UNIVERSIDAD
DE MÁLAGA

DOCTORAL THESIS:

PHOTOVOLTAIC SYSTEMS DISTRIBUTED MONITORING FOR PERFORMANCE OPTIMIZATION

AUTHOR: **FRANCISCO JOSÉ SÁNCHEZ PACHECO**

DIRECTORS: **PROF. DR. JUAN RAMÓN HEREDIA LARRUBIA**
PROF. DR. MARIANO SIDRACH DE CARDONA ORTÍN
PROF. DR. FRANCISCO PÉREZ HIDALGO

MÁLAGA, 2015

DR. D. JUAN RAMÓN HEREDIA LARRUBIA, PROFESOR DEL DEPARTAMENTO DE TECNOLOGÍA ELECTRÓNICA DE LA UNIVERSIDAD DE MÁLAGA, **DR. D. MARIANO DE SIDRACH DE CARDONA ORTÍN**, PROFESOR DEL DEPARTAMENTO DE FÍSICA APLICADA II DE LA UNIVERSIDAD DE MÁLAGA Y **DR. D. FRANCISCO PÉREZ HIDALGO**, PROFESOR DEL DEPARTAMENTO DE INGENIERÍA ELÉCTRICA DE LA UNIVERSIDAD DE MÁLAGA

CERTIFICAN:

Que la Tésis Doctoral realizada por D. Francisco José Sánchez Pacheco, con el título "Monitorización Distribuida en Sistemas Fotovoltaicos para la optimización de la Eficiencia *Photovoltaic Systems Distributed Monitoring for Performance Optimization*", de la cual somos directores, ha sido proyectada y desarrollada bajo nuestra supervisión.

Que el mencionado trabajo de investigación reúne todas las características científicas y técnicas para poder ser defendido públicamente. Asimismo, merece una alta valoración en cuanto a rigor, actualidad de planteamiento y metodología, de todo lo cual informamos como trámite preceptivo para su aceptación y posterior defensa pública en Málaga, a 12 de febrero de dos mil quince.

Dr. D. J.R. Heredia Larrubia

Fdo:_____

Dr. D. Mariano de Sidrach de Cardona Ortin

Fdo:_____

Dr. D. Francisco Pérez Hidalgo

Fdo:_____

DOCTORAL THESIS

PHOTOVOLTAIC SYSTEMS DISTRIBUTED MONITORING FOR PERFORMANCE OPTIMIZATION

WRITTEN BY:

FRANCISCO JOSÉ SÁNCHEZ PACHECO

DIRECTED BY:
PROF. DR. JUAN RAMÓN HEREDIA LARRUBIA
PROF. DR. MARIANO SIDRACH DE CARDONA ORTÍN
PROF. DR. FRANCISCO PÉREZ HIDALGO

TO APPLY TO THE DEGREE OF DOCTOR FROM THE UNIVERSITY OF MÁLAGA

Publicaciones y
Divulgación Científica

INDEX OF CONTENTS

INDEX OF FIGURES

CHAPTER 3: SMART MONITORING AND PLC COMMUNICATIONS MODULE

-

Chapter 4: SMCM MEASURING CHAINS UNCERTAINTY ESTIMATION

Chapter 5: MODEL VALIDATION WITH EXPERIMENTAL DATA

-

Chapter 6: MODEL APPLIED TO SMCM MONITORED DATA

Chapter 7: PV MODULES REAL-TIME PERFORMANCE RATING

-

Chapter 8: CONCLUSIONS, FUTURE RESEARCH LINES & SCIENTIFIC PRODUCTION

INDEX OF TABLES

Chapter 8: CONCLUSIONS, FUTURE RESEARCH LINES & SCIENTIFIC PRODUCTION

LIST OF SYMBOLS

Symbol	Name or description
a	Photovoltaic module temperature coefficient
b	Photovoltaic module temperature coefficient
$Drift(V_{AFE})$	Derate of the VAFE
$Drift(I_{AFE})$	Derate of the IAFE
$Drift(T_{AFE})$	Derate of the TAFE
Eg	Energy gap of the semiconductor material atom
FF	Fill Factor
FF_O	Ideal Fill Factor
FF_{Ot}	Translated ideal Fill Factor
FS_{OA}	Operational Amplifier Full Scale
G	Incident irradiance
Ge	Effective irradiance in the plane of the photovoltaic module
G_g	Global incident irradiance
G_0	Reference irradiance at STC
I	Current at the output of the photovoltaic cell/module
I_D	Diode current
Imp	Maximum power point current
I_{SC}	Photovoltaic module short circuit current
I_{SC0}	Photovoltaic module short circuit current at STC
I_{SCt}	Photovoltaic module translated short circuit current
I_0	Diode saturation current
I_{ph}	Cell/module photogenerated current
k_B	Boltzmann constant
k_{ISENS}	Hall effect current sensor sensitivity
k_{VC}	VAFE measuring chain constant
k_{VN}	VAFE measuring chain nominal constant
k_{IC}	IAFE measuring chain constant
k_{IN}	IAFE measuring chain nominal constant
k_{TC}	TAFE measuring chain constant

k_{TN}	TAFE measuring chain nominal constant
LF	Loss Factor
L^e_{DC}	Effective DC Losses
L^i_{DC}	Instant read PV Module DC overall Losses
L^t_{DC}	ROC translated DC overall Losses
NI_{ADC}	ADC digital counts of photovoltaic module current
$NOCT$	Normal Operating Cell Temperature
Ns	Number of series connected photocells
NT_{ADC}	ADC digital counts of photovoltaic module back-plane temperature
NV_{ADC}	ADC digital counts of photovoltaic module voltage
P	PV module output power
P_{DC}	Photovoltaic module DC generated power
P_i	Photovoltaic module instant power
P_{mLF}	Photovoltaic module maximum power with loss factor
Pmp	Maximum power point
Pmp_t, Pm_t	Translated maximum power point
Pmp_0	Maximum power point at STC
PR	Traditional Performance Factor
PR_{DC}	DC side Performance Ratio
PR^i_{DC}	Photovoltaic module instant DC performance ratio
PR^t_{DC}	Photovoltaic module translated DC performance ratio
q	Charge of the electron
R_{Ch}	Characteristic resistance
Rp	Parallel parasitic resistance
Rs	Series parasitic resistance
Rs_t	Translated series parasitic resistance
Sc_i	Uncertainty sensitivity coefficient
SR	Spectral Radiation
STC	Standard Test Conditions
S_W	Wind speed
T	Absolute temperature (K)
Ta	Ambient temperature

Tc	Photovoltaic cell temperature
Tc_t	Translated photovoltaic cell temperature
Tm	Photovoltaic module temperature
Tm_t	Translated photovoltaic module temperature
T_0	Reference module temperature at STC
U	Expanded uncertainty
$u(C)$	Uncertainty contribution of measuring chains calibrated constants
$u(R)$	Uncertainty contribution of reading unstable conditions
$u(D)$	Uncertainty contribution of components drift
$U_c(y)$	Combined uncertainty
$uD(X_i)$	Components drift uncertainty terms
$uD(V_{AFE})$	Uncertainty of VAFE drift
$uD(I_{AFE})$	Uncertainty of IAFE drift
$uD(T_{AFE})$	Uncertainty of TAFE drift
$uR(X_i)$	Reading uncertainty terms
V	Voltage at the output of the photovoltaic cell/module
Vq	ADC quantization voltage
V_D	Diode voltage
Vmp	Maximum power point voltage
V_{OC}	Photovoltaic module open circuit voltage
V_{OC0}	Photovoltaic module open circuit voltage at STC
V_{OCc}	Photocell open circuit voltage
V_{OCct}	Translated photocell open circuit voltage
V_{OCt}	Photovoltaic module translated open circuit voltage
v_{OC}	Normalized V_{OC} voltage
v_{OCt}	Translated normalized V_{OC} voltage
V_T	Thermal voltage
V_{Tt}	Translated thermal voltage
ΔT	Temperature difference
α	Photovoltaic module current temperature coefficient
αV_{IO}	Opamp input offset voltage thermal drift
β	Photovoltaic module voltage temperature coefficient

| δ | Photovoltaic module irradiance temperature coefficient |
| γ | Photovoltaic module power temperature coefficient |

A mis Padres
A mi mujer Pilar y a mis hijos Carlos y Alvaro
A mi hermano Carlos

ACKNOWLEDGEMENTS

AGRADECIMIENTOS

Esta Tésis Doctoral recoge los resultados del trabajo desarrollado durante más de 5 años ya. Ha sido una labor árdua, que ha requerido mucho tiempo, gran parte del cual se lo he quitado a mi Familia. Sin embargo, ha constituido para mi una oportunidad única de profundizar en un campo apasionante, al tiempo que me ha permitido compartir muchos fructíferos momentos con grandes profesionales que me han transmitido su buen saber hacer. Espero y deseo que esto sea un punto de continuidad habida cuenta de las perspectivas que este trabajo ha permitido vislumbrar.

Quiero expresar mi mayor agradecimiento a mis Directores de Tésis, los Dres. Juan Ramón Heredia Larrubia, Mariano Sidrach de Cardona y Francisco Pérez Hidalgo, por su constante apoyo y asesoramiento, durante todos estos años. Sus aportaciones en cuanto a los contenidos, estructura y valoración de los resultados experimentales han sido inestimables. Ha sido para mi un privilegio haber podido contar con ellos como Directores.

También quiero agradecer a los profesores del DIEM de la Universidad de Salerno, que tan amablemente me acogieron durante mi estancia en dicha Universidad. Tuve la oportunidad de contactar con los profesores Giovanni Spagnuolo y Giovanni Petrone, renombrados expertos en el área de la Tecnología Fotovoltaica cuyos conocimientos y sugerencias me ayudaron mucho en el desarrollo de la Tésis.

Mis compañeros de Departamento han constituido el elemento de apoyo necesario en esta andadura. Sus constantes palabras de ánimo me han servido para no cejar en el esfuerzo. Las sugerencias hechas por la profesora Ana Pozo y por el profesor David Trujillo han sido de gran ayuda. Muy particularmente, quiero agradecer al Profesor Pedro Sotorrío su inestimable ayuda y asesoramiento en varios apartados de la Tésis. También quiero agradecer el asesoramiento que me facilitó el profesor Lorenzo Sevilla.

Quiero agradecer asimismo el trabajo de revisión que han hecho los Dres. Damien Picault y Sonia Leva, que me han permitido acceder a la mención de Doctorado Internacional.

El tiempo robado a la Familia espero que no haya sido en vano. Han sido muchas las horas dedicadas los fines de semana y los días cogidos en períodos de vacaciones. El apoyo incondicional que en todo momento me ha transmitido mi mujer Pilar, así como mis Padres ha sido providencial para haber podido consolidar este trabajo.

Una vez echada la vista atrás, sin la participación de todas estas personas, uno no se imagina haber podido llegar hasta aquí y no puede menos que estar enormemente agradecido. No es posible compensar dichos esfuerzos, salvo con el compromiso personal de intentar transmitir sus conocimientos y sabios consejos cuando se me dé la oportunidad de poder hacerlo en la labor cotidiana que uno intenta llevar a cabo de la mejor manera posible.

The first was never to accept anything for true which I did not clearly know to be such; that is to say, carefully to avoid precipitancy and prejudice, and to comprise nothing more in my judgement than what was presented to my mind so clearly and distinctly as to exclude all ground of doubt.

The second, to divide each of the difficulties under examination into as many parts as possible, and as might be necessary for its adequate solution.

The third, to conduct my thoughts in such order that, by commencing with objects the simplest and easiest to know, I might ascend by little and little, and, as it were, step by step, to the knowledge of the more complex; assigning in thought a certain order even to those objects which in their own nature do not stand in a relation of antecedence and sequence.

And the last, in every case to make enumerations so complete, and reviews so general, that I might be assured that nothing was omitted.

Discourse on the Method, R. Descartes

Abstract

This Doctoral Thesis is entitled Photovoltaic Systems Distributed Monitoring for Performance Optimization. The aim of the concepts herein developed is to improve significantly the performance of photovoltaic plants. The amount of energy that a PV plant can generate depends mainly on the incident irradiance and on the ambient temperature as well, which will finally affect the PV module temperature.

There are different losses factors that may affect negatively their performance. Their consequences will affect directly the PV module operating parameters. The convenience to have real-time information of their behavior is evident. This will allow to obtain the module *I-V* fingerprint and quantify its performance according to applying real outdoor conditions (ROC). A further comparison with the values that should be theoretically obtained, will make possible to identify a PV module underperforming. The differences obtained will allow to quantify the associated losses.

An underperforming PV module will generate significant financial losses if it keeps working under these conditions.

This Thesis has been structured as follows: in chapter 2, an overview is made of the PV modules operational parameters and their dependence on applying atmospheric conditions. These are:

- Short circuit current: I_{SC}
- Oper circuit voltage: V_{OC}
- Current at máximum power point: I_{mp}
- Voltage at maximum power point: V_{mp}
- Power at maximum power point: P_{mp}

Furthermore, the translation procedures of referred parameters from Standard Test Conditions (STC) to Real Operating Conditions (ROC) are defined.

In chapter 3, the proposed monitoring system is described, as well as the Smart Monitoring and Communications Module (SMCM) configuration and the

PLC based physical communications layer. The SMCM is a smart device based on TI MSP 430 high performances low cost µController. This has allowed the development of a low cost monitoring system.

The main characteristics are:

- Developed with low cost components.
- The system can be tailored according to customer requirements.
- It allows to have real-time data of the PV module operating data, such as voltage (V), current (I) and module temperature (T_m), as well as the ambient conditions like the incident irradiance (G) and the ambient temperature (T_a).
- Data can be displayed to the end user by means of corresponding Graphic User Interface (GUI).
- Real-time identification of underperforming or defective PV module.
- Data Tx/Rx by means of PLC technology over already existing DC power lines.

In chapter 4, the SMCM, as an electronic measurement device, associated uncertainty is quantified.

In chapter 5, the proposed model is validated using consolidated data obtained in the UMA RREE Lab. The procedure applied has been to generate the *I-V* curve values from proposed model, according to reported ambient conditions and then the results are compared in order to quantify the resulting Relative Error (RE).

A total of 10 sets of measurements have been made under different conditions. The *I-V* curves at STC have been obtained and further translated to ROC. The Relative Error (RE) of main operational parameters such as short circuit current (I_{SC}), open circuit voltage (V_{OC}), power at maximum power point (P_{mp}) and corresponding voltage (V_{mp}) and current (I_{mp}) as well has been calculated.

In chapter 6, the same procedure has been applied to the SMCM obtained experimental results generated in the EPS PV Lab installed Isofoton PV modules, once they have been previously validated. One of the PV modules has been equipped with one SMCM, which has been in charge of monitoring its operational

parameters (*V, I* and T_m), and further transmit them to the CCS, by means of the PLC technology using already existing DC power lines. The SMCM-CCS version is in charge of data routing to the CCS for further processing. Additionally, it processes the parameters of the calibrated cell which gives the effective incident irradiance and the ambient temperature sensor (Pt-100 RTD).

In chapter 7, previously described procedures are applied to quantify the Performance Ratios (PR) and corresponding Losses. The losses that a PV module can be affected of can be reflected in corresponding PR and can be divided in two major groups. On one hand, we have the losses due to the fact that the PV module is not working under STC. These losses are considered as non-avoidable. On the other hand, we have the losses due to a misfunction of the PV module or abnormal conditions non related to the applying atmospheric conditions. These can be due to a total or partial shadowing, either momentary or permanent, dust, soiling, etc… These losses are considered as avoidable and can be amended with corresponding corrective actions.

In this chapter, a comparison protocol is proposed between the two different PR concepts. Being the PV module working under given known real operating conditions (ROC), a first experimental *PR* is obtained, which is called PR^i_{DC}. On the other hand, the new concept of PR obtained by means of the ROC translated paramters is obtained, which has been called PR^t_{DC}. The comparative analysis of both *PR* will allow to quantify the losses that are applying to the PV module and their possible causes.

The amount of energy that a PV plant can generate, either grid connected or stand-alone depends initially on the efficiency of the PV cell technology for given ambient conditions. Under these premises, the energy generated can be significantly constrained due to both predictable and unpredictable losses factors (*LF*).

Finally, in chapter 8, the genera conclusions are described, together with the scientific production and the future research lines.

ABSTRACT

Chapter 1

INTRODUCTION

Current trends in energy supply and use are unsustainable – economically, environmentally and socially. Without decisive action, energy-related greenhouse-gas (GHG) emissions would lead to considerable climate degradation with an average 6°C global warming. We can and must change the path we are now on; sustainable and low-carbon energy technologies will play a crucial role in the energy revolution required to make this change happen. Energy Efficiency, many types of renewable energy, carbon capture and storage (CCS), nuclear power and new transport technologies will all require widespread deployment if we are to achieve a global energy-related CO_2 target in 2050 of 50 % below current levels and limit global temperature rise by 2050 to 2° C above pre-industrial levels.

… And it follows [1]: "*Photovoltaic (PV) energy is one of the most promising emerging technologies. The cost of PV modules has been divided by five in the last six years; the cost of full PV systems has been divided by almost three. The levelised cost of electricity of decentralised solar PV systems is approaching or falling below the variable portion of retail electricity prices that system owners pay in some markets, across residential and commercial segments. For bulk power on grid, PV electricity can already be competitive at times of peak demand, especially in areas where peak electricity is provided by burning oil products. And there remains ample room for improvements…*"

1.1 THE ROLE OF THE PHOTOVOLTAIC ENERGY NOWADAYS

It is a matter of fact that Renewable Energies play an important role in the Green House Gases (GHG) emissions reduction [1]. Figure 1.1 is a graph of the potential contribution of the different technologies in emissions reduction. The solar PV has a potential contribution of 20 %, but, furthermore, the electricity efficiency improvements can contribute a 23 % more.
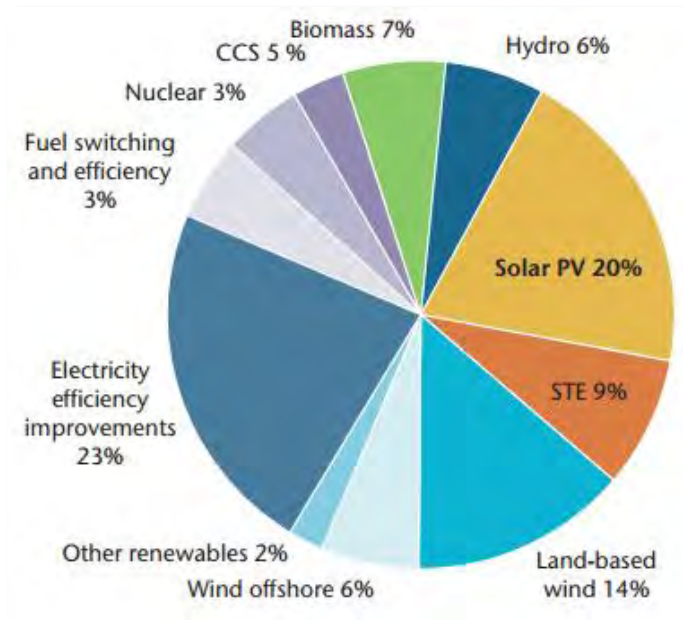
Figure 1.1. Cumulative technology contributions to power sector emission reductions in ETP 2014 hi-Ren scenario (source: IEA)

Figure 1.2 shows the cumulative PV based energy production by countries, as per 2013 [1].
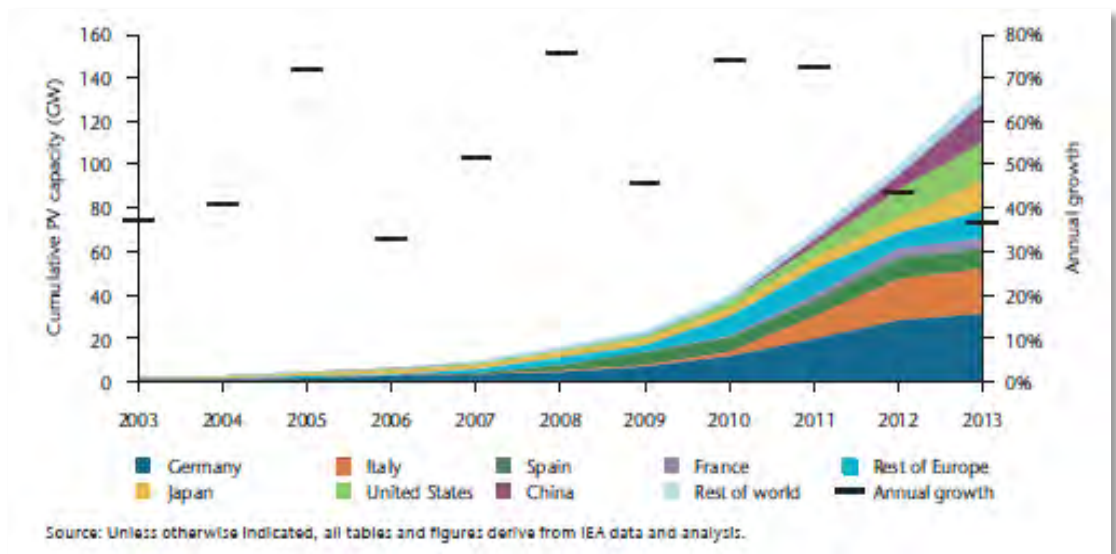
Figure 1.2. Cumulative PV energy production capacity (source:IEA)

1.2 THE CONVENIENCE OF MONITORING

Electricity production PV power plants of medium to large dimensions are very sensitive to optimal performance from operational and financial points of view [2][3][4]. Projects shareholders expect to have the maximum benefit of their investment and have a prompt pay-back. PV plants monitoring is becoming a real need, since any malfunction can create important revenue losses [5]. In this sense, the International Energy Agency (IEA) states clearly the need to know exactly the PV performance data [2][6].

Different adverse circumstances may lead to a significant decrease in the conversion of solar radiation into electricity production [7]. Most relevant adverse conditions are due to:

- Atmospheric and ambient variables like temperature, humidity, wind speed and air mass index
- Permanent or temporary shadowing, dust, soiling
- Devices degradation / failures

Several of these power losses might apparently be due to incident radiation or occasional shadowing conditions [8]. This being the case, it is somewhat difficult to determine the root cause of any potential failure.

The fact to have reliable real time data of every single PV module functional parameters, namely voltage, current and back-plane temperature can help to determine their optimal performance and evaluate any problem root cause. In case of system failure, since proposed solution is able to identify the defective module, immediate corrective actions can be undertaken, which improves maintenance activities. In case of non-monitored plants, a defective module might be masked into the string with which it is associated and no major evidence would arise.

Nowadays, there are different possible solutions available in the market and referred in the literature. These solutions are based on general purpose industrial monitoring and control systems (SCADA), on application specific systems designed for PV plants monitoring, or in some cases this is performed by µinverters endorsed to the PV modules. All these options represent a significant cost of the system itself and of the installation in the plant. These solutions are tailored mainly for domestic or small scale facilities and not always suitable to monitor at PV module level.

Regarding the transmission of the monitored data, here again the possible solutions are based on standard industrial communications configurations, which require additional wiring installation; another option is based on radio communications topologies, expensive and highly sensitive to noise and communications problems. Finally, if the case of module level monitoring, in the literature, most of the solutions are based on costly magnetic coupling.

Furthermore, the data mining and processing of the monitored parameters can help to improve the PV plant performance. For this purpose, it is proposed a concept of Performance Ratio that helps to real-time identify a PV module that is underperforming according to the applying real outdoor conditions.

1.3 THE PV MODULES EFFECTIVE PERFORMANCE RATIO ESTIMATION

Once the PV module functional parameters have been monitored, the main advantage is that this information can help to quantify the PV module real time Effective Performance Ratio (EPR). This EPR by difference with the traditional one, gives a more accurate information of the module operation, taking into account the applying outdoor ambient conditions. This being done, the resulting values help to identify in real time any defective module, working below the expected values.

1.4 THE CHALLENGE OF MONITORING AT LOW COST

Arrived at this point, the convenience of monitoring at PV module level is clear and justified to be convenient.

Now the challenge is to define a monitoring structure which were suitable for complying with requested objectives. Mainly, these are related to tight the costs as low as possible of:

- System electronic components
- Data transmission and reception (Tx/Rx)
- System deployment

The main challenges were to develop a monitoring device, embedded in a whole monitoring system that might be cost competitive. If the monitoring module cost were excessive, it might not be justified in terms of investment in the monitoring system by the PV plant owners. On the other hand, the overall monitoring system, including the data Tx/Rx communications layers is also an important issue in terms of installation costs. Furthermore, the system deployment cost-effectiveness would be questioned if finally its usefulness were not demonstrated.

Maintenance costs due to non-identified defective modules may have an important impact. The identification of a defective PV module in a string requires a skilled technician that would have to analyze each single module in a time consuming activity.

As an orientation example, in a 100 kW PV which might invoice 50.000 €/year, an accumulated continuous 10 % of not detected losses could represent a lack of incomes of around 5.000 €/year. Considering that the proposed monitoring system has an estimated materials cost of around 10 €/module (which is a 2 % of a 250 Wp PV module cost), a 550 PV panels plant monitoring system deployment would represent an investment of roughly 5.500 €. The return of the investment is done in one year of PV plant operation.

1.5 THE OBJECTIVES OF THE THESIS

The work performed and the results obtained in order to comply with above referred challenges have been detailed in the present Thesis. In essence, the objectives have been:

- To demonstrate the possibility to monitor the PV modules operational parameters at module granularity level
- The possibility to receive and transmit monitored data using the already existing direct current (DC) power line, applying the Power Lines Carriers technology
- To implement an overall monitoring system at the lowest possible cost
- To demonstrate the Effective Performance Ratio proposed model advantages

1.6 THE STRUCTURE OF THE THESIS

On the basis of these premises, this thesis describes all the tasks that have been undertaken to comply with them and which have helped to demonstrate the viability of the idea. It includes:

- The models definition
- Modules and Tx/Rx lines simulation
- Laboratory prototypes and test benches
- The field experimental results

The present Thesis is structured as follows:

After this introductory chapter, in chapter 2 an overall review is made of the PV cells and modules functional parameters, as well as their dependence on the applying outdoor ambient conditions. The identification of these parameters behavior is essential to define the monitoring system. Additionally, the translation criteria of referred parameters to real outdoor operating conditions have been depicted which will be necessary to further estimate the proposed EPR and subsequent resulting Losses Factors (LF). The different mathematical models; of the cell, the module, the translation criteria and the resulting Performance Ratios and Losses coefficients are deployed.

Chapter 3 is devoted to the PV modules monitoring concept. A description is made of the proposed Smart Monitoring and Communications Module (SMCM), together with the Power Lines Carrier application to the monitoring system as physical communication layer. The electronic design, simulation and laboratory prototypes are full depicted.

Afterwards, in chapter 4, the uncertainty related to above referred SMCM in terms of measuring device is described and quantified.

In chapter 5, the models proposed in chapter 2 are validated by means of consolidated field experimental data. This has allowed to confirm the viability of the proposed models.

In chapter 6, the same procedure has been applied to the monitoring data resulting from the experimental measurements made at the Escuela Politécnica Superior (EPS) Photovoltaic Lab, where two Isofotón ISF-245 PV modules have been installed together with a laboratory instrumentation test bench for experimental purposes.

In chapter 7, a detailed analysis is made of monitored data obtained by means of the SMCM, with the purpose of quantifying the PR and subsequent LF´s.

Finally, chapter 8 is devoted to the conclusions and future research lines that can result from present research work.

1.7 REFERENCES

[1] IEA. International Energy Agency. Technology Roadmap. Solar Photovoltaic Energy. 2014 Edition.

[2] L. Cristaldi, M. Faifer, A. Ferrero and A. Nechifor, "On line monitoring of the efficiency of photo-voltaic panels for optimizing maintenance schedule". I2MTC 2010 - International Instrumentation and Measurement Technology Conference, Austin, TX, 3-6 may 2010.

[3] L. Dorobantu, M.O. Popescu and C.L. Popescu, "Yield loss of photovoltaic panels caused by depositions". The 7th International Symposium on Advanced Topics in Electrical Engineering, Bucharest, may 2011.

[4] G. Petrone, G. Spagnuolo, R. Teodorescu, M. Veerachary and M. Vitelli, "Reliability Issues in Photovoltaic Power Processing Systems". IEEE Transactions on Industrial Electronics, Vol. 55, No. 7, july 2008.

[5] B. Marion, K. Adelstein, K. Boyle, H. Hayden, B. Hammond, T. Fletcher, B. Canada, D. Narang, A. Kimber, A. Kimber, L. Mithcell, G. Rich and T. Townsend, "Performance parameters for grid-connected PV systems". Conference Record of the Thirty-first IEEE Photovoltaic Specialists Conference, 2005.

[6] IEA. International Energy Agency. Performance Prediction of Grid-Connected Photovoltaic Systems using Remote Sensing. Report IEA PVPS T2-7: 2008.

[7] A. Detrick, A. Kimber and L. Mitchel, "Performance Evaluation Standards for Photovoltaic Modules and Systems". Conference Record of the Thirty-first IEEE Photovoltaic Specialists Conference, 2005.

[8] S. Vergura, G. Acciani, V. Amoruso and G. Patrono, "Inferential Statistics for Monitoring and Fault Forecasting of PV Plants". IEEE International Symposium on Industrial Electronics, ISIE 2008.

Chapter 2

PV Cell and Module Models and Monitoring

In chapter 1, it has been justified the convenience of PV modules monitoring, in order to have reliable information related to their behavior and by extension to know how the PV plant is performing. A PV modules monitoring system is a very important resource which makes possible to empower different aspects once it is implemented. On one hand, it allows the user to have real time information of the behavior of the Photovoltaic plant; it can store data for further retrieving. Furthermore, according to the data processing algorithms, it may issue the corrective actions to be generated. For this purpose, a detailed description is made of the main operating parameters of the photocell and by extension of the PV module, which will be further monitored.

2.1 OPERATIONAL PARAMETERS OF THE ILLUMINATED PHOTOCELL

A solar cell is in essence a p-n semiconductor based device capable of generating electricity from the incident sunlight, by means of the PV process [1]. Since 1954, when the first efficient photovoltaic cells were manufactured, up to date, the technology has made possible to reach efficiencies in the surrounding of the 45 % [2].

In the dark, a PV cell behaves like a p-n junction diode and requires an external voltage source to allow a given amount of current through the diode (Figure 2.1). The current through the cell (I_D) would be defined by the voltage of the external power supply (V_D) when in direct polarization and when in reverse polarization, the current obtained is the dark saturation current (I_O) [1].
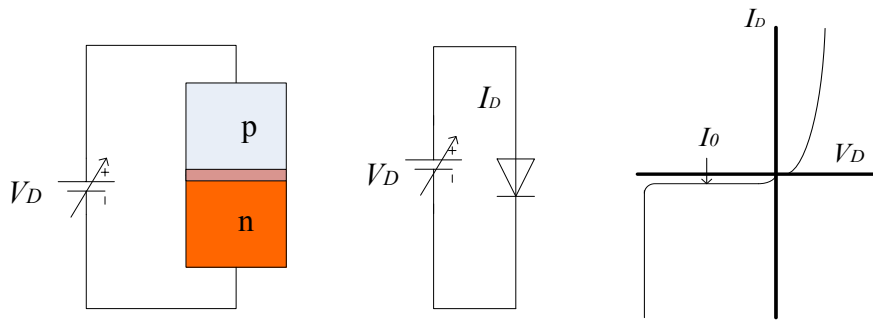
Figure 2.1. The photocell in the dark equivalent diode and characteristic curve

The expression that characterizes both parameters is the typical characteristic curve of the diode:

$$I_D = I_0 \left(e^{\frac{V_D}{V_T}} - 1 \right)$$

(2.1)

Where V_D is the voltage across the diode; V_T is the thermal voltage, given by equation (2.2) and which value at 25 ºC is considered to be around 25 mV for Silicon.

$$V_T = \frac{k_B \cdot T_C}{q}$$

(2.2)

Where k_B is the Boltzmann constant (k_B=1,38 · 10^{-23} J/K); T_C is the absolute temperature of the photocell under ambient conditions and q is the charge of the electron (q=1,60 · 10^{-19} C).

On the other hand, the diode dark saturation current (I_O) is given by equation (2.3), according to [1]:

$$I_0 = 1{,}5 \cdot 10^5 \, e^{\left(-\frac{E_g}{k_B \cdot T}\right)} A/cm^2 \qquad (2.3)$$

Where E_g is the energy gap of the semiconductor material used for the photocell manufacturing (1,2 eV in case of Silicon). This makes the photocell energy conversion efficiency dependent upon the wavelength of the incident photons (Figure 2.2.) [4].
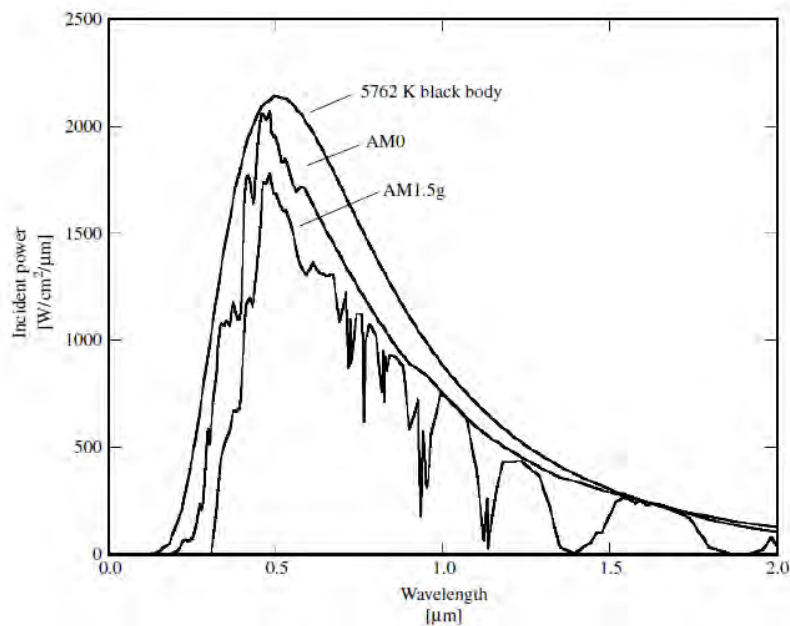
Figure 2.2. Spectral distribution of sunlight of the sun as a 6000 K black body, with AM0 and AM1,5

When the photocell is being submitted to the sun irradiance, the PV process begins and it starts generating electrons in movement to create the electric current.

An ideal photocell can be represented by an ideal photo-generated current source (I_{ph}) and a diode in parallel, as per Figure 2.3, [3]:
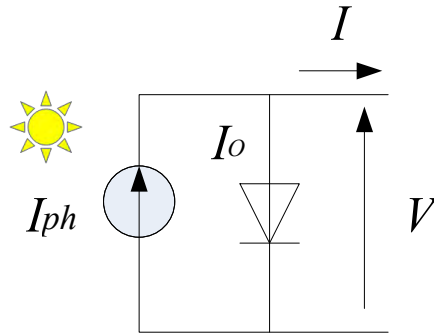
Figure 2.3. Simplified model of the illuminated photocell

Its characteristic equation is given by equation (2.4), which relates the voltage at the output of the cell with the current that it might supply, depending on the irradiance incident on it:

$$I = I_0\left(e^{\frac{V}{V_T}} - 1\right) - I_{ph} \qquad (2.4)$$

Resulting characteristic curve, given in Figure 2.4.
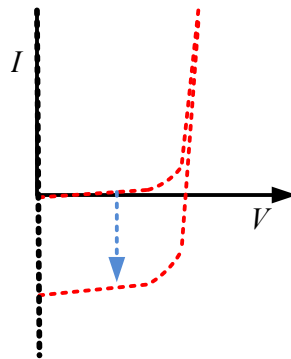
Figure 2.4. Characteristic curve of the illuminated photocell

Finally, considering:

$$e^{\frac{V}{V_T}} >> 1 \qquad \text{and} \qquad I_{ph} >> I_0$$

After changing the axes criteria, equation (2.4) results in following expression and the graph of Figure 2.5:

$$I = I_{ph} - I_0 \left(e^{\frac{V}{V_T}} \right) \tag{2.5}$$
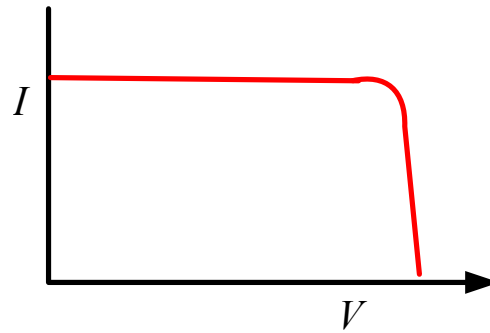
Figure 2.5. Characteristic curve of the illuminated ideal photocell

The symbol generally used to represent is shown in Figure 2.6.
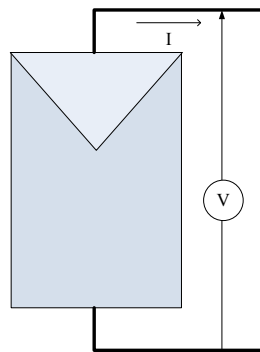
Figure 2.6. Electric symbol of the PV cell (and module)

Once the ideal illuminated photocell has been modeled as per equation (2.5), Figure 2.7 gives the main parameters that finally characterizes it. In this figure, both the I-V curves and the P-V curve have been represented, as well as the Maximum Power Point (MPP), which is the maximum value of electric power that the photocell can deliver. These parameters are:

- I_{SC} : short circuit current (V = 0 V)
- V_{OC}: open circuit voltage (I = 0 A)
- V_{mp}: Voltage at MPP
- I_{mp}: Current at MPP
- P_{mp} : Power at MPP
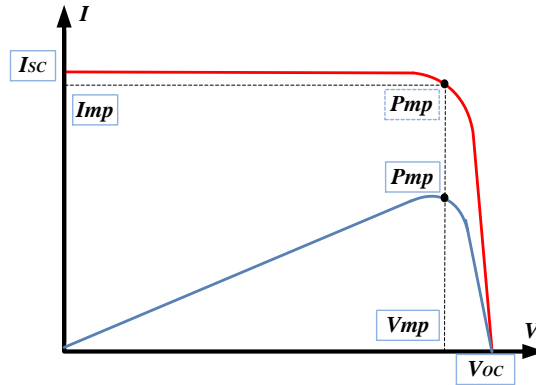
Figure 2.7. I-V-P photocell characteristic curve and main operating parameters

2.1.1. Short Circuit Current (I_{SC}).

The short circuit current (I_{SC}) is the value of the maximum current that the illuminated cell can supply according essentially to the incident irradiance (G) and the ambient temperature (T_a), under short circuited connection of the cell´s contacts. In the ideal case, I_{SC} is equal to the photo-generated current I_{ph} (equation 2.6).

$$I_{SC} = f(G, T_a)$$

$$I_{SC} = I_{ph} \tag{2.6}$$

2.1.2. Open Circuit Voltage (V_{OC})

This parameter gives the maximum voltage that can be obtained in the PV cell, any time no load is connected and no current is supplied by the cell:

$$V_{OC} = \frac{k_B T}{q} \cdot \ln\left(1 + \frac{I_{ph}}{I_0}\right) \tag{2.7}$$

Where k_B is the Boltzmann constant, T is the absolute temperature, q is the charge of the electron and I_{ph} and I_0 are already referred photo-generated and dark saturation currents.

The value of V_{OC} is dependent up on the properties of the semiconductor, since I_0 is as well, as stated by Green in [1]. Known V_T, it can be assumed that the PV cell is open-circuited. This means that no current will be transferred to a load connected (I=0 A). Subsequently, the voltage across of the PV cell will be the open circuit voltage (V_{OC}).

2.1.3. Diode dark saturation current (I_0)

When the PV cell is short circuited, the current (I_{SC}) is essentially equivalent to the photogenerated current (I_{ph}). Solving equation (2.5) for I= 0 A and V= V_{OC}; that means that no current will be transferred to the load (I=0 A.), the voltage across the PV module is the so called open circuit voltage (V_{OC}):

$$0 = I_{ph} - I_0 \left(e^{\frac{V_{OC}}{V_T}} \right)$$

And solving for I_0, it is obtained the equation that allows to calculate the value of the diode dark saturation current, as indicated in equation (2.8).

$$I_0 = I_{SC} e^{\left(-\frac{V_{OC}}{V_T} \right)} \tag{2.8}$$

2.1.4. Maximum Power Point

The Maximum Power Point (MPP) identifies the coordinates of the I-V curve where the value of the power delivered by the cell reaches the maximum value under applying irradiation and ambient temperature, being all other parameters in the best conditions.

$$P_{mp} = V_{mp} \cdot I_{mp} \tag{2.9}$$

The value of this parameter and its position in the *P-V* curve will vary upon different parameters and conditions, as it will be further explained.

2.1.5. Fill Factor. Parasitic and characteristic resistances

The ideal *I-V* curve shape of Figure 2.5 will vary significantly if the losses that the PV cell can be affected of are considered. These losses are mainly due to internal parasitic resistances, *Rs* and *Rp*. These components are depicted in Figure 2.8, which shows the electrical model considering referred parasitic resistances.
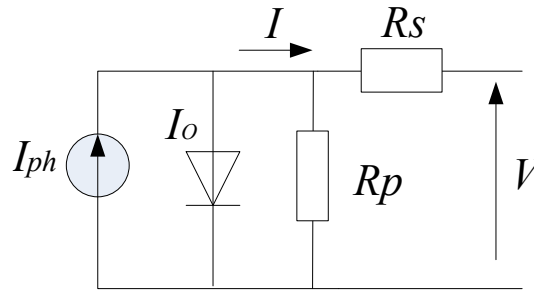
Figure 2.8. One diode electrical model of the PV cell with parasitic resistances

The series resistance *Rs* is mainly due to the PV cell inner bus bar metallic contacts and the semiconductor region. Its value is usually $< 1\ \Omega$, but it may have a significant impact in the shape of the *I-V* curve, mainly in the region of V_{OC}.

The effects of the parasitic resistances are depicted in Figure 2.9, where it can be seen the relationship established between the areas occupied by the rectangles defined by *Imp* and *Vmp* on one hand and by I_{SC} and V_{OC} on the other one.
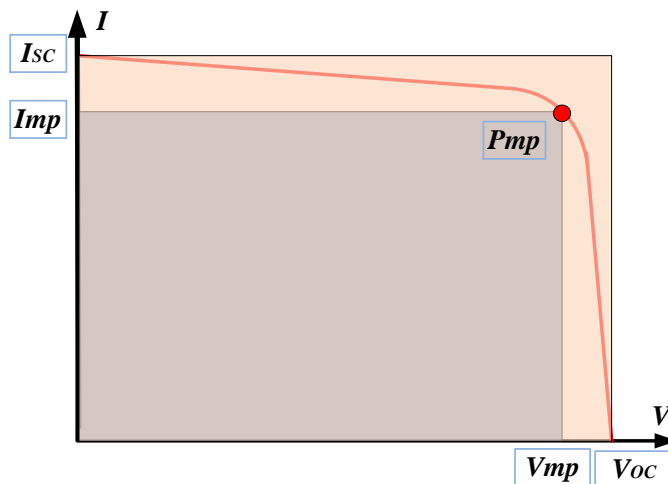
Figure 2.9. PV cell Fill Factor graph

In an ideal case, where no losses are reported, both figures would have the same dimensions. Nevertheless, as it has been seen previously, the effect of the parasitic resistances makes the MPP to move downwards.

The term that relates both figures is the so called Fill Factor (FF), which can be expressed as per equation (2.10), according to [1].

$$FF = \frac{V_{mp}I_{mp}}{V_{OC}I_{SC}} \tag{2.10}$$

This factor gives a magnitude of the maximum power that a PV cell may generate, under the operating conditions. It may reach values between 0,7 and 0,85.

In the specific case that the parasitic resistance were neglected ($Rs = 0\ \Omega$), ideally the Fill Factor value can be expressed empirically as a function of the normalized voltage v_{OC} [1], as indicated in equation (2.11).

$$FF_0 = \frac{v_{OC} - \ln(v_{OC} + 0,72)}{v_{OC} + 1} \tag{2.11}$$

Where v_{OC} is the normalized voltage at V_T, given by equation (2.12).

$$v_{OC} = \frac{V_{OC}}{\frac{kT_c}{q}} \implies v_{OC} = \frac{V_{OC}}{V_T} \tag{2.12}$$

The slope given by the relationship of V_{OC} and I_{SC} is called the characteristic resistance Rch, given in equation (2.13) and depicted in Figure 2.10.

$$Rch = \frac{V_{OC}}{I_{SC}} \tag{2.13}$$
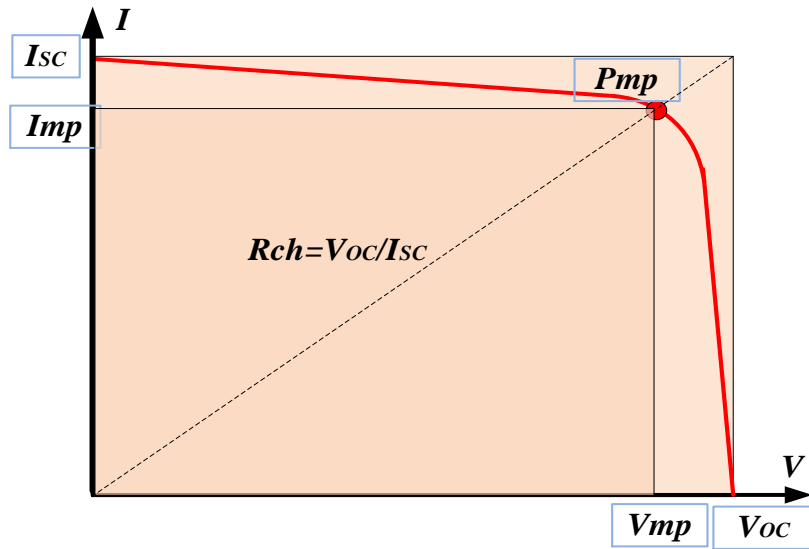
Figure 2.10. PV cell characteristic resistance *Rch*

In order to establish a relationship between *FF* and *FF₀*, which would give an idea of the cell ideality, it can be considered that [1]:

$$FF = FF_0\left(1 - \frac{Rs}{Rch}\right) \tag{2.14}$$

Equation (2.14) gives a maximum value for *FF* when *Rs*=0 Ω, resulting in *FF=FF₀*. Solving *Rs* from equation (2.14), it can be deducted that:

$$Rs = Rch\left(1 - \frac{FF}{FF_0}\right) \tag{2.15}$$

Substituing equation (2.13) in (2.15), it results equation (2.16), which is the expression that empirically expresses the value of *Rs*, as a function of the characteristic parameters of the photocell.

$$Rs = \left(1 - \frac{FF}{FF_0}\right)\left(\frac{V_{OC}}{I_{SC}}\right) \tag{2.16}$$

The effect of the parallel resistance *Rp* represents the leakages due to the solar cell crystal defects and impurities. The value of *Rp* is significant, and for ease of calculation, considered ∞ and hence removed from the electrical model. This parasitic resistor affects mainly the slope of the I-V in the region of I_{SC}. All these considerations are depicted in Figure 2.11. The values of *Rp* and *Rs* that finally affect the PV cell, will define the coordinates of the MPP.
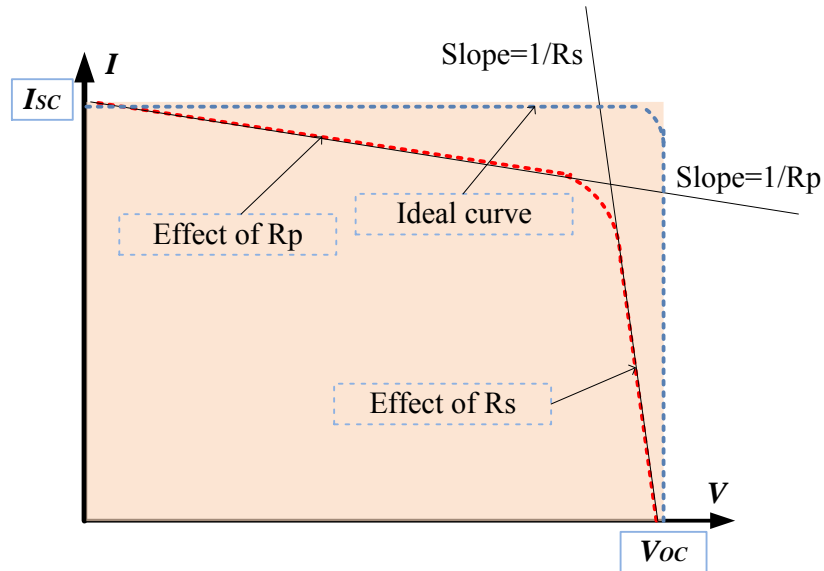
Figure 2.11. Effect of the parasitic resistances on the I-V PV cell characteristic

2.2 PV MODULE MATHEMATICAL MODELS

In order to compare measured PV module operating parameters with the values that theoretically should be obtained, under the applying atmospheric conditions, a mathematical model of the PV module operational parameters (Figure 2.12) is required.
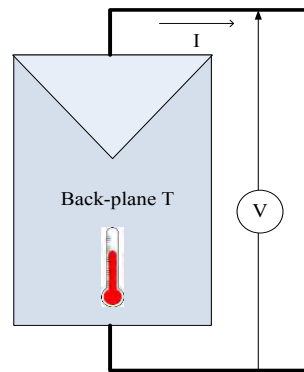
Figure 2.12. PV module operational parameters.

There are several options that have already been described in the literature. The most detailed and extensive one is to consider the two diodes model, as described in [10], by Adamo et al.

Nevertheless, the single diode option has been considered (Figure 2.13a) and for ease of operations, the option without parallel loss resistance (Rp) has been selected, which, being accurate, significantly simplifies the mathematical model [11] and [12] (Figures 2.13b).
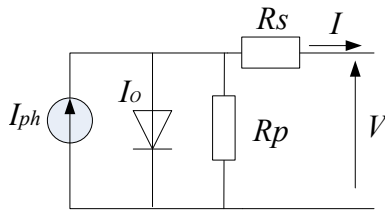
Figure 2.13a. PV cell one diode equivalent model with Rp and Rs
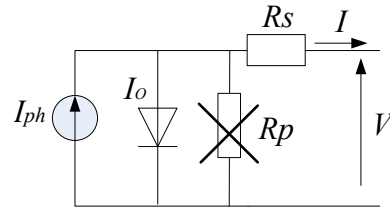
Figure 2.13b. PV cell one diode equivalent model without Rp

It is suitable in order to obtain the *I-V* fingerprint, which involves the PV module main electrical operating parameters: (Figure 2.14).

- I_{SC} : short circuit current (V=0 V)
- V_{OC} : open circuit voltage (I=0 A)
- V_{mp}: Voltage at MPP
- I_{mp}: Current at MPP
- P_{mp} : Power at Maximum Power Point
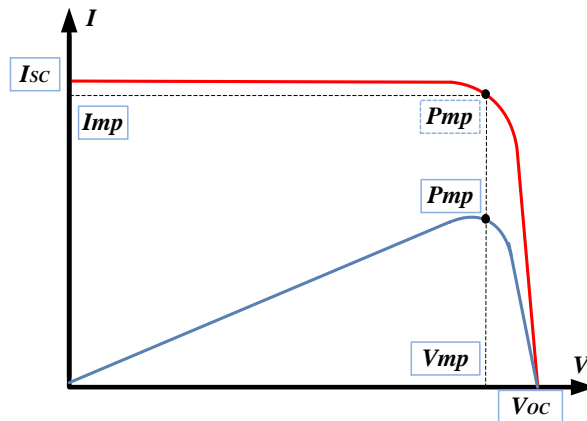
Figure 2.14. PV module electrical operational parameters

The expression that characterizes the one diode based single exponential model of a PV module (Figure 2.13a) is given by equation (2.17).

$$I = I_{ph} - I_0\left(e^{\frac{V+IR_s}{n \cdot N_s \cdot V_T}} - 1\right) - \frac{V + IRs}{Rp} \tag{2.17}$$

Where V and I are respectively the voltage and current supplied by the PV module (Figure 2.3); I_{ph} stands for the photo-generated current; n is the diode ideality factor; N_s is the number of series connected cells of the PV module; V_T is the equivalent diode thermal voltage and Rp and Rs represent the ohmic losses that affect the final energy yield.

One of the constraints of equation (2.17) is that it is an implicit one, which requires significant computational resources to solve it. Beside traditional computational environments, other possible solutions have been described in the literature. Petrone et al. in [13] describe a solution based on the use of the Lambert W-function. Furthermore, Merino et al. in [14] propose the so-called Reverse Decomposition Method to solve the PV cell electrical model.

In order to simplify one step ahead the analysis process, in this case and since in comparison, $Rp \gg Rs$, it is generally accepted to neglect Rp (Figure 2,13b), and hence, equation (2.17) can be written as follows:

$$I = I_{ph} - I_0\left(e^{\frac{V+IR_s}{n \cdot N_s \cdot V_T}} - 1\right) \tag{2.18}$$

Above equation represents the non-implicit simplified mathematical one diode model of the illuminated PV module. This equation is based on six variables, namely I, V, I_{ph}, I_0, V_T and Rs. Once solved equation (2.18), the PV module fingerprint I-V curve can be obtained. This can be done any time the values of I_{ph}, I_o and V_T are known. It has been considered the option based on PV module

manufacturer´s data sheets, as in [15]. This can apply to the photo-generated current (I_{ph}) and consequently to the PV module output voltage in absence of load, that is, the open circuit PV module voltage (V_{oc}).

Given all these data, finally, the PV module fingerprint *I-V* characteristic curve can be drawn. For this purpose, starting from equation (2.18) and solving for V, we obtain equation (2.19) is obtained:

$$V = V_T \cdot n \cdot N_s \cdot \ln\left(1 - \frac{I - I_{ph}}{I_0}\right) - I \cdot Rs \qquad (2.19)$$

Which can be solved for $I_{ph}=I_{SC}$. This equation will be used in order to determine the theoretical value of the PV module output voltage, for the range of current (*I*) between 0 A and I_{SC} for given outdoor conditions.

Calculated values will be compared with real measurements and the result will help us to determine the PV module instant Performance Ratio.

2.3 PV MODULES PARAMETERS. REFERENCE TO STC AND NOCT

A PV Module is an array structure of PV cells combined in series and parallel connections. The array is assembled into an aluminum frame, with the front covered with a tempered glass and the back protected with a tedlar cover (Figure 2.15). This affects the response of the cells and of the module, to the ambient temperature and incident irradiance and, hence, this must be taken into account for further estimation of their performance
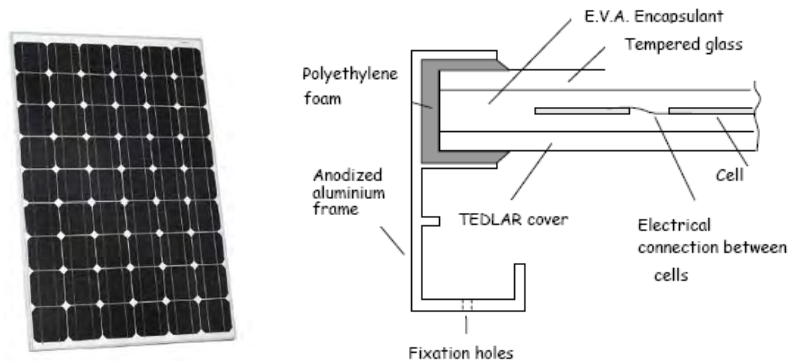
Figure 2.15. PV module array and mechanical structure

.   The nominal operational parameters depend upon the final series-parallel cells array configuration and, in essence, come from the parameters of the cells that conform the array (Figure 2.16).
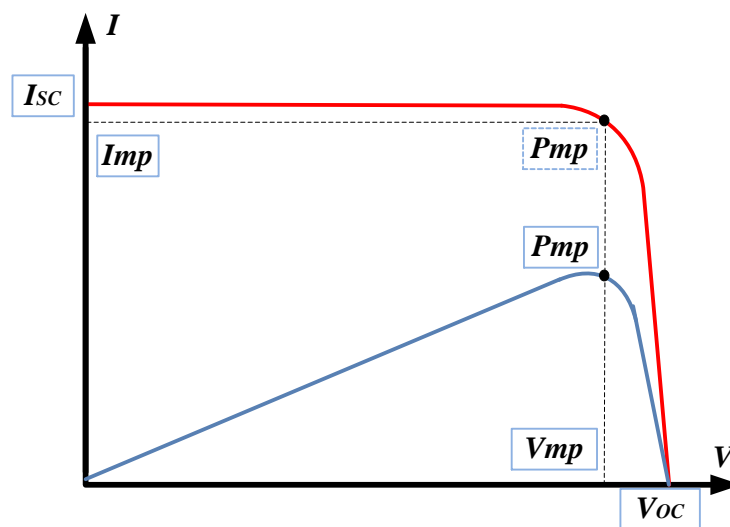
Figure 2.16. PV module I-V (red line) and P-V (blue line) characteristic curve

These parameters are obtained and certified in laboratory environments and detailed in the manufacturer´s data sheets (Tables 2.1 and 2.2). In order to establish common criteria that might make possible the comparison and analysis of these parameters, they are referred to two different test conditions, according to [6]:

a) Standard Test Conditions – STC:

Most of the PV cells and modules manufacturers and qualification laboratories perform the qualification tests at the so-called Standard Test Conditions (STC). According to [6], STC corresponds to:

 – Irradiance on the plane of the PV module: 1000 W/m^2

 – PV cell temperature: 25°C

 – Solar spectral irradiance (Air mass): AM 1,5

Table 2.1 reports referred parameters of Isofotón ISF-245 PV module.

Table 2.1. Isofotón ISF-245 PV module data-sheet electrical parameters at STC

Electrical parameter	Value
Rated Power (*Pmax*)	245 W
Open-circuit Voltage (V_{OC})	37,3 V
Short-circuit Current (I_{SC})	8,70 A
Maximum power point Voltage (*Vmax*)	30,2 V
Maximum power point Current (*Imax*)	8,12 A
Efficiency	14,8 %
Power tolerance (% *Pmax*)	+/-3%

b) Normal Operating Cell Temperature – NOCT:

Alternatively, it is also common to define the operating parameters to different applying conditions, the so named as Normal Operating Cell Temperature (NOCT) [6], considering an open-rack mounted module in the following standard reference environment:

 – Tilt angle: 45° from the horizontal

 – Total irradiance: 800 W/m^2

 – Ambient temperature: 20 °C

 – Wind speed: 1 m/s

Table 2.2 gives Isofotón ISF-245 PV module parameters, referred to NOCT.

Table 2.2. Isofotón ISF-245 PV module data-sheet electrical parameters at NOTC

Electrical parameter	Value
Maximum Power (*Pmax*)	176 W
Open-circuit Voltage (V_{OC})	34,2 V
Short-circuit Current (I_{SC})	7,02 A
Maximum power point Voltage (*Vmax*)	26,8 V
Maximum power point Current (*Imax*)	6,56 A

2.4 PV CELL AND MODULE TEMPERATURE ESTIMATION

One of the critical parameters that will affect the overall performance of the PV cell and of the PV module is the cell temperature (T_c) that it reaches during operation. The temperature has different effects on the PV cell operating parameters. It is more relevant on the V_{OC}, and consequently on the P_{mp}, while its effect on the I_{SC} is less significant [1]. This effect can be quantified by means of corresponding temperature coefficients, supplied by the PV cell manufacturer.

Since it is technically somewhat difficult to measure the cell temperature when this one is assembled in a module frame, it can be calculated in two different ways:

a) **Procedure based on NOCT value**

This procedure is based on the Nominal Operating Cell Temperature (NOCT), which is a parameter supplied by the PV cell manufacturer. This parameter refers to the temperature that the cell would reach under operation at specific ambient conditions, namely an air temperature of 20 ºC, an incident irradiance of 800 W/m^2 and a wind speed of 1 m/s [4]. According to this, the cell temperature can be given by equation (2.20).

$$T_c = T_a + \frac{NOCT - 20}{800 W/m^2} \cdot G \tag{2.20}$$

Where T_a is the ambient temperature (ºC), *NOCT* is the manufacturer reported cell temperature (ºC) and *G* is the incident irradiance (W/m²).

b) Procedure based on the module temperature

Since above procedure is not exempt of a significant uncertainty, and technical difficulty as well, in case of cells assembled in module frame, the cell temperature can be estimated based on the module measured temperature, as per the thermal model indicated in equation (2.21) [5].

$$T_c = T_m + \frac{G}{G_0} \cdot \Delta T \tag{2.21}$$

Where T_m is the back-plane temperature module (ºC), *G* is the incident irradiance on the plane of the module (W/m²), G_0 is the reference irradiance (1000 W/m²) and ΔT is the difference temperature between the cell and back-plane temperature (2 to 3 ºC for c-Si and tedlar).

In case that the back-plane temperature could not be measured, but the wind speed (S_W) were known or estimated, the module temperature can be given by equation (2.22) [5].

$$T_m = G \cdot \left(e^{a+b \cdot S_W} \right) + T_a \tag{2.22}$$

Where *G* is the incident irradiance on the module surface, T_a is the ambient temperature (ºC), S_w is the wind speed (m/s) measured at a height of 10 meters and *a* and *b* are empirical coefficients that depend on the PV module technology.

2.5 TRANSLATION CRITERIA TO REAL OPERATING CONDITIONS

Although previously referred test conditions references, STC and NOCT as well are generally accepted, one of the problem that arises is that these conditions

are difficult to comply and probably will never be met. Furthermore, if the aim is to analyze the PV module performance under real operating conditions (ROC), a procedure must be applied that can help to predict the values of the PV module operating parameters. Once these parameters have been estimated, they can be compared with the field measured PV modules operating parameters under applying ambient conditions in order to quantify the resulting performance ratio.

The Real Operation Conditions (ROC) refer to the effective incident irradiance (G), the ambient temperature (T_a) and the wind speed (S_W) as the most relevant ones. Additionally, for a more accurate estimation of the PV module performance ration, the module temperature (T_m) is required to be also considered. Other parameters affecting the performance ratio will be detailed in chapter #7 referred to the losses of the PV module performance.

Figure 2.17 (Isofotón) depicts clearly the effect of the incident solar irradiance (G) on the short-circuit current (I_{SC}) of the PV module. As it can be seen, I_{SC} decreases as G decreases. The irradiance also has an effect on V_{OC}, although it is not so relevant.
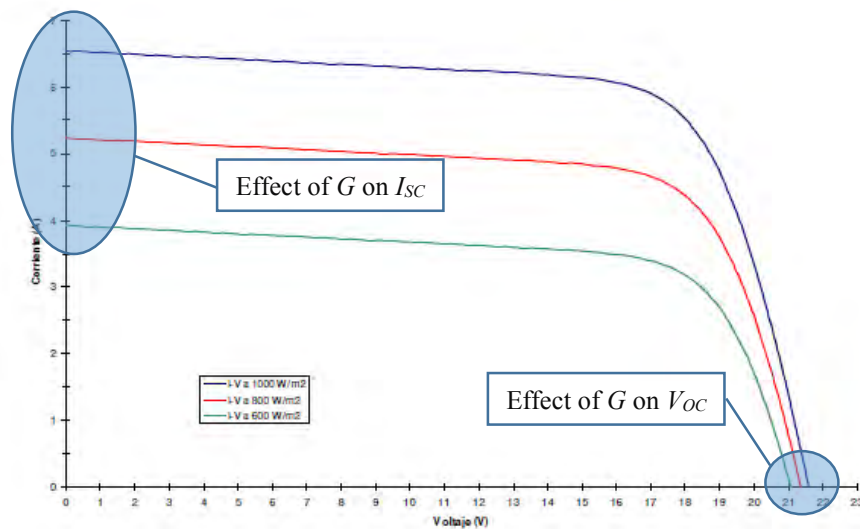
Figure 2.17. Variation of *I-V* curve depending on incident solar irradiation at constant cell temperature (source: Isofoton)

The effect of the cell temperature (T_C) on the module performance can be seen in Figure 2.18. An increase on the cell temperature has a negative impact on the value of the open circuit voltage (V_{OC}). As the cell temperature increases, the result is a significant decrease of V_{OC}.
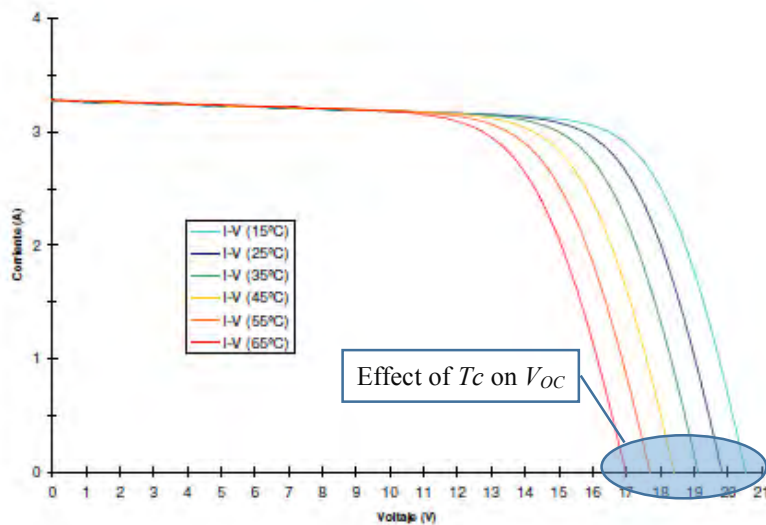
Figure 2.18. Variation of *I-V* curve depending on cell temperature at constant incident solar irradiation (Source: Isofoton)

In order to estimate the values of the PV module operating parameters under real applying outdoor conditions, a translation procedure, not exempt of uncertainty must be applied to STC data sheet reported parameters. This procedure applies to PV module voltage (V) and current (I) and specifically to I_{SC} and V_{OC}, in order to obtain the new translated *I-V* and *P-V* fingerprint of the PV module.

The translation procedures are essentially based on the different temperature coefficients that affect the main electrical parameters of the PV cell/module. A detailed description of a translation procedure that takes into account the different temperature coefficients is made in [8]. It is considered not only the ones that apply to I_{SC} (α_{Isc}) and V_{OC} (β_{Voc}), but furthermore, specific coefficients are defined for *Imp* (α_{Imp}) and *Vmp* (β_{Vmp}).

Nowadays, there are essentially two references that describe the possible translation criteria: the proposed by the IEC (on one hand) and the proposed by the NREL on the other one.

An accurate procedure has been described by King et al. in [5]. This procedure has the constraint that every parameter is translated using its own specific temperature coefficients, which differ for the different currents, voltages, power and irradiance. These coefficients are empirically determined. This requires a significant quantity of field experiments data, which are not always available.

Alternatively, Marion et al. [25] describe an accurate procedure based on the obtention of the temperature coefficients by means of field experiment data and applying the bilinear interpolation method. This procedure requires the obtention of 4 different *I-V* reference curves. The interpolation is made to characterize the V_{OC} at two different module temperatures and the I_{SC} for two different irradiances.

More recently, in 2009, the IEC published the IEC 60891 standard *Photovoltaic devices – Procedures for temperature and irradiance corrections to measured I-V characteristics* [7]. The herein proposed procedures depend on the available historical PV module data. It requires to empirically determine the values of R_s and of the curve adjusting factor (*k*), with a significant amount of reliable experimental data.

Above procedures and standards, have the constraint that they require reliable historical data under different performing conditions. On the other hand, the temperature coefficients available in the PV modules manufacturer´s data sheets are only referred to the PV module current, voltage and power, for the whole operating range.

A simple procedure that can be applied to model the I-V curve of a PV module performing under outdoor conditions and that can be based on manufacturer´s data sheets is described in [9].

This procedure defines the different models to apply to each of the operating parameters, taking as a reference manufacturer´s data sheet STC reported parameters. The equations that apply to every parameter take into consideration corresponding temperature coefficients, usually expressed in ºC^{-1}.

- α: Current correction factor for PV module temperature.
- β: Voltage correction factor for PV module temperature.
- δ: Voltage correction factor for irradiance at module temperature.
- γ: Maximum power correction factor for module temperature.

These equations are:

$$I_{SCt} = I_{SC0} \cdot \frac{G}{G_0} \cdot [1 + \alpha(T_m - T_0)] \tag{2.23}$$

$$V_{OCt} = V_{OC0} \cdot [1 + \beta(T_m - T_0)] \cdot \left[1 + \delta \cdot \ln\left(\frac{G}{G_0}\right)\right] \tag{2.24}$$

Equations (2.23) and (2.24), together with PV mathematical model seen previously, allow to obtain the corresponding I-V and P-V curves, from which the translated maximum power point (P_{mt}) point can be identified.

Nevertheless, in case that the PV module were known to be working at MPP as is the case of grid connected PV power plants, the Osterwald power translation model can be applied [26].

$$P_{mpt} = P_{mp0} \frac{G}{G_0} \cdot [1 + \gamma(T_m - T_0)] \tag{2.25}$$

Where 0 subscript variables are the manufacturer´s data sheets STC referred ones; G is the irradiance in the plane of the module (W/m^2); G_0 is the reference irradiance at STC (1000 W/m^2); α is the current temperature coefficient (ºC^{-1}); T_m is the module back-plane temperature; T_0 is the module temperature at STC; β is the voltage temperature coefficient (ºC^{-1}), δ is the voltage irradiance temperature coefficient (ºC^{-1}) and γ is the module power temperature coefficient (ºC^{-1}).

As it can be seen, above equations are referred to the module temperature (T_m) and to the incident irradiance (G).

Accordingly, both the cell temperature (T_c) and the module temperature (T_m) must be corrected using equations (2.20), (2.21) and (2.22), to applying ambient temperature (T_a), effective irradiance (G) and wind speed (S_w), when applicable.

$$T_{ct} = T_a + \frac{NOCT - 20}{800W/m^2} \cdot G \tag{2.26}$$

$$T_{mt} = G \cdot \left(e^{a+b \cdot S_W} \right) + T_a$$

(2.27)

In the same way, the next step will be to translate the cell thermal voltage (V_T) to this new applicable cell temperature, as indicated in equation (2.28):

$$V_{Tt} = \frac{k_B \cdot T_{Ct}}{q}$$

(2.28)

And furthermore, the normalized voltage (v_{OC}) must also be translated, as indicated in equation (2.29):

$$v_{OCt} = \frac{V_{OCct}}{V_{Tt}}$$

(2.29)

This will allow us to determine the translated value of FF_0

$$FF_{0t} = \frac{v_{OCt} - \ln(v_{OCt} + 0,72)}{v_{OCt} + 1}$$

(2.30)

While FF remains unchanged (equation 2.14).

Additionally, loss resistances values must be translated to the applying conditions. Parallel resistance Rp is not considered in the adopted model. In case of Rs, it results:

$$Rs_t = \left(1 - \frac{FF}{FF_{0t}} \right) \left(\frac{V_{OCct}}{I_{SCct}} \right)$$

(2.31)

2.6 PV PLANTS MONITORING SYSTEMS

As stated previously, the main challenge of the monitoring of PV plants is to have available real-time information of PV modules operation parameters. The availability of this information, together with the previously estimated translated data to applying ambient conditions will help us to estimate the performance of the PV modules and,by extension, the performance of the whole PV plant. With this procedure, any defective PV module or working under estimated performance can be immediately detected and then corresponding correcting actions to be taken.

The possibility to have reliable real time data of PV modules by means of the acquisition of their operational voltage and current as well as their operating temperature, in comparison with PV module manufacturer´s Standard Test Conditions (STC) reported can be of a great help to evaluate the different losses and optimize its performance [17].

In this sense, the EN standard 61724 "*Photovoltaic system performance monitoring. Guidelines for measurement, data exchange an analysis*" [16], defines clearly the parameters to be monitored, to be calculated and the data interchange format. Finally, a proposal is made for the performance estimation of the PV systems.

Referred parameters are essentially grouped into four major topics. The first group is related to ambient atmospheric conditions, which at least are the most relevant ones in order to quantify the PV module performance. These are the sun irradiance, the ambient temperature and the wind speed as well. The second group is dedicated to the PV module DC electrical parameters, namely voltage and current supplied and also the module back-plane temperature. The third group comprises the parameters related to the AC side of the installation, mainly related to the inverters operation and both from the DC and AC point of view. Finally, the fourth item is dedicated to the system performance estimation. These parameters are summarized in table 2.3.

Table 2.3. PV Plants Parameters to be Monitored

General parameter	Specific parameter
Solar radiation and meteorological data	− Direct and Diffused radiation − Ambient temperature and humidity − Wind speed and direction
PV modules/ strings	− DC voltage (V) − DC current (I) − Module temperature (Tm)
Inverters	− DC input (V/I/P) − AC output (V/I/P) − Inverter efficiency − Power factor (cos φ) − Grid frequency
PV plant performance	− PV plant performance and efficiency

A monitoring system can be deployed in up to three different topologies (Figure 2.19).

a) In the first option, the information is supplied by the DC /AC inverter. These devices give information related to the AC power delivered to the grid and some manufacturers give information of the corresponding DC power at the input of the inverter either measured, or estimated.

b) In a second option, the monitoring is performed at string level. The aggregated DC power delivered by all the PV modules that comprise the string is reported.

c) In a third possibility, the monitoring is performed at PV module level. This means that the system is capable of delivering information of the operating conditions of each single module. This information, through corresponding Graphic User Interface (GUI) application, can further be processed and presented to the end user.

Additionally, the information related to the atmospheric ambient conditions must always be reported as mandatory, since they are the point of reference for the PV plant performance estimation.
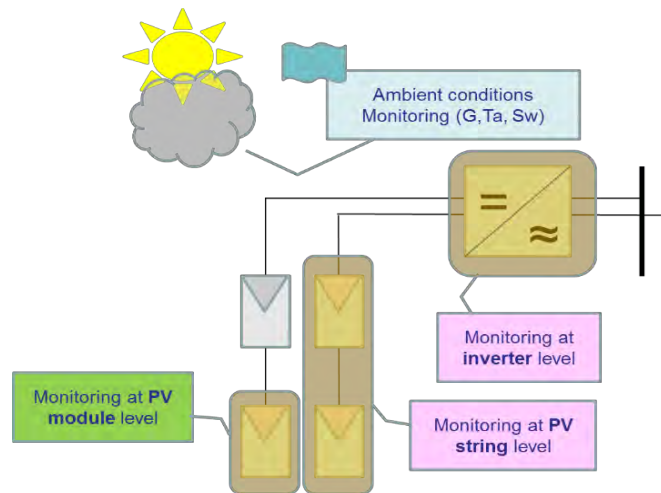
Figure 2.19. Different Monitoring Levels

A PV monitoring system allows Data logging, storing, user representation, retrieval and transmission as well. This will ensure following benefits:

- The correct operation of the plant
- To determine the performance of the different PV plant components
- To identify devices malfunction which may subsequently generate corrective and preventive maintenance actions

In order to define the system configuration, layout and integration, following points have to be considered:

- Hardware and Software for PV modules parameters data monitoring and transmission
- Hardware for atmospheric ambient conditions monitoring
- Hardware, Firmware and Software for data processing, user information and corrective actions to be taken

The monitoring system configuration will depend on the PV system layout and dimensions, as well as on the working conditions under which it will be submitted. Since the PV systems can be tailored for many type of applications, from low scale up to huge power plant, working under different conditions, several scenarios can be considered, each with different requirements and constraints.

Different solutions can be adopted with scaled upgrades of Hardware and Software (Hw/Sw) resources and cost:

- Systems configured around already existing industrial data acquisition platforms
- Dedicated systems developed specifically for PV plants applications
- System based on the PV modules low cost Smart Monitoring and Communications Module (SMCM), which is described in this thesis

Additionally, a specific chapter must be dedicated to the data communications in the monitoring system. In case of high dimensions PV plants, connectivity and communications topologies are a critical issue for real time monitoring and control. Different options can be considered :

- Wired technology: additional cabling network must be implemented. Cost impact.
- Wireless technology: radio systems must be deployed around the whole PV plant (zigbee, bluetooth, etc…). Communications problems.
- PLC technology: takes profit of already existing power wiring between PV modules and connection points. This option means important savings in the installation costs.

The communications hierarchy levels are described in Figure 2.20:

- Level 1: between primary sensors and signal conditioning / monitoring modules
- Level 2: between monitoring modules and Central Computer System (CCS)
- Level 3: Between CCS and end users interfaces
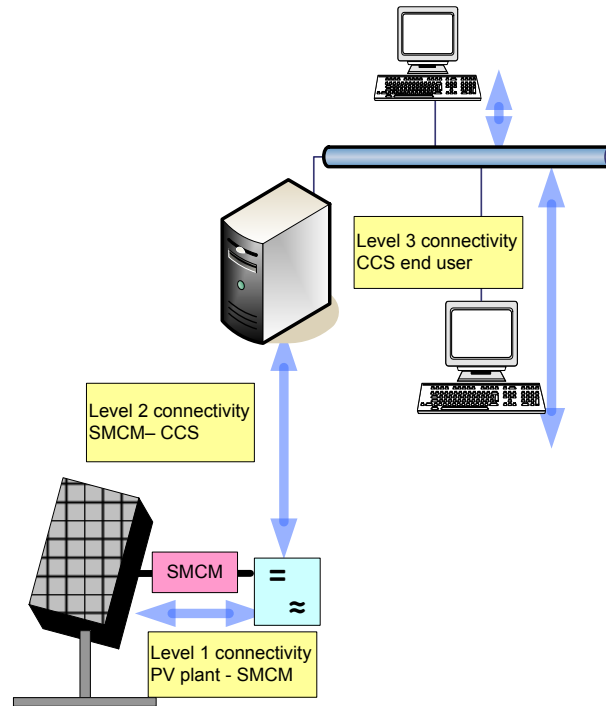
Figure 2.20. Data communications hierarchy levels

2.6.1 Requirements of a PV Plant Monitoring System

In order to define a PV plants Monitoring System (PVPMS) architecture, most important requirements to be taken into consideriation are:

- PV plant size and dimensions
- Geographical location
- Data monitoring and logging technology
- Data Tx and Rx communications layer into system integration
- Data transmission requirements (baud rate, distance, line specifications)
- Data processing and Graphic User Interface (GUI) format for end user interface and information generation
- Final control elements requirements
- Hardware, firmware and software integration
- Total system cost

For the deployment and implementation of the monitoring system, several possible solutions can be considered, as described in following paragraph.

2.6.2 Commercial specific PV plants monitoring systems

Systems based on specific PV plants monitoring systems are currently available in the market. They are based on PC architecture or dedicated programmable logic controllers. They process data at string level and use inverters generated parameters for PV plant performance evaluation. Some manufaturers supply specific data acquisition modules. These options require manufacturer´s proprietary application software for system supervision.

They are mainly intended to comply with following requirements:

- Real Time Data Acquisition
- Operation supervision (energy metering, alarms, data transmission and storing, meteorological parameters)
- Web access for remote supervision and control capabilities. Wired / wireless communications protocol
- Allow MPPT plant operation
- Grid monitoring (voltage stability, power generation, phase angle supervision)

But, they have also some constraints:
- PC based + DAS + Management and propietary user interface Sw
- Not fully end user configurable
- Closed systems from programming point of view

2.6.3 General purpose industrial Data Acquisition Systems

Another possibility is based on general purpose industrial Data Acquisition Systems (DAS). This option has the advantage to use broadly tested industrial systems and to give to the end user the possibility to develop its own software application, according to PV plant management requirements.

They are usually based on PC platforms and use RS232/RS485 (for digital) or 4-20 mA industrial standard current loop (for analog) wired data transmission. Referred options require additional wiring for both monitoring and data transmission. Some of them use radio modules for wireless communications. This

is a constraint if monitoring system deployment is large. On the other hand, radio systems are not exempt of operation problems, due to noise, antennas mistuning, etc… In any case, this means an important additional installation cost.

The main advantages of this option are:
- Modularity, adaptability and expansion capabilities
- All type of primary parameters sensors (G, Ta, S_W)
- Communications between sensors and CCS wired or wireless
- Web access is also granted in most cases
- Allow data transmission, storing and display
- Software development tools allow customer self-development according to the plant operation requirements

Meanwhile, main constraints are:
- These systems are already available in the market from different makers at considerable costs
- Not properly suitable for monitoring at PV module level

Several monitoring systems of this type have already been presented [18] and more recently [19], which are considered essential in order to improve the PV facility efficiency.

In Figure 2.21, the layout of the industrial type monitoring system installed in the EPS PV Lab is depicted.
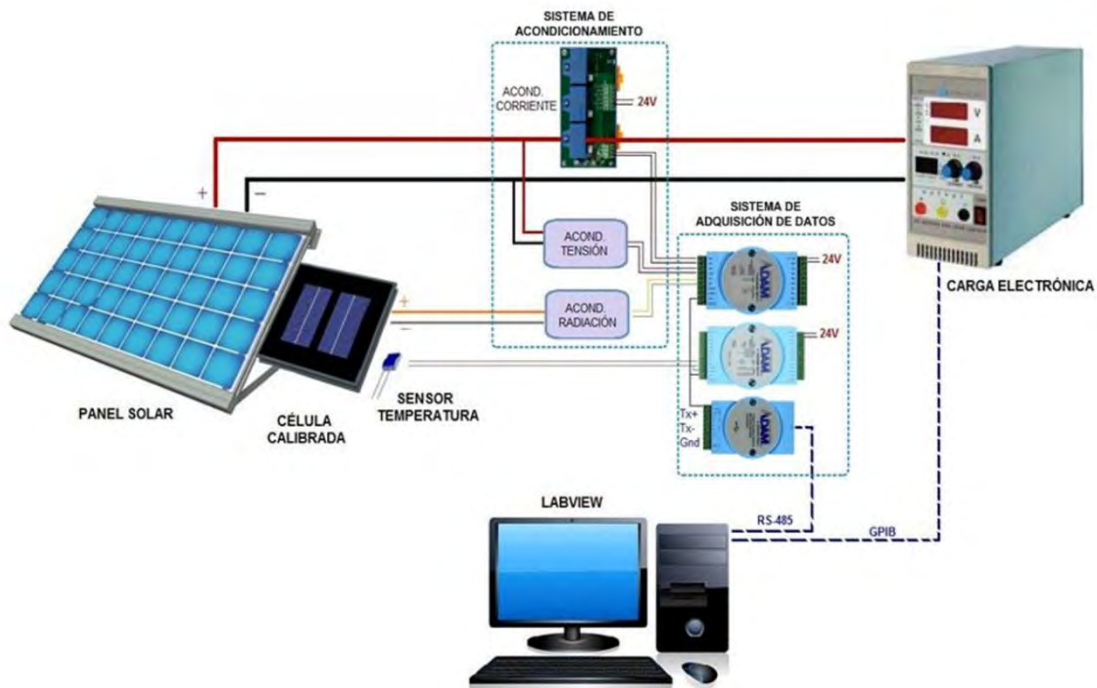
Figure 2.21. Industrial type DAS for PV modules monitoring at EPS PV Lab

2.6.4 Custom Design Monitoring Systems

The third option is based on PV custom design application specific monitoring system. It is specifically designed to comply with PV plants requirements, from monitoring, communications as well as management and operation point of view. These systems are scalable and can be plant deployed according to monitoring needs and financial available budget. Supervisory, operations and management activities can be further defined and implemented since plant management application Sw is end user developed. In our case, taking into consideration all these advantages, this is the option adopted.

The main advantages of monitoring at PV module level are:

- The use of low cost devices
- Real Time Data availability (V, I and T)
- Real Time defective PV module detection
- No delay on maintenance/corrective actions to be taken
- End user programmable and reconfigurable

- PLC based communications layer (uses already existing DC power wiring for data Tx –reduces communications cost)
- PC based + SMCM + Management and propietary user interface SW
- Not affected by radiation noise

Nevertheless, they have some constraints:
- Must be installed in each PV module
- Data Tx / Rx sensible to line conditions

In the literature, several options have been described. In [20], Román et al. present a monitoring module with a magnetic coupling to the DC line. In [21], Carullo et al. describe an in-situ PV modules calibration system; meanwhile, Guerriero et al. in [22] write about a wireless communications based PV modules monitoring device.

In 2011, Sánchez et al. in [23] presented in the IEEE PowerEng Conference, the first approach to the SMCM proposal, based on low cost concept based on the PLC technology for data transmission.

More recently, in [24], corresponding experimental results and uncertainty quantification were published. This is the model that has allowed to implement the field experiments in order to validate the proposed concept of low cost Real Time monitoring for PV plant efficiency improvement.

2.7 References

[1] M. Green, *Solar Cells, Operating Principles, Technology and System Applications.* University of New South Wales. 1992.

[2] M. Green, K. Emery, Y. Hishikawa, W. Warta and E. Dunlop, *Solar cell efficiency tables (version 43)*, Progress in Photovoltaics, Volume 22, Issue 1, pages 1–9, January 2014.

[3] A. Mc Evoy, T. Markvart and L. Castañer, *Solar Cells. Materials, Manufacture and Operation.* Elsevier. 2013.

[4] A. Luque, S. Hegedus, *Handbook of Photovoltaics Science and Engineering.* Wiley, 2003.

[5] D. King, W. Boyson and J. Kratchovil, *Photovoltaic Array Performance Model.* Sandia Report SAND2004-3535, Sandia National Laboratories, 2004.

[6] EN 61646:208, *Thin-film terrestrial photovoltaic (PV) modules. Design qualification and type approval.* AENOR, 2008.

[7] IEC 60891:2009, *Photovoltaic devices – Procedures for temperature and irradiance corrections to measured I-V characteristics.* International Electrotechnical commission, 2009.

[8] D. King, J. Kratochvil, W. Boyson and W. Bower, *Field experience with a new performance characterization procedure for photovoltaic arrays.* Sandia National Laboratories, 1998.

[9] B. Marion, *A method for modeling the current-voltage curve of a PV module for outdoor conditions.* Progress in Photovoltaics, Research and Applications, 2002.

[10] F. Adamo, F. Attivisimo, A. Di Nisio and M. Spadavecchia, *Characetrization and Testing of a Tool for Photovoltaic Panel Modeling,* IEEE Transactions on Instrumentation and Measurement, Vol. 60, N. 5, May 2011.

[11] L. Cristaldi, M. Faifer, M. Rossi, and S. Toscani, *A Simplified Model of Photovoltaic Panel,* IEEE International Instrumentation and Measurement Technology Conference (I2MTC), 2012.

[12] A. Chouder, S. Silvestre, N. Sadaoui, and L. Rahmani, *Modeling and simulation of a grid connected PV system based on the evaluation of main PV module parameters,* Simulation Modelling Practice and Theory, Elsevier, 2012.

[13] G. Petrone, G. Spagnuolo and M. Vitelli, *Analytical model of mismatched photovoltaic fields by means of Lambert W-function,* Solar Energy Materials and Solar Cells 91, Elsevier, 2007.

[14] S. Merino, F.J. Sánchez-Pacheco, P. Rodríguez, and C. Sánchez, *Photovoltaic Cells electrical model resolution by applying Reverse Decomposition Method,* Proceedings of the Applications of Computer Algebra (ACA) Congress, 2013.

[15] D. Sera, R. Teodorescu and P. Rodríguez, *PV panel model based on data sheet values,* IEEE Int´l. Symposium on Industrial Electronics (ISIE), 2007.

[16] EN 61724, *Photovoltaic system performance monitoring. Guidelines for measurement, data exchange and analysis,* april 2000. CENELEC.

[17] S. Vergura, G. Acciani, V. Amoruso, G.E. Patrono, and Francesco Vacca, *Descriptive and Inferential Statistics for Supervising and Monitoring the Operation of PV plants*. IEEE Transactions on Industrial Electronics, (Vol. 56, No. 11), 2009.

[18] L. Cristaldi, M. Faifer, A. Ferrero and A. Nechifor, *On-line monitoring of the efficiency of Photo-Voltaic panels for optimizing maintenance scheduling*. IEEE International Instrumentation and Measurement Technology Conference, 2010.

[19] A. Carullo and A. Vallan, *Outdoor Experimental Laboratory for Long-Term Estimation of Photovoltaic-Plant Performance*, IEEE Transactions on Instrumentation and Measurement, 2012.

[20] E. Román, R. Alonso, P. Ibáéz, S. Elorduizapatarietxe and D. Goitia, *Intelligent PV Module for Grid-Connected PV Systems*, IEEE Transactions on Industrial Electronics, 2006.

[21] A. Carullo, S.Corbellini, A. Luoni, and A. Neri, *In Situ Calibration of Heterogeneous Acquisition Systems: The monitoring System of a Photovoltaic Plant*, IEEE Transactions on Instrumentation and measurement, (Vol. 59, No. 5), may 2010.

[22] P. Guerriero, V. d'Alessandro, L. Petrazzuoli, G. Vallone, and S. Daliento, *Effective Real-Time Performance Monitoring and Diagnostics of Individual Panels in PV Plants,* IEEE International conference on Clean Electrical Power (ICCEP), 2013.

[23] F.J. Sánchez-Pacheco, P.J. Sotorrío-Ruiz, J.R. Heredia-Larrubia, F. Pérez-Hidalgo, M. Sidrach-de-Cardona, *Low cost DC lines PLC based Photovoltaic*

plants parameters smart monitoring communications and control module. IEEE III International Conference on Power Engineering (POWERENG 2011), Energy and Electrical Drives, 2011.

[24] F.J. Sánchez-Pacheco, P.J. Sotorrío-Ruiz, J.R. Heredia-Larrubia, F. Pérez-Hidalgo, M. Sidrach-de-Cardona, *PLC-Based PV Plants Smart Monitoring System: Field Measurements and Uncertainty Estimation.* IEEE Transactions on Instrumentation and Measurement (TIM), 2014.

[25] B. Marion, J. del Cueto and B. Sekulic, *Modeling Current-Voltage Curves Using Bilinear Interpolation.* NREL/CP-520-36232, 2004.

[26] C. R. Osterwald, *Translation of Device Performance Measurements to Reference Conditions / Device Performance*, Solar cells, 18,3-4 Pages 269-279, Elsevier, 1986.

Chapter 3

Smart Monitoring and PLC Communications Module - SMCM

In chapter 2, a detailed description of the operational parameters of PV cells and of the PV modules parameters has been made, with a reference to the ambient conditions that affect their operation. In this chapter, a detailed description is made of the Smart Monitoring and Communications Module (SMCM) both in the standard and in the Central Computer System (CCS) version, that have been developed as the necessary hardware and firmware for the real time estimation of the PV modules performance. These modules allow the measurement and transmission of PV modules operating parameters for further routing by means of the existing DC power lines, on the basis of the Power Lines Carrier (PLC) technology to the CCS for subsequent analysis and processing.

3.1 MONITORING SYSTEM ARCHITECTURE

The overall performance of a PV plant depends on the operation of each of the elements that configure it (Figure 3.1). Any one of them may introduce a given factor of losses, which will make the PV plant performance decrease significantly. The main consequence is the financial losses it can generate.

One of the problems is the contribution to these losses that can be attributed to the PV modules and the amount of energy that they are missing of supplying at a given moment under given ambient conditions. The problem in this case is the lack of information corresponding to the PV modules operating parameters and their evaluation in order to determine their performance.
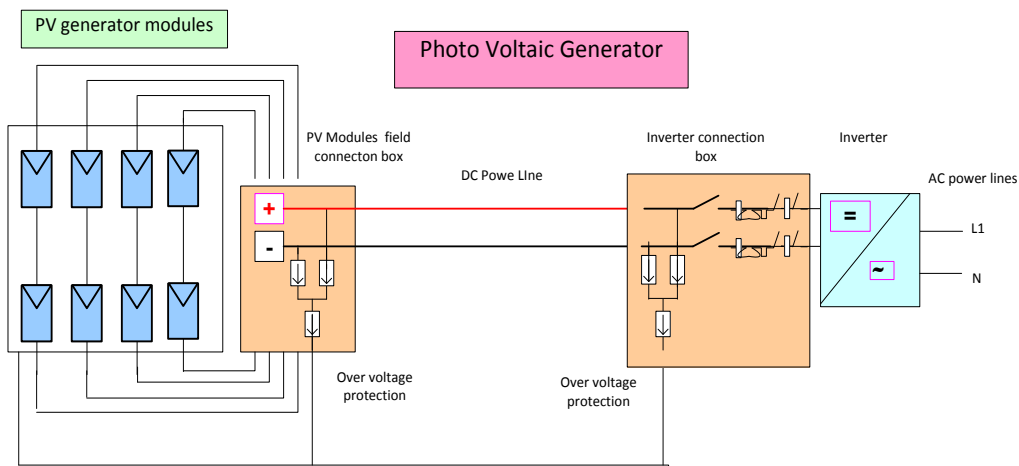
Figure 3.1. PV plant general layout

The focus has been put on the DC side of the PV generators and, specifically, on the PV modules.

The aim of the proposed SMCM is to supply real time reliable data related to the instant operational parameters of each of the PV modules that conform the PV plant layout (Figure 3.2).

The system is implemented around the SMCM, in charge of the the real-time PV modules parameters, namely voltage (V_{PV}), current (I_{PV}) and back-plane temperature (T_{PVBp}) monitoring and data transmission. This module is designed to transmit information to a PC based Central Control System (CCS) using as a communication layer, the basis of the Power Lines Communications (PLC) technology. The use of already existing DC power wiring for data transmission avoids extra costs, since no additional wiring is needed [1][2]. A laboratory prototype has been developed, which has made possible to perform field trials and measurements in order to validate the proposed idea. Additionally, an estimation has been made of the uncertainty related to the measurement of V_{PV}, I_{PV} and T_{PVBp} performed by the SMCM [3].
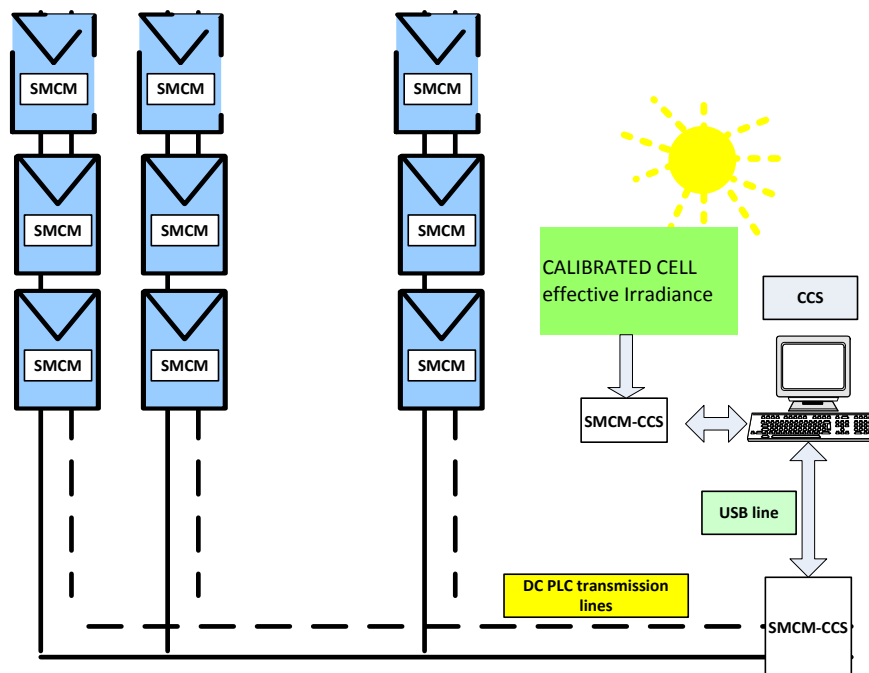
Figure 3.2. SMCM Plant deployment schematic

The main characteristics of the SMCM based monitoring system are:

- Developed with low cost devices
- System can be tailored to customer´s requierements
- Real-time Data availability (V, I and T_m, T_a, G)
- End user representation through corresponding GUI
- Immediate defective PV module detection
- PV plant maintenance (either predictive or corrective) actions can be more efficient ; direct PV defective module identification
- End user programmable and reconfigurable (opened system)
- PLC based communications layer, using already existing power wiring for data Tx/Rx (reduces communications costs)
- PC based + SMCM + Management and propietary user interface software

The proposed monitoring system architecture is shown in Figure 3.3. It is composed of a low cost μController based SMCM installed in each PV plane, the PC based CCS as system supervisor with which it communicates bidirectionally, an interface module (SMCM-CCS) to digitally connect the CCS to the DC line and the data transmission path. This transmission path uses already existing DC power lines as a PLC based technology physical communications layer (red dotted and dashed lines).
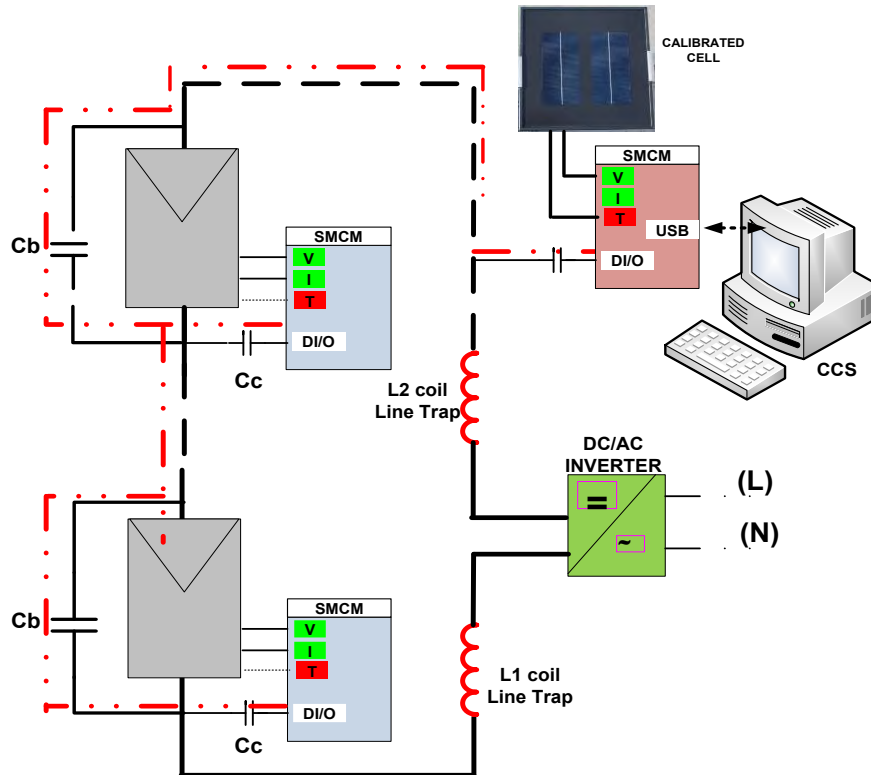
Figure 3.3. Monitoring system architecture

The coupling of the SMCM to the DC power line for data Tx/Rx can be implemented in different ways. One of them is by a magnetic coupling. This option has the constraints of cost and wiring manipulation requirements.

Considered as a more efficient option, the capacitive coupling has been considered [4]. In order to implement a low impedance data transmission path, each PV module has a bypass capacitor (Cb) connected in parallel. Line trap coils L1 and L2 perform a filtering of data signal carrier, so that no harmonics are transferred to the DC/AC inverter.

The SMCM has an output enabled line transceiver with capacitive coupling (Cc) to the DC power line.

Data reception and routing to the CCS is performed by the SMCM-CCS version, which behaves as a data concentrator of the data coming from the PV plant deployed SMCM. This device receives also information of the incident irradiance (G) and ambient temperature (Ta), supplied by the reference cell. It is connected to the CCS via USB.

3.2 SMCM DESIGN CONSIDERATIONS

From the electronic design point of view, several considerations have been taken into account. They have conditioned the electronic design, board dimensions, operating characteristics, power consumption and cost.

A. Components cost:

The aim has been to develop a low cost device which might be inserted in the PV module connection box. This requirement is mandatory, since the additional cost of the installation of a monitoring system must tight as much as possible, so that to minimize the financial impact. This has led to following considerations:

- Selection of low cost electronic devices, including the μController.
- The coupling to the DC line has been made by capacitances, instead of magnetic devices, since these are more expensive.
- The current sensor is not invasive and requires no interruption of the DC line, so no additional hand-work is required for device wiring.
- The SMCM final printed circuit board dimensions must fit into the PV module connection box, so that it uses the already existing ones. Final version will be designed using Surface Mounted Technology (SMT).
- For data Tx and Rx no commercial transceiver has been used, which are quiete expensive. Instead of it, a general purpose driver has been used with corresponding signal conditioning circuitry.

B. Supply voltage:

The SMCM is directly connected to the associated PV module which acts as its own power supply. This means that:

- The SMCM cannot suppose an excessive load to the PV module in terms of consumed power.
- The DC supply voltage of the SMCM must be from 0 to +12 VDC, since the voltage regulators used for internal supply can support a considerable range of input power variation (large line regulation).

3-6

- Since the SMCM supply voltage is from 0 to + 12 VDC, rail-to-rail single supply operational amplifiers must be used.

C. Functional configuration

In order to optimize the SMCM functionality/cost, both the SMCM and the SMCM-CCS version are based on the same design. The only difference are the external elements that can be connected; that is, the PV module voltage/current for the first ones and the calibrated cell and ambient temperature for the CCS version. This philosophy allows us to use the same design and a specific components configuration for each option.

D. PV back-plane temperature measurement

As previously described, one of SMCM functions is the measurement of the PV back-plane temperature. Although in the prototype, a PT-100 RTD temperature sensor endorsed to the PV module has been used, in the original design, in order to reduce the components cost. The aim was to use the μController internal temperature sensor capability. For this purpose, an estimation of the temperature gradient and impedance has to be calculated from the back-plane to the SMCM μController (Figure 3.4).
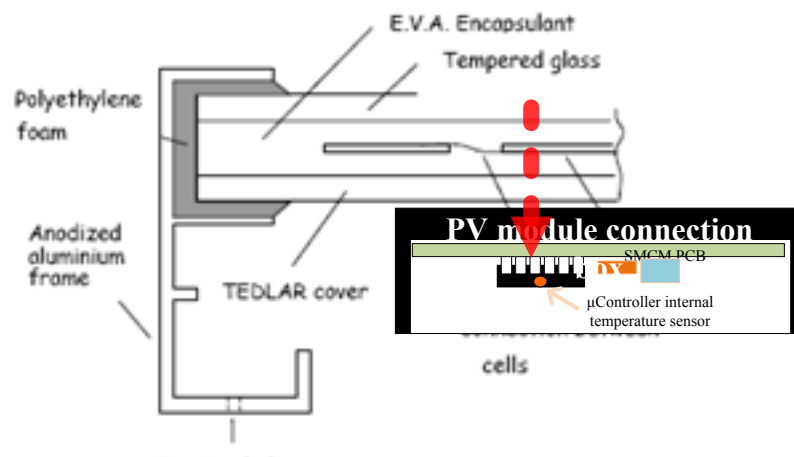
Figure 3.4. Back-plane temperature measurement using the MSP 430 μController internal temperature sensor and thermal resistivity

E. SMCM-CCS version USB connection to the PC

The CCS version of the SMCM is based on the standard SMCM and configured to perform two different functions: on one hand, it has the functionality to operate as a data node concentrator which routes all the received data to the CCS PC. Additionally, this device monitors the incident radiation given by the calibrated cell output; the ambient temperature and all this information is routed to the CCS PC for further processing and performance estimation.

3.3 SMART MONITORING AND COMMUNICATIONS MODULE STRUCTURE

As it has previously described, the SMCM is the element around which, all the monitoring system has been implemented. It is endorsed to each single PV module and performs the two basic functions of monitoring the PV module operating parameters, namely the voltage and current photogenerated as well as the temperature of the back-plane and then the transmission through the DC power line, of all the data resulting from the monitoring. The SMCM is a smart device in the sense that it can support bidirectional communications. It receives in a polling sequence from the CCS, the SMCM identification code which wakes it up and in response, it delivers the monitored data according to a given data format.

The detail of the SMCM structure is given in Figure 3.5. The SMCM incorporates a low cost MSP 430 µController, specific Analog Front Ends signal conditioning for V, I and T measurement as well as an Analog Front End for Data Transmission (Tx)/Reception (Rx) through capacitive coupling.
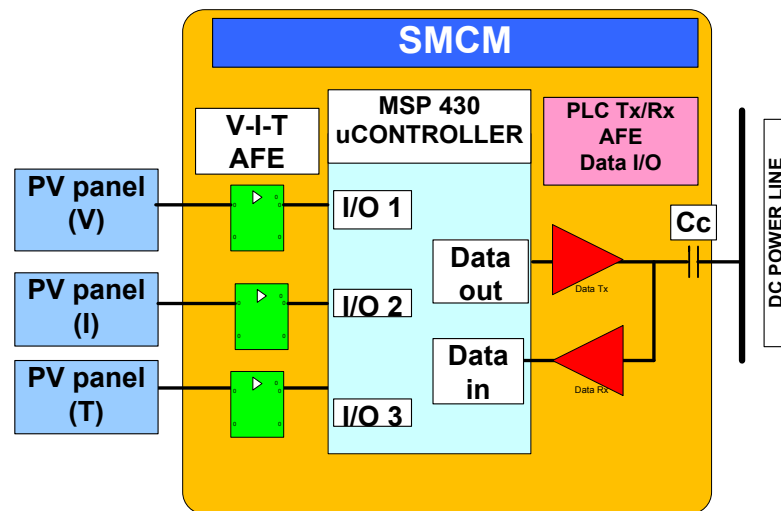
Figure 3.5.   SMCM block diagram for *V-I-T* PV module parameters monitoring and Data Transmission (Tx) and Reception (Rx)

3.3.1 MSP 430 µController.

The core element of the SMCM is Texas Instruments® MSP430 µController [5]. This µController has been selected among other ones basically because its cost (< 1 €/piece), low power consumption in standby, has an internal Analog to Digital Converter (ADC) and temperature sensor. The data bus is composed of an 8 bits general purpose I/O bus that can be user configured as digital inputs or outputs and analog inputs for further conversion to digital by the ADC. One of the I/O lines is used for Tx/Rx of data and identification codes.

Its main characteristics are:

- Low supply-voltage range: 1,8 to 3,6 V
- Ultralow power consumption
    - Active mode: 220 µA at 1 MHz, 2,2V
    - Standby mode: 0,5 µA
    - Off mode (RAM retention): 0,1 µA
- Five power-saving modes
- Ultrafast wake-up from standby mode in less than 1 µs
- 16-Bit RISC architecture, 62,5 ns instruction cycle time
- Clock module

  – Internal frequencies up to 16 MHz

  – External digital clock source

- 16-Bit Timer with two capture/compare registers

- Universal Serial Interface (USI) supporting SPI and I2C

- Brownout detector

- 10-Bit 200-ksps A/D converter with internal reference, sample-and-hold and autoscan

- Serial onboard programming. No external programming voltage needed

- On-chip emulation logic with spy-by-wire interface

All these characteristics make possible the compliance of "smart" concept. In Figure 3.6, it can be seen its internal functional block diagram.
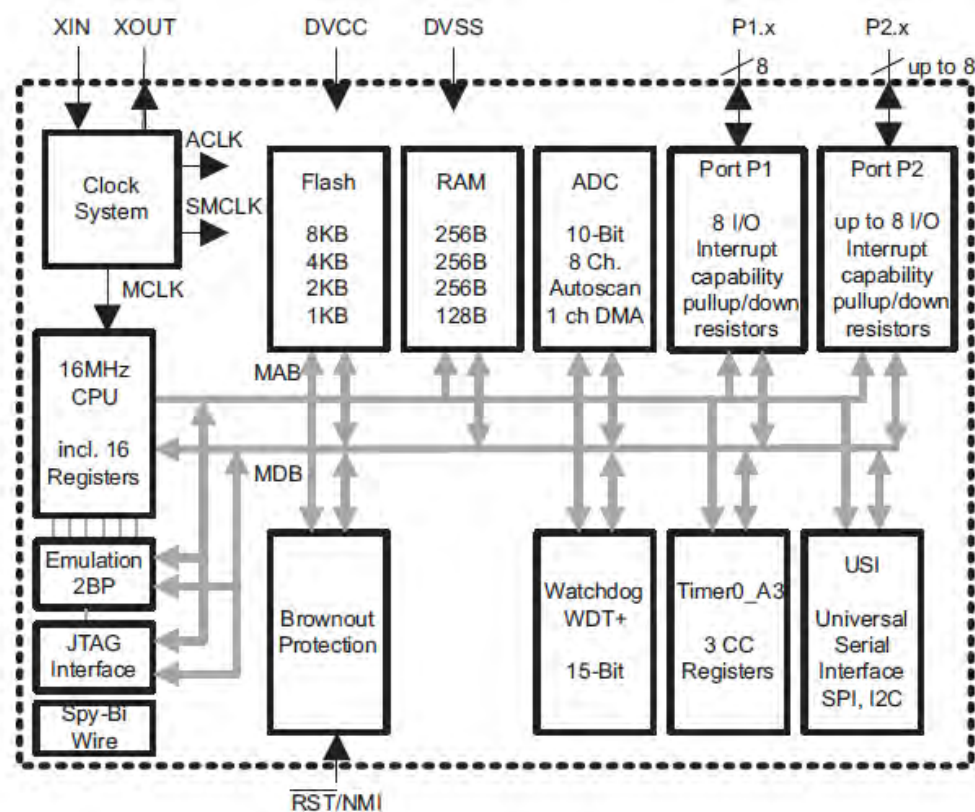
Figure 3.6.   MSP 430 µController functional block diagram.

In order to speed-up the first prototype, it has been used the TI MSP 430 launch-pad development kit. The main characteristics of this kit are:

- USB debugging and programming interface featuring a driverless installation and application UART
- serial communication with up to 9600 Baud
- Supports all MSP430G2xx and MSP430F20xx devices in PDIP14 or PDIP20 packages
- Two general-purpose digital I/O pins connected to green and red LEDs for visual feedback
- Two push buttons for user feedback and device reset
- Easily accessible device pins for debugging purposes or as socket for adding customized extension boards
- High-quality 20-pin DIP socket for an easy plug-in or removal of the target device

Another of the advantages is that all the µController pins are user available and can be connected to an expansion board.

Figure 3.7 shows the functional block diagram of the MSP 430 launch-pad.
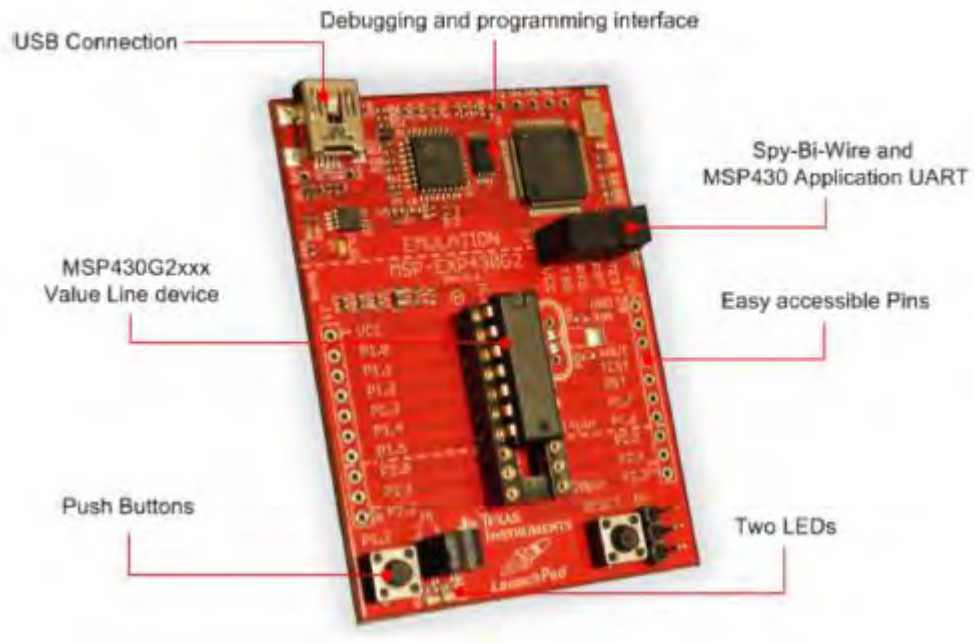
Figure 3.7.   MSP 430 launch-pad

3.3.2 Analog Front End for PV module Voltage (V_{PV}) signal conditioning and measurement.

One of the parameters that the SMCM is due to monitor is the PV module output voltage. This parameter can range from 0 V up to V_{OC}, according to the manufacturer data sheet with maximum values in the surroundings of 40 VDC. Since the µController ADC input can be maximum 3,6 VDC, a first conditioning must be done to convert the signal to acceptable values.

The PV module output voltage (V_{PV}) monitoring Analog Front End (AFE) block diagram is depicted in Figure 3.8.
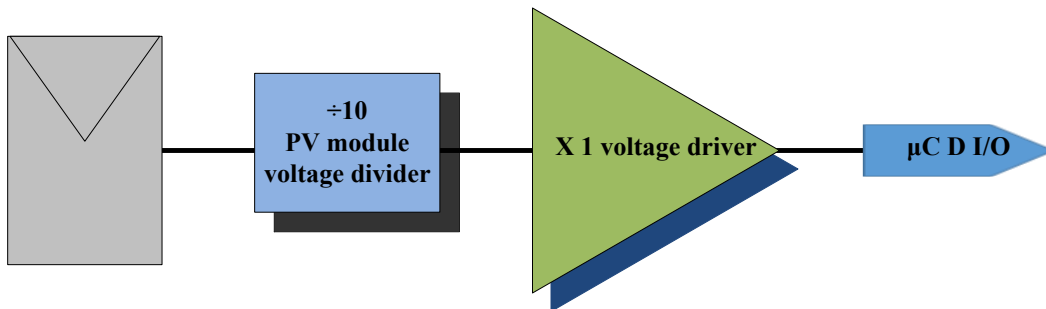
Figure 3.8. SMCM AFE for PV module Voltage monitoring block diagram

It is configured of a by 10 resistors based voltage divider. The signal is then applied to a high input impedance, unity gain voltage follower (TLC271 Opamp) and further routed to one of MSP430 analog inputs for Analog to Digital Conversion. This solution is simple, efficient and very stable from the temperature point of view. The TLC 271 Opamp has low offset voltage drift and high input impedance and manufactured with a technology that provides stable offset voltage.

Figure 3.9. shows the schematic diagram of referred signal conditioning configuration.
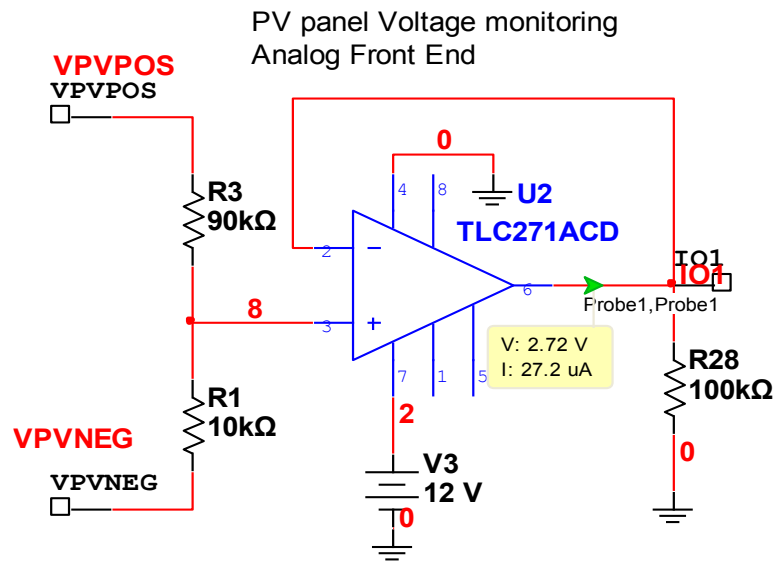
Figure 3.9. SMCM AFE for PV module Voltage monitoring schematic diagram

Figure 3.10. shows the simulated circuit, where it can be seen the signal conditioning and the resulting 3 V output of the Opamp, for a PV module generating 30 V connected to the equivalent circuit of the DC power line.
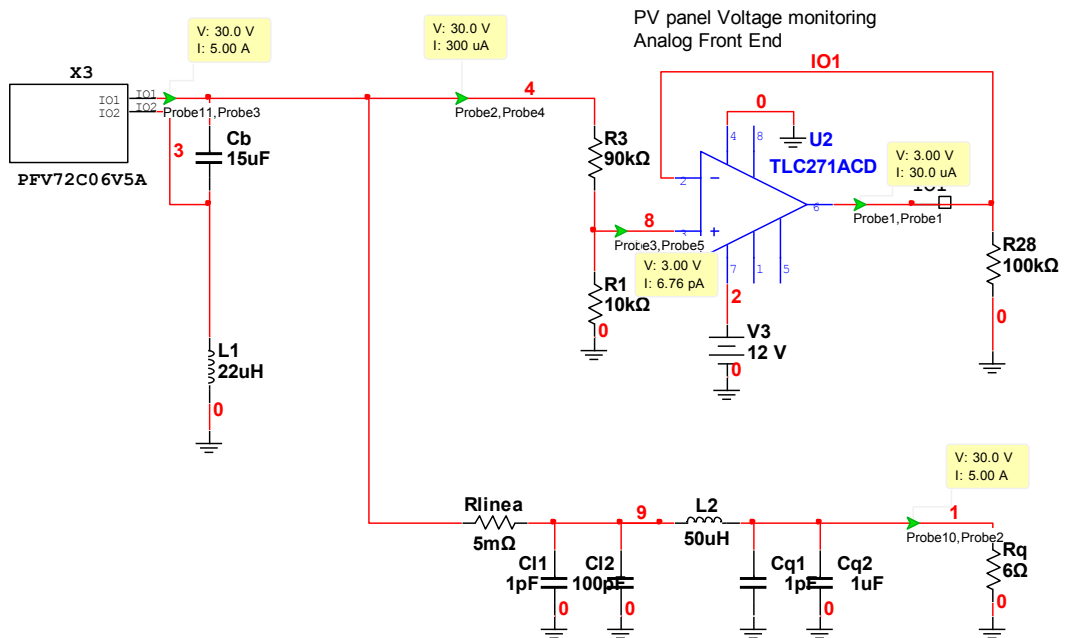
Figure 3.10. SMCM AFE for PV module Voltage monitoring simulated model

3.3.3 Analog Front End for I~PV~ signal conditioning and measurement.

Current (I_{PV}) measurement requires a different solution. A non-invasive hall-effect sensor configuration has been used. The output current of the PV module is sensed by this current transducer and its output is fed into a unity gain voltage follower for further connection to the µController input. Figure 3.11 shows the functional block diagram of this module.
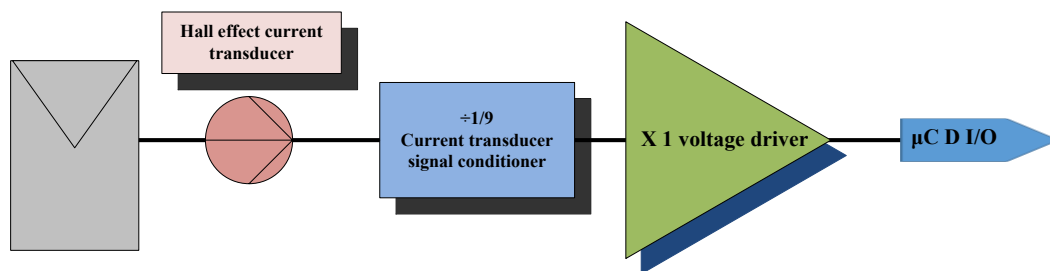
Figure 3.11. SMCM AFE for PV module Current monitoring block diagram

The hall-effect current sensor used is the Premo HCT06DSR5 model [6]. This is a hall-effect bidirectional current sensor, which supplies 0,625 V for a 6 A span, with an offset of 2,5 V.

Since µController input voltage must be maximum 3,6 V, a voltage divider has been implemented, which multiplies voltage by 0,9. Under these conditions, in case a PV module were supplying 6 A, maximum current sensor output voltage generated would be 3,125 V; after voltage divider, the signal obtained is 2,81 V. This signal is then applied to a unity gain voltage follower amplifier based on TLC271 Opamp, which output is applied to MSP430 µController input for AD conversion.

One of the characteristics of the HCT06DSR5 current sensor is that it has a 2,5 V direct voltage output reference. This signal is supplied by an internal Zener diode and hence very stable from temperature variations point of view. This output is directed to the µController input and is used as a reference for system integrity checking and even calibration.

Figure 3.12 shows the schematic functional diagram of referred configuration. The schematics shows also the results of the electrical simulation.
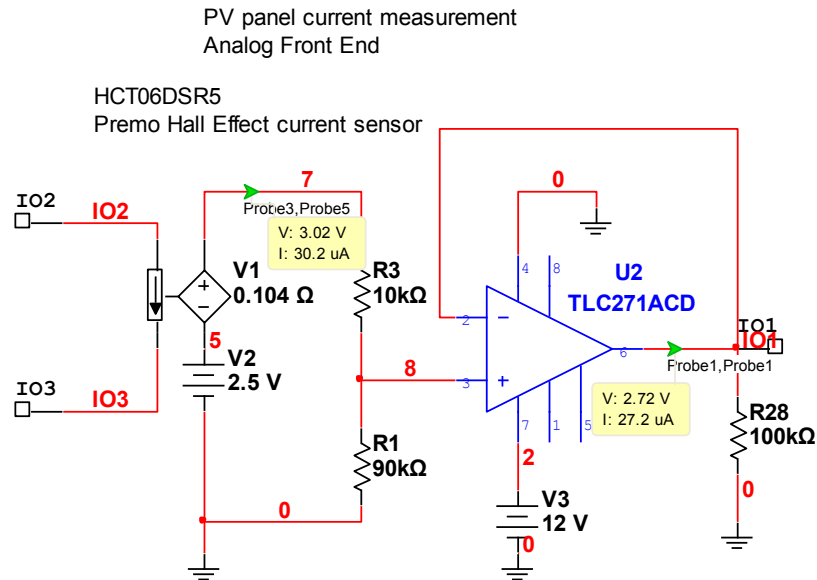
Figure 3.12. SMCM AFE for PV module Current monitoring functional diagram

3.3.4 Analog Front End for T_{PVBp} signal conditioning and measurement.

PV module backplane temperature (T_{PVBp}) measurement is made using a platinum PT 100 type Resistance Temperature Detector (RTD) endorsed to the PV module back-plane. The AFE has been implemented around a standard Wheatstone bridge RTD signal conditioning and amplifier module (Figure 3.13).

The configuration is designed to supply an amplifier output value of 3 V, for a PV module back-plane temperature of 100 ºC. In this case, the RTD resistor value should be 138,5 Ω. For a temperature of 0 ºC, the RTD resistance would be 100 Ω and the amplifier would deliver 0 V.
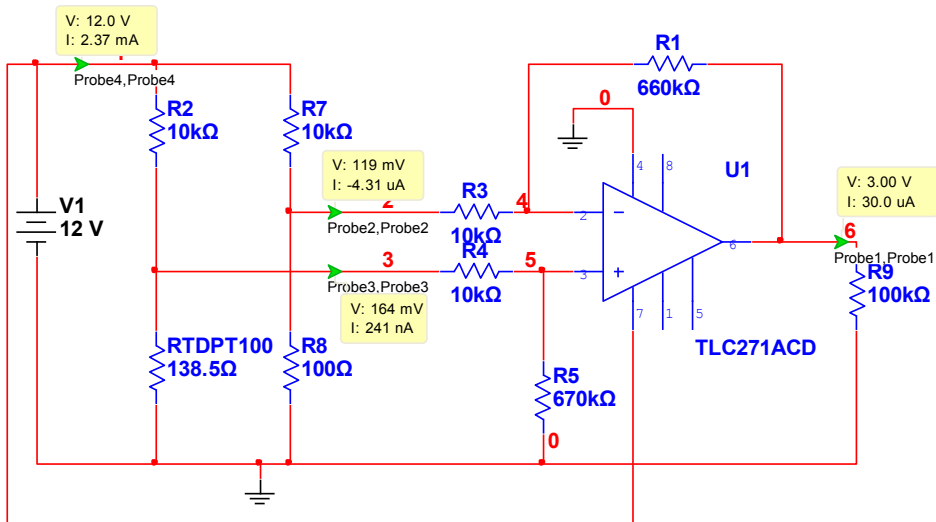
Figure 3.13. SMCM AFE for PV back-plane PT100 Temperature measurement

3.3.5 Analog Front End for Data Transmission (Tx) and Reception (Rx).

The system is intended to be working in the CENELEC B band (95-125 kHz), according to EN50065-1 [7], which is open for end users applications and allows standard as well as proprietary communications protocol. In this case, a 100 kHz signal transmission rate is used (Figure 3.14).
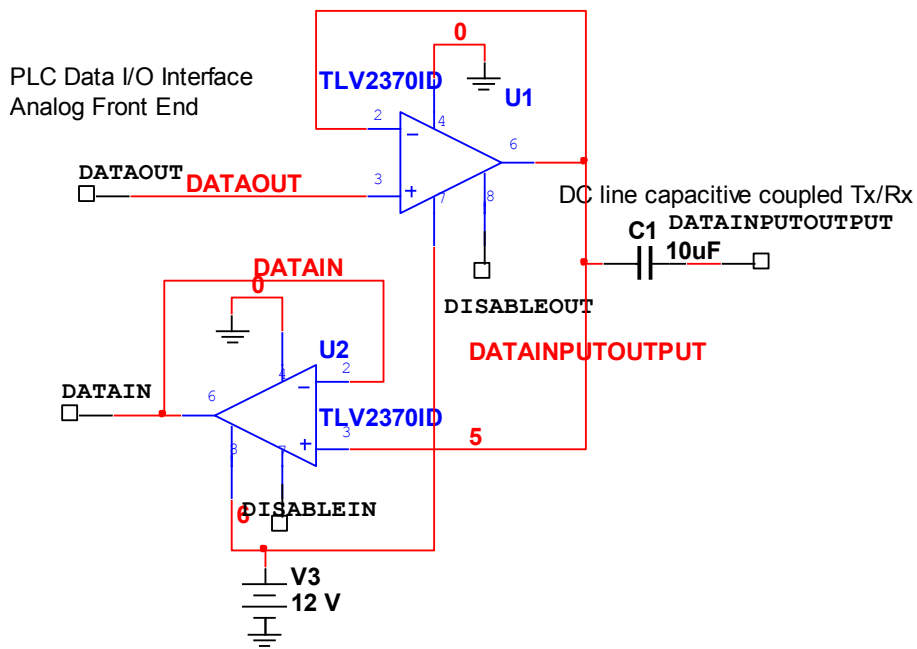
Figure 3.14. SMCM AFE for Data I/O, with capacitive coupling

All data processed by SMCM are further routed to the CCS. Transmitted data structure is based on CENELEC EN 61724 standard [8]. Each transfer is identified with PV module ID #, each data separated by a Field Separator (FS) character (ASCII 44) and ends with an End Of Line (EOL) character (ASCII 13), as depicted in Figure 3.15.

Figure 3.15. Transmitted data structure, according to CENELEC EN 61724

Transmitted data are:

- Header (AA_h): used as synchronization byte
- PV module identification number ($XXXX_h$)
- PV module temperature (TT_h)
- Field separator (ASCII 44)
- PV module current (II_h)
- Field separator (ASCII 44)
- PV module voltage (VV_h)
- End Of Line – EOL – (ASCII 13)

3.3.6. SMCM-CCS configuration

A specific version SMCM-CCS has been assembled, which acts as a data concentrator and interface between the DC PLC line and the CCS, via USB, using MSP430 Launch-pad capabilities.

SMCM–CCS version Data Reception Analog Front END (RxAFE) is depicted in Figure 3.16. Data capture is made by capacitive coupling. Due to the PLC transmission path impedance, the transmitted signal suffers a significant attenuation and distortion. Hence, at the SMCM-CCS receiver, the received one is submitted to a signal conditioning. The first step has been to amplify it with an amplifier (TLV2372) with a gain of x21; its output is then applied to a differential

comparator with hysteresis cycle implemented (LM211), which delivers squared logic level signal, -as a replica of initially transmitted data- and which feeds the MSP 430 µController digital input.
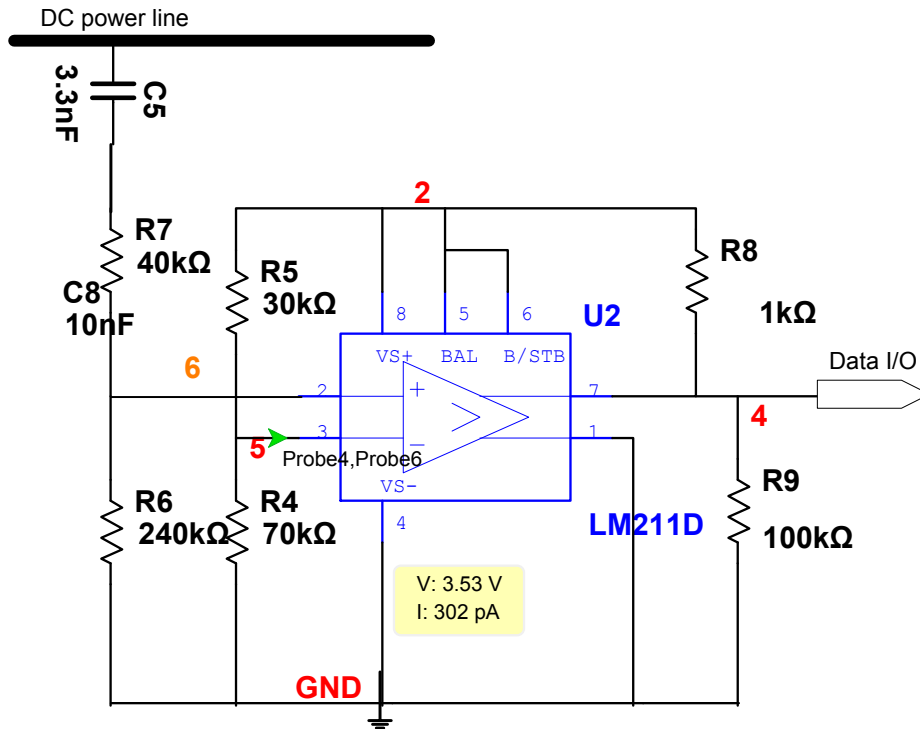
Figure 3.16. SMCM-CCS Data Rx AFE

Environmental conditions are required to be known in order to determine correct PV modules operation [9]. This module receives also data from Atersa calibrated and compensated cell, which supplies information related to global radiation (100 mV @ 1000 W/m^2) in the plane of the PV modules, as well as ambient temperature given by a PT100 RTD.   The MSP 430 launch-pad based SMCM prototype, together with the SMCM-CCS version for data gathering are shown in Figures 3.17 and 3.18.
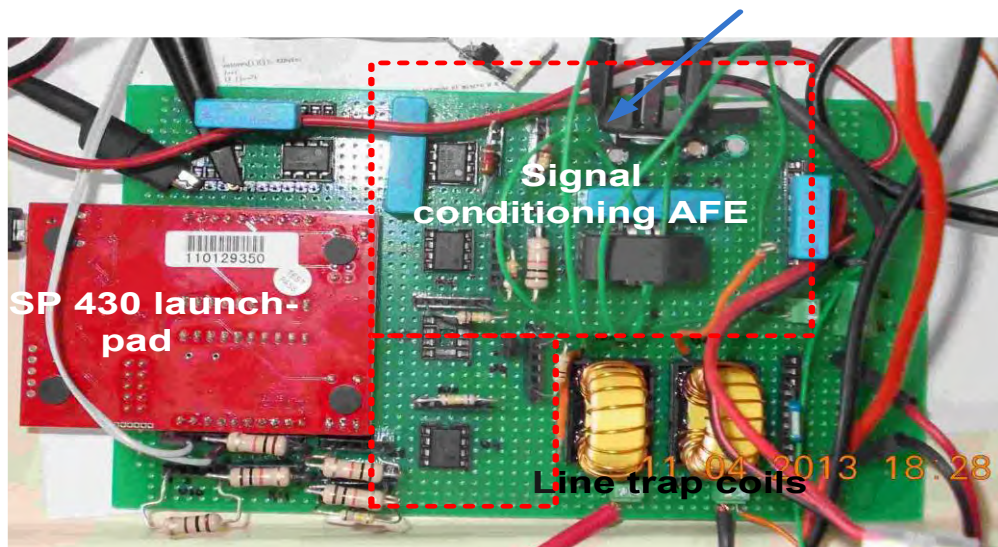
Figure 3.17. SMCM Launch-pad based prototype
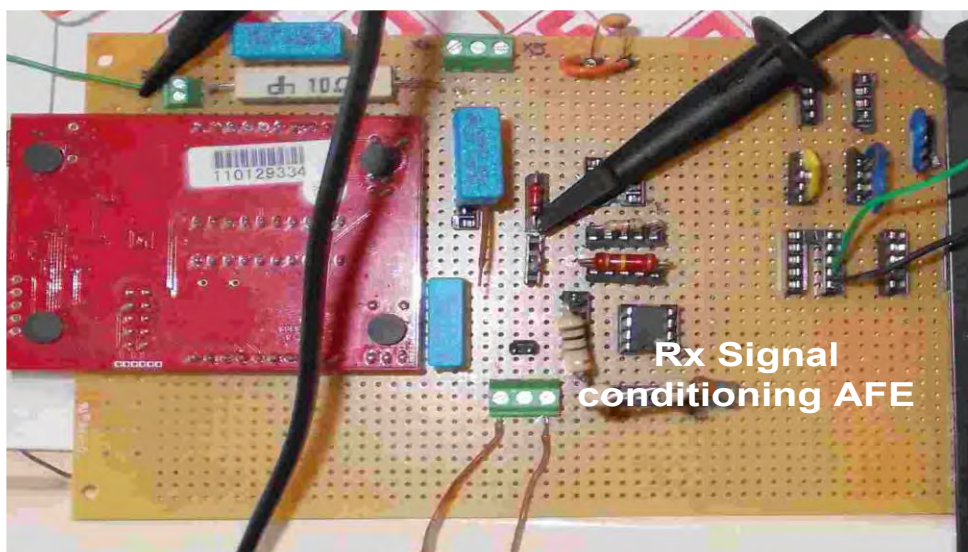
Figure 3.18. SMCM-CCS Launch-pad based prototype

3.4 PLC LINE AND TX AND RX DATA ANALYSIS

The transmission of the monitored data to the CCS by means of the DC power line is a key issue in order to tight the installation costs as low as possible. In our case, the Power Lines Carriers (PLC) technology has been used. The main advantages of this solution has a twofold consideration: on one hand, the problems and costs of radio based systems are voided; on the other hand, no additional wiring installation is required. For the viability of the proposed monitoring system, the confirmation that this technology might be applied in the PV plants scenarios had not been demonstrated so far.

In this paragraph, a first approach to the idea viability has been made, by simulation of the transmission of data over a line that simulates a 1000 m length line, with its associated impedance connected to a PV module and an DC/AC inverter. In this case, it has been estimated the signal attenuation as well as an AC analysis in order to estimate the harmonics that might be seen by the inverter input. In the second part of the paragraph, a description is made of the simulation of the data transmission applied to the EPS PV Lab composed of two PV modules and corresponding load simulating the Inverter input. Additionally, the real measurements are depicted, together with the corresponding analysis and subsequent conclusions.

3.4.1 DC lines PLC data transmission simulation and validation

Data monitored by the SMCM must be forwarded to the CCS for further analysis. The option of using the DC power line as physical transmission layer is due mainly to following reasons:

- No additional wiring is required which means an important saving in installation man power and materials
- Radio Tx/Rx modules are not required and hence installation costs are not affected
- System is not affected of noise in radio signals

Main advantages of PLC lines have been deeply described [10], [11], but data transmission using PLC technology is not exempt of problems [12], such as line impedance and signal attenuation. It has been implemented taking into account

recommendations of the IEEE Guide for Power-Line Carrier Applications (IEEE Std. 643) [13].

In order to evaluate transmission line behavior, a model has been chosen [14]. Figure 3.19 shows the electronic diagram of the PLC line simulation (TINA TI®) model.
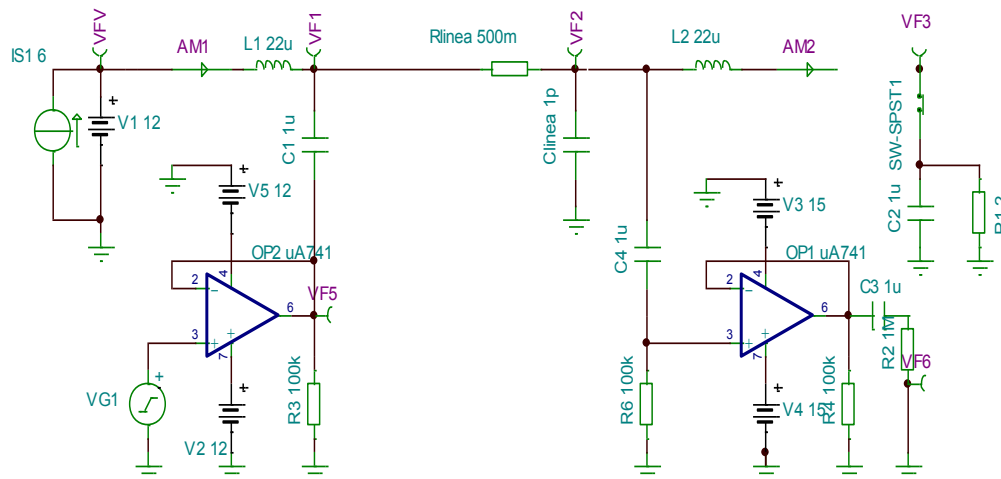
Figure 3.19. PLC line data transmission simulation

One of the concerns is the type of coupling to the PLC DC line. Several solutions can be adopted. One is through magnetic coupling using Transmission Lines Transformers (TLT). In the proposed solution, the capacitive coupling has been implemented [15]. Major reason is the lower cost of capacitors vs TLT.

The simulation model of Figure 3.19 has helped to evaluate the possibility to transmit data and receive them at the SMCM-CCS for further routing to the PLC. The impact on the waveform shape, distortion, attenuation and possible harmonics have been characterized.

In order to evaluate proposed system topology functionality, two different actions have been taken. On one hand, PLC transmission line has been simulated and on the other hand, a laboratory prototype has been assembled. Figure 3.19 shows the simulated electrical diagram using TINA-TI® spice electronics simulation software. Detailed model has been developed in [16].

The design of the transmission line has been implemented to simulate real scenarios, considering a 1000 m (≈ 3000 feet) DC cable length, with its resistive (Rline) and capacitive (Cline) equivalent impedance values. Input impedance of typical EMC filters at the input of DC/AC inverters has been considered as well.

SMCM-PLC line driver has been simulated, performing the transmission of a 100 kHz square signal. The transmitter coupling to the DC line is made by C1 capacitor. DC line is coupled for this transmission rate, using two 22 µH terminal suppression coils, one at the PV panels end (L1) and the other one just before the inverters entry (L2). Data recovery is made by OP1. Its output is able to show received data at the end of the line (Figure 3.19).

Following simulation results have been obtained. Figure 3.20 shows waveforms at the transmitter level (VF1), modulated signal on the DC line (VF5) as well as received signal at the end of the DC line (VF6). As it can be seen, the received simulated signal is clearly defined.
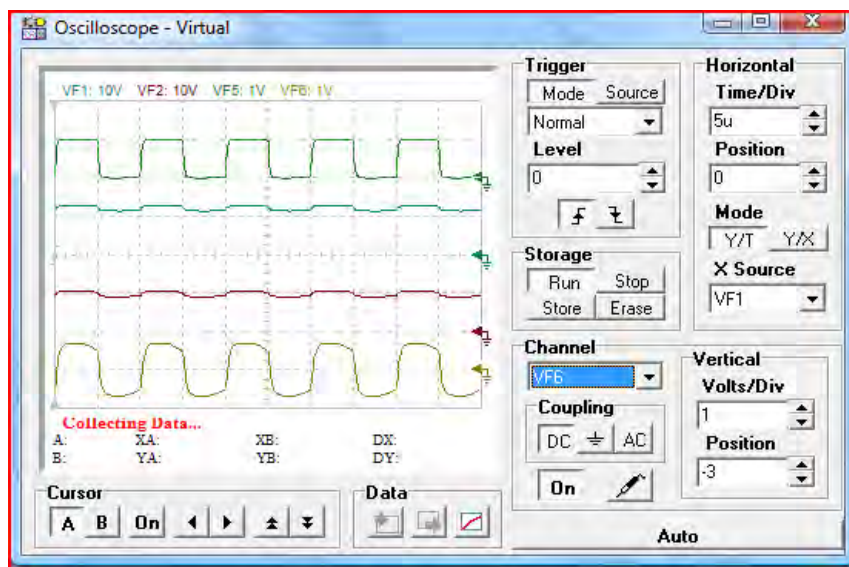
Figure 3.20. Data transmitted waveforms at transmitter level (VF1), DC line modulated signal (VF5) and received signal at the end of DC line (FV6)

Figure 3.21 shows DC levels at the PV generator side (VFV), at the DC line – PLC (VF1), as well as the signal at the inverter side (VF3). Effect of L1 and L2 suppression coils can be clearly seen. AC transmitted signal components are duly filtered at the purely DC segment of the transmission line.
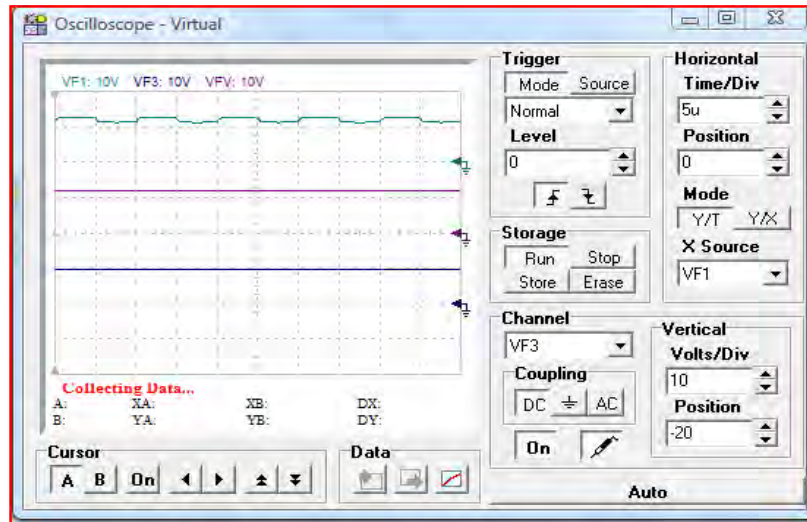
Figure 3.21. PLC line voltage waveforms at the DC line

In figure 3.22, the graphic of the Fourier analysis at the inverter level (VF3) is shown. It can be seen that magnitude of present harmonics are not significant, at the end of the PLC line (Figure 3.22). No AC component is transferred to the inverter.
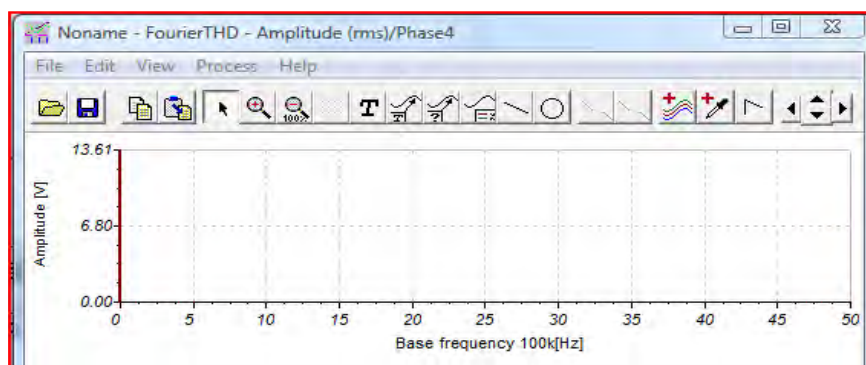
Figure 3.22. Fourier analysis of signal at the inverter level (VF3); Spectrum analysis

In Figure 3.23, THD calculation results are presented, indicating main carrier presence and no consecutive harmonics.
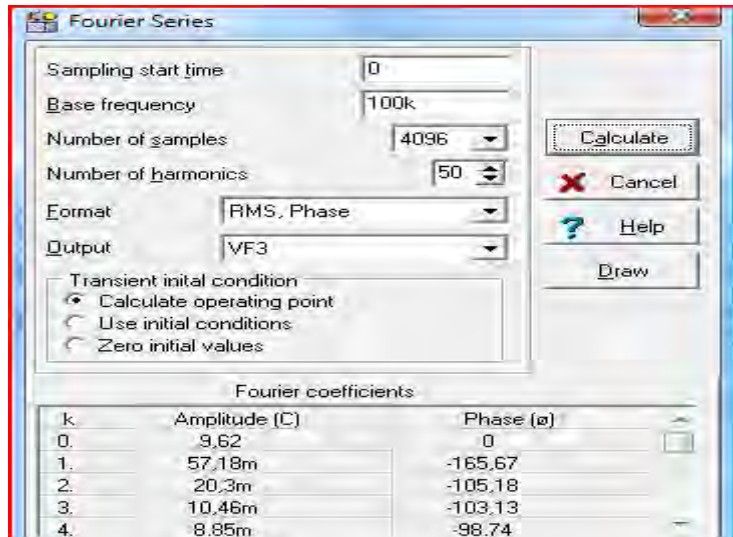
Figure 3.23. Fourier analysis of signal at the inverter level (VF3). THD calculation

Figure 3.24 shows the characteristic impedance at the head of the PLC transmission line. The major impedance appears at the proximity of the 100 kHz (signal carrier base frequency).
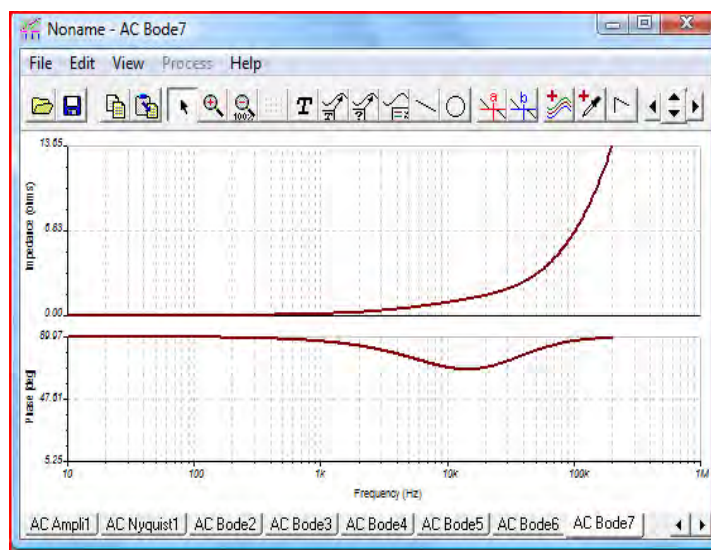
Figure 3.24. AC transfer characteristic and impedance at the transmission point (VF1)

Figure 3.25 shows the laboratory test bench mounted to implement the DC PLC line. It simulates the line impedance to evaluate empirical data for simulation comparison. This test bench includes all components specified in electric diagram of figure 3.19. Power resistors have been necessary to dissipate all the heat generated by transferred current.
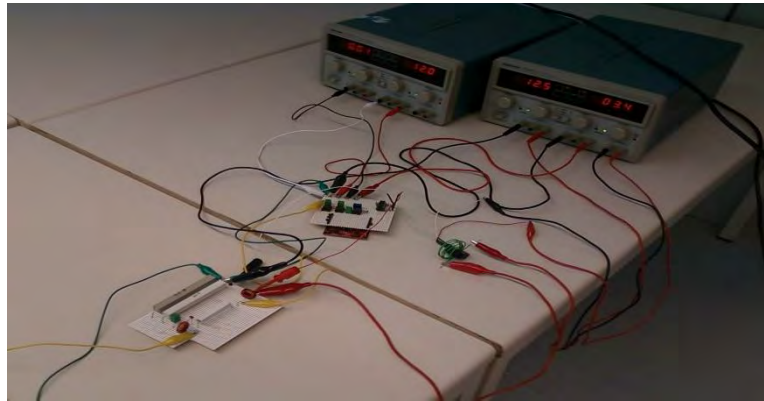
Figure 3.25. Laboratory test bench for PLC line testing

As it can be seen in figure 3.26, the experimental laboratory test bench obtained results are quiete similar to the results of simulation. In the lab, spikes and noise are much more significant, although with no major effect on the receiver side, since HF filtering is made. No significant AC harmonic is detected at the DC side of the PLC line (inverter proximity). So, no negative effect is expected from inverter point of view.

Figure 3.26. Test bench signals. Square signal by μController (CH1). Received signal at the end of the PLC line (CH2). DC signal at the inverters input (AC filtered)(CH3)

3.4.2 Bypass capacitors for PV modules low impedance data path implementation.

Once the concept of DC PLC data transmission has been seen to be viable, the following step was to validate the previous concept in the scenario of the EPS PV Lab test bench.

One of the problems that arised was related to the impedance seen by the Data Tx SMCM AFE, since from the PV module up to the CCS input, a complex signal path was figured-out. The aim of ensuring the data reception required to consider alternative data paths that voided all the PV modules internal parasitic parameters influence (Rs, Rp, parasitic capacitances, etc …). The proposed solution has been to implement a bypass capacitor (Cb) in parallel with each PV module. This ensured a controlled low impedance path for the data transmitted from the SMCM, as depicted in Figure 3.27.
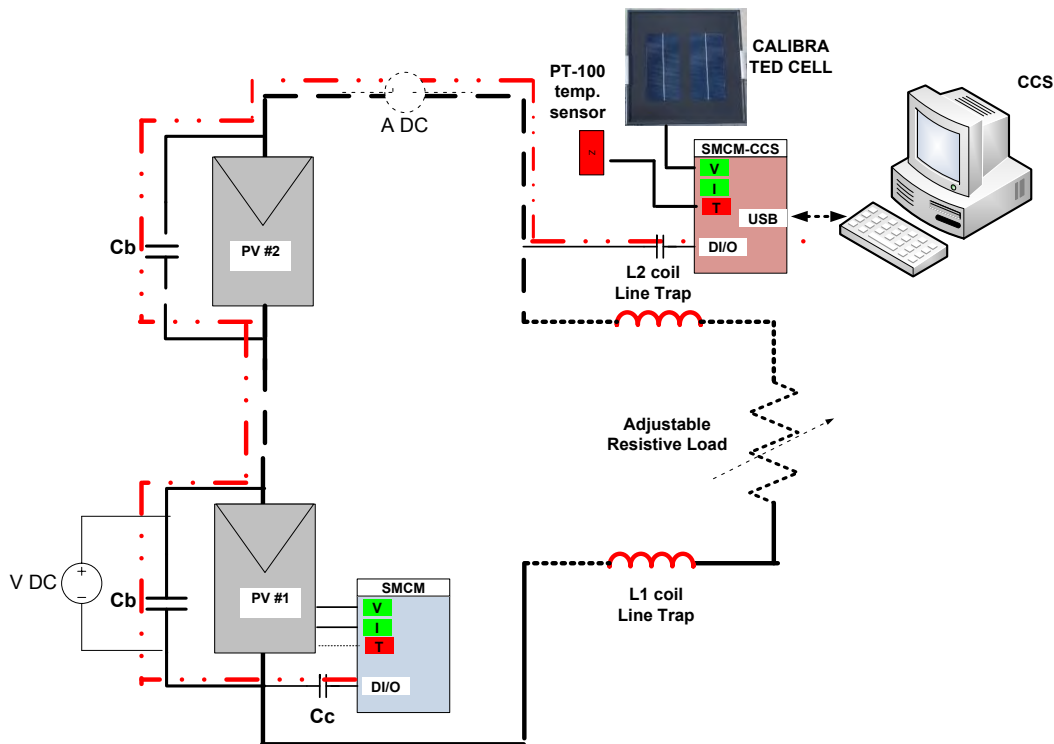
Figure 3.27. PV modules parallel low impedance data path bypass capacitors

3.4.3 EPS Renewable Energies LAB validation of simulated model and experimental data.

The model depicted in Figure 3.28 shows the Multisim (National Instruments) based simulation model. This model comprises a PV module, as well as the transmission line simulation components, including the inverter input.

The proposed model incorporates the 15 µF bypass capacitor that simulates the low impedance capacitive data path for the transmitted signal for a x 12 PV modules string.
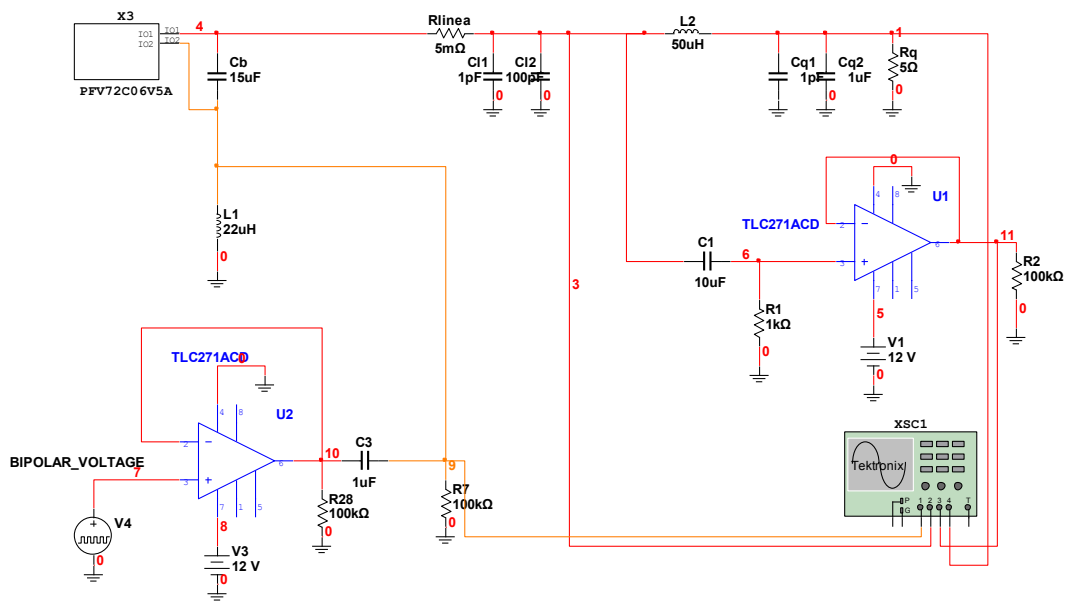
Figure 3.28. PLC data Tx EPS PV Lab est bench signals simulation model

Figure 3.29 shows the simulated waveforms of the transmitted data (CH1), the waveform of the data on the PLC line (CH2) and finally, the recovered signal (CH4) applied to the µController.
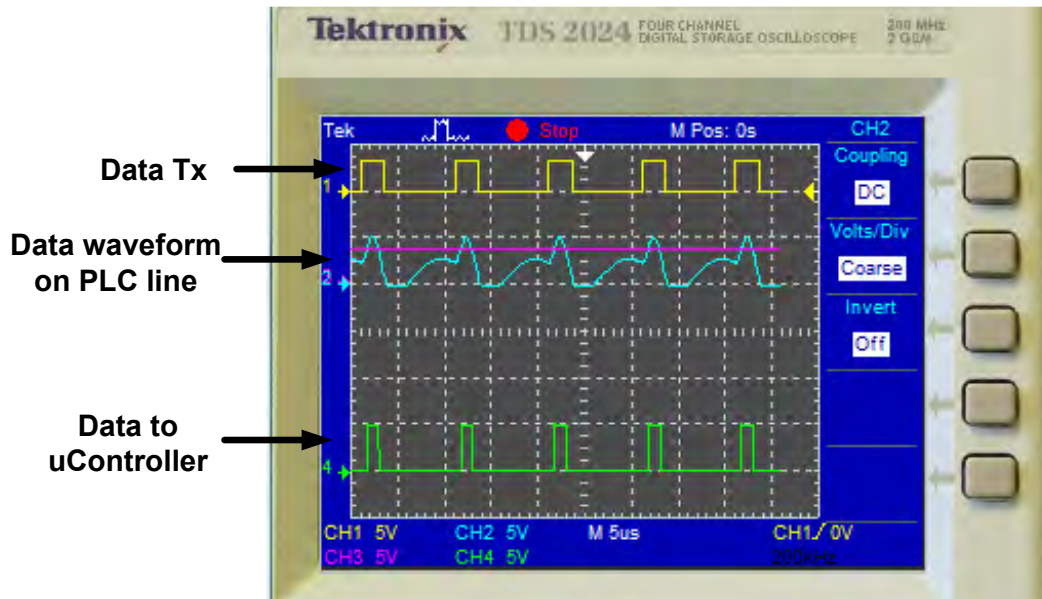
Figure 3.29. PLC data Tx simulated transmitted and received signals

For validation purpose, the configuration implemented simulates two series connected 24 V, 5 A PV modules, with its corresponding bypass capacitors (Cb). It simulates a string with maximum 1000 m (≈3000 feet) DC cable length, with its resistive (Rline) and capacitive (Cl1 and Cl2) equivalent impedance values. Equivalent input impedance of typical EMC filters at the input of DC/AC inverters has been considered as well. Line trap coils (L1 and L2) represent a high impedance at the data signal frequency, while for the DC power signal, this impedance is insignificant.

Field measurements of generated, PLC transmitted and received data are shown in Figure 3.30. Oscilloscopes picture shows in CH1 the data generated in the PV module SMCM. CH2 shows the distorted data waveform on the PLC line. Finally, CH3 shows the data that arrives to the µController input, after corresponding conditioning.

Data Tx

Data waveform on PLC line

Data to uController
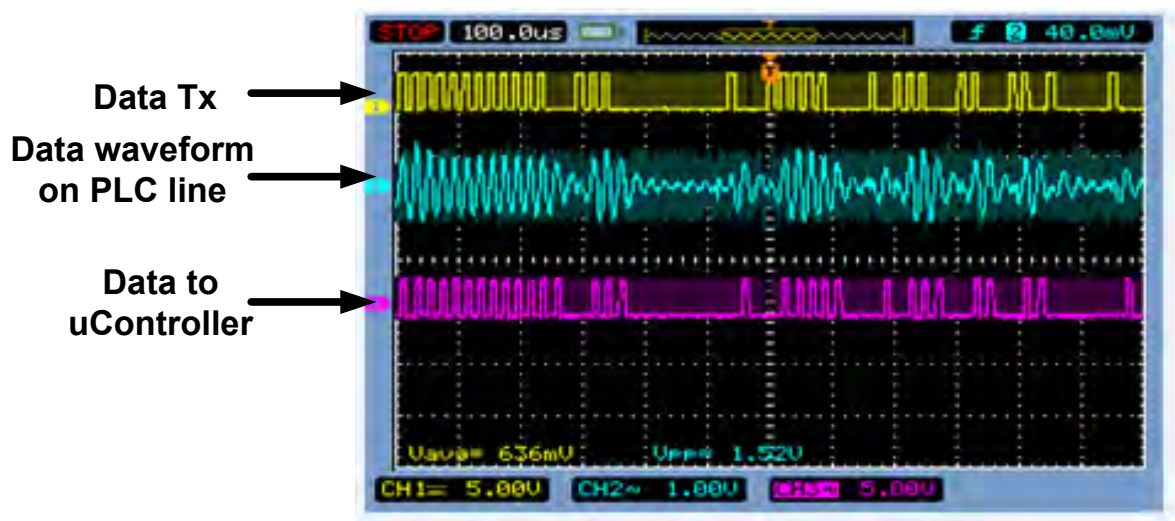
Figure 3.30. PLC data Tx EPS PV Lab test bench transmitted and received signals

3.5 SMCM GRAPHIC USER INTERFACE

All single module parameters are real time processed by CCS. A Graphic User Interface (GUI) application has been developed to allow the representation of all the information generated by the SMCM. This application has been developed under National Instruments Labview® environment. Figure 3.31 shows the GUI screen shot, where each single PV modules parameters can be visualized. In the "Temperature Map" option, PV modules temperature is displayed. Meanwhile, in the "Power Map" option, the actual Maximum Power Point at which every PV module is working under present ambient conditions is displayed. This tool is useful to detect any malfunction in real time. A scaled color based display allows operator to sightsee any operation fault, alarm situations being displayed in red.

The color scale is related to the percentage to the Maximum Peak Power (MPP) that under actual conditions, according to the information supplied by the calibrated cell (*Gg* and *Ta*), each single PV module should be generating.

Figure 3.31. Graphic User Interface for power and temperature visualization

If an adverse condition is applying, that affects to the PV module MPP or its temperature, the label color would be changing. In case of extreme failure, the PV module alarm label would be displayed blinking in red. This criteria applies both to the PV modules back-plane temperature and to the power generated as well. The option is operator selectable. Figure 3.32 shows the operator interface to introduce PV module parameters manufacturer´s nominal values, which will be used to determine the different values in percentage for the display options
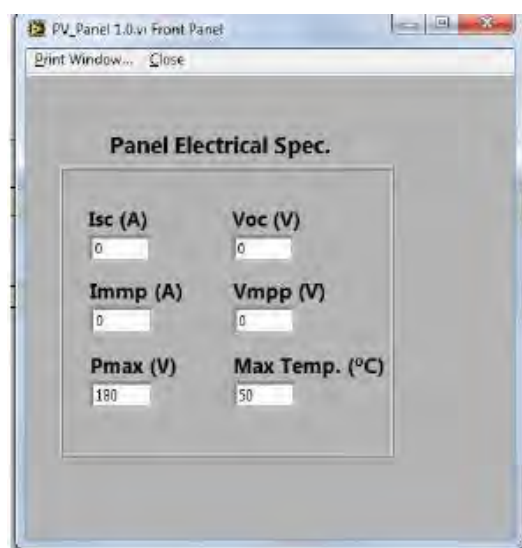
Figure 3.32. GUI operator interface for PV module parameters insertion

3.6 CONCLUSIONS

The possibility to real-time monitor the operating parameters of PV modules requires the adequate electronics to both perform this task and transmit the monitored data to the CCS. In this chapter, a detailed description is made of the SMCM hardware design and simulation of the different AFE. The AFE described are the necessary to monitor the PV modules operating parameters, namely voltage, current and module temperature and data transmission as well. For the current measurement, a non-invasive hall-effect current sensor has been used.

Additionally, a customized version of the SMCM is in charge of the monitored data reception and further routing to the CCS. This data concentrator has required a specific signal conditioning electronics, due to the signals level of noise. All the components used are standard industrial devices, which cost allows to tight the monitoring system overall cost.

The PLC based data transmission hardware AFE design and simulation is described and the viability demonstrated experimentally. The specifically designed low impedance data path by means of the PV modules bypass capacitors (Cb) has been demonstrated to be effective. This low cost solution also contributes to the initial objective to design a low cost system. The line trap coils are required to adapt the data transmission line impedance (in this case, the DC power line), to the digital data transmission electronics. They are only required at the head and trail of each modules string.

3.7 REFERENCES

[1] E. Román, R. Alonso, P. Ibañez, S. Elorduizapatarietxe and D. Goitia, *Intelligent PV Module for Grid-Connected PV Systems*, IEEE Transactions on Industrial Electronics, 2006.

[2] F.J. Sánchez-Pacheco, P.J. Sotorrío-Ruiz, J.R. Heredia-Larrubia, F. Pérez-Hidalgo and M. Sidrach-de-Cardona, *Low cost DC lines PLC based Photovoltaic plants parameters smart monitoring communications and control module*. POWERENG2011 III International Conference on Power Engineering, Energy and Electrical Drives, 2011.

[3] A. Ferrero and S. Salicone, *Decision Making in the Presence of Measurement Uncertainty: an Approach in terms of the Theory of Evidence*. IEEE 9th International Conference on Probabilistic Methods Applied to Power Systems KTH, June 2006.

[4] M. P. Sibanda, P. A. Janse van Rensburg, and H. C. Ferreira, Passive, *Transformerless Coupling Circuitry for Narrow-Band Power-Line Communications*, IEEE International Symposium on Power Line Communications and Its Applications, ISPLC 2009.

[5] Texas Instruments MSP 430 μControllers family data sheets. http://focus.ti.com.

[6] J. G. Webster, *The measurement, instrumentation and sensors handbook*, CRC press. ISBN 0-8493-2145-X.

[7] EN 50065-1, *Signaling on low-voltage electrical installations in the frequency range 3 kHz to 148,5 kHz. Part 1: General requirements, frequency bands and electromagnetic disturbances,* CENELEC 2012.

[8] EN 61724, *Photovoltaic system performance monitoring. Guidelines for measurement, data exchange and analysis,* CENELEC April 2000.

[9] L. Cristaldi, M. Faifer, M. Rossi and F. Ponci, *A Simple Photovoltaic Panel Model Characterization Procedure and Evaluation of the Role of Environment Measurements*, IEEE Transactions on Instrumentation and Measurement, (Vol. 61, No. 10, October 2012).

[10] S. Galli, A. Scaglione, Z. Wang, *For the Grid and Through the Grid:The Role of Power Line Communications in the Smart Grid*, Proceedings of the IEEE | (Vol. 99, No. 6), June 2011.

[11] Jianming Liu, Bingzhen Zhao, Jiye Wang, Yi Zhu, Jing Hu, *Application of Power Line Communication in Smart Power Consumption*, IEEE International Symposium on Power Line Communications and Its Applications, ISPLC 2010.

[12] T.P. Surekha, Dr. T. Ananthapadmanabha, and Dr. C. Puttamadappa, *Analysis of effect of Power line Channel Characteristic Parameters in Broadband Power Line Communication (BPLC) systems*, Power Systems Conference and Exposition, PSCE '09. IEEE/PES 2009.

[13] IEEE Std 643-2004, *643 IEEE Guide for Power-Line Carrier Applications*, IEEE Power Engineering Society, 2004 (revision of IEEE Std. 643-1980).

[14] D. Guezgouz, Y. Raingeaud, J-C. Lebunetel, *SPICE model for the PLC propagation channel in the high frequency range*. 2010 IEEE International Symposium on Power Line Communications and Its Applications (ISPLC).

[15] Mloyiswa P. Sibanda, Petrus A. Janse van Rensburg, and Hendrik C. Ferreira, *Passive, Transformerless Coupling Circuitry for Narrow-Band Power-Line Communications*. IEEE International Symposium on Power Line Communications and Its Applications, ISPLC 2009.

[16] B. A. Mork, D. Ishchenko, X. Wang, A.D. Yerrabelli, R.P. Questan and C.P. Kinne, *Power Line Carrier Communications System Modeling,* presented at the International Conference on Power Systems Transients, June 19-23, 2005, Paper No. IPST05 – 247.

Chapter 4

SMCM MEASURING CHAINS UNCERTAINTY ESTIMATION

The SMCM has been described from the electronics and functionality point of view in chapter 3. As an electronic measurement device, it is not exempt of uncertainty in the obtained results. The electronic components and configuration for the monitoring of the PV modules functional parameters give an information that in fact cannot be considered as absolutely loyal to the true data. The task described in this chapter is related to the estimation and quantification of the uncertainty, according to the IEC 98-3 standard, that comes from the Guide for the Uncertainty Measurement proposed by the Bureau International des Poids et Mesures de Paris. The quantification of the measurement chains uncertainty will be further used to define the acceptance margin of the PV modules Performance Ratios, obtained by means of SMCM monitored PV modules operational parameters.

4.1 INTRODUCTION TO THE UNCERTAINTY IN THE MEASUREMENTS

The SMCM is in itself an electronic measurement device that combines analog and digital electronic components for signal conditioning and conversion purposes and hence not exempt of uncertainty in the measurement process [1][2][3].

The framework in which the measurement standard uncertainty is quantified is the Guide to the Expression of Uncertainty in Measurement (GUM) [1], although more recent works highlight significant improvement approaches to traditional method [3].

As stated in [4], a "measurement" is a set of operations having the object of determining a value of a quantity with corresponding uncertainty [2][5].

Standard uncertainty components are classified in Type A and Type B, upon the method employed in its quantification [1]. Type A components are obtained from repetitive measurements of considered parameter. Type B components, in our case, and taking into account that the test bench is a laboratory prototype, they have been quantified on the basis of the SMCM electronic components manufacturers´ specifications. Three major contributions have been identified:

a) Contribution of measuring chain calibrated constants u(C).
b) Standard Uncertainty related to the unstable ambient conditions impacting on the PV module u(R).
c) Contribution to the overall Standard Uncertainty due to the SMCM electronic components drifts u(D).

4.2 MEASURING CHAINS STANDARD UNCERTAINTY ESTIMATION

The assembled prototype has made possible to perform the calibration and further quantification of standard uncertainty of SMCM measuring chains for PV module V_{PV}, I_{PV} and T_{PVBp} as referred in [6].

As stated previously, characteristic functions for the three measuring chains, voltage (VAFE), current (IAFE) and temperature (TAFE) are given by equations (4.1), (4.2) and (4.3).

$$VAFE : V_{PV} = NV_{ADC} \cdot V_q k_{VC} \tag{4.1}$$

$$IAFE : I_{PV} = \left[\left(NI_{ADC} \cdot V_q \cdot k_{IC}\right) - 2,5V\right] \cdot k_{ISENS} \tag{4.2}$$

$$TAFE : T_{PVbp} = NT_{ADC} \cdot V_q \cdot k_{TC} \tag{4.3}$$

Where NV_{ADC}, NI_{ADC} and NT_{ADC} are the digital values in counts (c), resulting from the AD conversion process of corresponding analog parameters; Vq is the ADC quantization voltage, given by $Vq = FS_{ADC}/(2^n-1)$, where FS_{ADC} is the ADC full scale range, namely 3,6 V divided by the ADC number of possible counts (c) minus one, where n is the ADC number of bits; in this case 10, accordingly, the value of $Vq=3,6$ V/1024, which gives a result of $Vq=3,52$ mV.

Measuring chains constants used k_{VC}, k_{IC} and k_{TC} are the corrected ones, instead of the nominal ones. According to the GUM [1], possible systematic errors must be corrected before performing the measurement uncertainty estimation. K_{ISENS} is the HCT06DSR5 hall-effect current sensor sensitivity.

According to the current sensor manufacturer´s data sheets, this device is calibrated to give an output of 0,625 V for a current of 6 A and hence, K_{ISENS} results to be 9,6 A/V. This sensor is capable of measuring positive and negative currents. Its output has an offset of 2,5 V, which is the value of the output under no current conditions. In the IAFE characteristic function (4.2), this offset is considered.

As referred previously, actual measuring chains constants differ from the nominal ones, which depend on nominal components parameters values. These are: $k_{IN}=1,11$ A/V and $k_{VN}=10,00$ V/V. On the other hand, k_{TN} is the TAFE sensibility. It comes from the Wheatstone bridge differential amplifier configuration, that, in this case, has been calibrated in the range of 0 ºC ($RTD=100$ Ω) which would give 0 V at the output of the amplifier and 100 ºC ($RTD=138,5$ Ω) giving 3 V at the output of the amplifier, hence $K_{TN}=100$ ºC/3 V= 33,33 ºC/V.

In order to quantify actual calibrated values, a set of experimental data have been processed. Regarding k_{TC}, a reference voltage of 0,962 V to simulate a T_{PVBp} of 24 ºC has been applied. For the k_{IC} evaluation, a reference voltage of 2,494 V has been applied, which is equivalent to a I_{PV} current of -0,057 A. Finally, for k_{VC} estimation, a 24 V reference voltage has been applied to simulate the PV module output voltage. Results are summarized in Table 4.1.

Table 4.1. Measuring chain calibrated constants calibration

	k_{TC} (ºC/V)	k_{IC} (A/V)	k_{VC} (V/V)
Nominal values:	33,33	1,11	10,00
Applied reference voltages	0,962 V @ 24 ºC	2,494 V @ -0,057 A	24,003 V @ 24 V
1	24,955	1,100	11,893
2	24,864	1,100	11,914
3	24,864	1,100	11,893
4	24,774	1,100	11,914
5	24,774	1,100	11,872
6	24,774	1,100	11,852
7	24,864	1,098	11,831
8	24,774	1,100	11,872
9	24,774	1,100	11,934
10	24,864	1,100	11,872
μ kx_ic	**24,828**	**1,100**	**11,885**

According to above results calibrated constants actual mean values result to be: k_{TC}=24,828 ºC/V, k_{IC}=1,10 A/V and k_{VC}=11,885 V/V. These constants values will be further considered when measuring real data.

Furthermore, once this potential systematic error has been corrected, the different contributions to the uncertainty in the measuring chains constants estimation have been evaluated. After k_{TC}, k_{IC} and k_{VC} have been calculated, their contribution to the Combined Uncertainty has been quantified considering them as type A. Accordingly, a total of 10 series of 30 consecutive readings have been made under given PV module working conditions. These results obtained are summarized in Table 4.2.

Table 4.2. Uncertainty estimation of measuring chains calibration constants

#	VAFE k_{VM}	IAFE k_{IM}	TAFE k_{TM}
1	11,95	0,994	24,801
2	11,96	0,994	24,795
3	11,95	0,997	24,815
4	11,98	1,036	24,822
5	12,14	1,002	24,830
6	12,05	1,001	24,827
7	11,94	1,015	24,800
8	11,95	0,999	24,832
9	11,96	1,002	24,829
10	11,98	1,012	24,835
μ	11,98	1,005	24,819
Var	0,003453	0,000149	0,000188
Std. Dev	0,062	0,013	0,015
Sens. Coeff	1,000	1,000	1,000
divisor	1,000	1,000	1,000
uC (k_{XiM})	**±0,062 V**	**±0,013 A**	**±0,015 ºC**

4.3 MEASUREMENT UNCERTAINTY ESTIMATION DUE TO AMBIENT CONDITIONS

The second contribution to the Combined Uncertainty is related to the unstable ambient conditions impacting on the PV module which might affect the readings in an unknown way.

In this sense, a run of measurements has been made under known ambient conditions (G=226,63 W/m^2, Ta=24,06 ºC). A total of 30 successive readings have been processed by the SMCM, at a rate of 16 ksa/s (kilosamples/second); that is, the 30 readings have been made in 1,87 ms. This fulfills the criteria that in a less than 2 ms of time frame, no ambient conditions changes are expected that might affect the PV module operation [7]. In Table 4.3 columns NT_{ADC}, NI_{ADC} and NV_{ADC} show the output of the SMCM µController AD converter (digital counts from 0 to 1023). Columns T_{PVBp}, V_{PV} and I_{PV} show corresponding duly converted engineering values. Applying procedures described in [1], which stipulate that:

$$uR(X_i) = Sc_i \cdot Sdev(X_i) \tag{4.4}$$

and considering that *Sci* is the sensitivity coefficient (*Sc$_i$*=1) and *Sdev(x$_i$)* is the Standard deviation of measured data, resulting uncertainty values are as follows: *uR(V$_{PV}$)*=±0,442 V, *uR(I$_{PV}$)*=±0,013 A and *uR(T$_{PVBp}$)*=±0,095 ºC.

Table 4.3. Stable conditions consecutive readings (*G*=226,63 W/m^2 , *Ta*= 24,06 ºC)

#	*NT$_{ADC}$*	*NI$_{ADC}$*	*NV$_{ADC}$*	*T$_{PVBp}$* (ºC)	*V$_{PV}$*(V)	*I$_{PV}$*(A)
1	257	663	799	30,07	33,871	0,485
2	256	662	795	29,95	33,701	0,466
3	257	662	789	30,07	33,447	0,466
4	256	662	777	29,95	32,938	0,466
5	257	663	774	30,07	32,811	0,485
6	257	663	772	30,07	32,726	0,485
7	260	662	771	30,42	32,684	0,466
8	257	663	774	30,07	32,811	0,485
9	257	662	782	30,07	33,150	0,466
10	256	662	790	29,95	33,489	0,466
11	256	662	799	29,95	33,871	0,466
12	257	663	800	30,07	33,913	0,485
13	257	663	796	30,07	33,744	0,485
14	256	662	788	29,95	33,404	0,466
15	257	664	780	30,07	33,065	0,504
16	256	663	774	29,95	32,811	0,485
17	257	662	771	30,07	32,684	0,466
18	257	663	772	30,07	32,726	0,485
19	256	663	775	29,95	32,853	0,485
20	256	663	782	29,95	33,150	0,485
21	256	662	790	29,95	33,489	0,466
22	257	664	798	30,07	33,828	0,504
23	256	662	798	29,95	33,828	0,466
24	256	663	795	29,95	33,701	0,485
25	256	663	787	29,95	33,362	0,485
26	256	664	777	29,95	32,938	0,504
27	257	663	774	30,07	32,811	0,485
28	257	664	773	30,07	32,769	0,504
29	256	662	772	29,95	32,726	0,466
30	256	663	776	29,95	32,896	0,485
			μ	30,022	33,204	0,480
			Var	0,003285	0,19684	0,000174
			Std. Dev	0,095	0,442	0,013
			Sens.Coeff	1,000	1,000	1,000
			divisor	1,000	1,000	1,000
			uR(x$_i$)	**±0,095ºC**	**±0,442V**	**±0,013A**

4.4 Measuring Chains Electronic Components Drift Uncertainty Estimation

The third contribution to the Combined Uncertainty is due to the measuring chains AFE electronic components drift. In this case, the standard uncertainty related to the electronic components drift u(D) contribution to Combined SMCM measurement Uncertainty is quantified considering [1] as follows:

$$uD(x_i) = Sc_i \cdot \left[Drift(x_i) / \sqrt{3} \right] \tag{4.5}$$

where $Drift(x_i)$ is each measuring chain quantified drift, considering they have a uniform distribution and hence the divisor is $\sqrt{3}$ (= 1,73) and Sc_i are corresponding sensitivity coefficient factors.

This approach is made separately for the three measuring chains. In all of them, one of the contributions is due to the μController internal Analog to Digital Converter (ADC).

The term that globally quantifies the ADC overall uncertainty contribution is the so defined Total Unadjusted Error (TUE) and is related to the ADC Vq quantization voltage. According to the μController manufacturer´s [6] data sheets, this TUE is quantified to be ±5LSB. In this case, referred TUE is ±17,6 mV, which represents an uncertainty of ±0,49 % of the 3,6 V μController maximum input voltage.

The TLC 271 Opamp generates an uncertainty due to the input offset voltage thermal drift (αV_{IO}), quantified to be 2 μV/ºC, which represents a maximum drift of 0,1 mV in an operating temperature range of 50 ºC. This gives a ±0,01 % of drift in the considered full scale (FS_{OA}) input voltage of 3,6 V. Total derate in the V_{AFE} is $Drift(V_{AFE})$=±0,4983 %, hence, the resulting uncertainty is $uD(V_{AFE})$=$Drift(V_{AFE})/\sqrt{3}$=±0,29 % or ±0,107 V related to the 37,3 V PV module open circuit voltage (Voc).

The hall effect current sensor has an offset voltage temperature drift of ±0,5 mV/ºC. This represents an uncertainty of ±0,75 % of full scale. Considering also

the ±0,01 % of the Opamp, and ±0,488 % of the ADC, this results in $Drift(I_{AFE})$=1,2983 % that represents an estimated components drift uncertainty $uD(I_{AFE})$=$Drift(I_{AFE})/\sqrt{3}$=±0,75 %, or ±0,065 A of the 8,7 A PV module short circuit current (Isc).

Regarding the PV back-plane temperature measurement AFE, the contribution of the PT100 RTD sensor is due to its temperature drift to be of ±0,8 % in the range of 100 ºC. This, added to the OA amplifier drift (±0,01 %) and ADC drift (±0,488%), gives a total of $Drift$ (T_{AFE})=±1,6783 % which represents an uncertainty $uD(T_{AFE})$=$Drift$ $(T_{AFE})/\sqrt{3}$=0,97 % that corresponds to ±0,242 ºC referred to STC Tm=25 ºC. These data are summarized in Table 4.4.

Table 4.4. Uncertainty estimation of electronic components drift

VAFE components drifts uncertainty	
Total drift Voltage AFE (±V)	0,1858
Sensitiviy coefficient (*Sc*)	1
Divisor ($\sqrt{3}$)	1,7321
Voltage AFE *uD(V_{PV})*	**±0,107 V**
IAFE components drifts uncertainty	
Total drift Current AFE (±A)	0,1651
Sensitiviy coefficient (*Sc*)	1
Divisor ($\sqrt{3}$)	1,7321
Current AFE *uD(I_{PV})*	**±0,065 A**
TAFE components drifts uncertainty	
Total drift RTD temp sensor (±ºC)	0,324
Sensitiviy coefficient (*Sc*)	1
Divisor ($\sqrt{3}$)	1,7321
Temp. AFE *uD(T_{PVBp})*	**±0,24 ºC**

Taking into account previous data, combined and expanded standard uncertainty can be quantified for the three measuring chains. Following the GUM recommendations [1], this can be expressed as:

$$u_c(y) = \left[\sum uC(kx_{i_M})^2 + \sum uR(x_i)^2 + \sum uD(x_i)^2 \right]^{\frac{1}{2}} \qquad (4.6)$$

Furthermore, it follows that the expanded uncertainty is given as:

$$U = k \cdot u_c(y) \qquad (4.7)$$

where k is the coverage factor. In this case, with $k=2$, a confidence level of 95 % can be considered.

Table 4.5 summarizes obtained results of combined and expanded uncertainty values.

Table 4.5. Uncertainty estimation of voltage, current and temperature measuring chains

Source	Type	Value	Divis.	Sens Coeff	Standard Uncertainty
$uR(V_{PV})$	A	0,442	1	1	0,442
$uC(V_{PV})$	A	0,062	1	1	0,062
$uD(V_{PV})$	B	0,107	1,73	1	0,062
				combined uncertainty	**0,451**
				coverage factor	**2,000**
			Voltage AFE expanded uncertainty (±V)		**0,901**
$uR(I_{PV})$	A	0,013	1	1	0,013
$uC(I_{PV})$	A	0,013	1	1	0,013
$uD(I_{PV})$	B	0,065	1,73	1	0,038
				combined uncertainty	**0,042**
				coverage factor	**2,000**
			Current AFE expanded uncertainty (±A)		**0,084**
$uR(TV_{PVBp})$	A	0,095	1	1	0,095
$uC(T_{PVBp})$	A	0,015	1	1	0,015
$uD(TV_{PVBp})$	B	0,242	1,73	1	0,140
				combined uncertainty	**0,170**
				coverage factor	**2,000**
			PV BP Temp. expanded uncertainty (±ºC)		**0,340**

4.5 CONCLUSIONS

As an electronic measurement device, the SMCM is not exempt of uncertainty in the results delivered. In this sense, applying the recommendations of the GUM of the BIPM, it has quantified its uncertainty of both A type and B type, due to 3 different contributions. On one hand, the contribution of the calibrated constants has been quantified as well as the related to the unstability of the applying ambient conditions; being both A type. Additionally, the contribution to the electronic components drift has also been quantified, being this B type. It has resulted that the different contributions give an uncertainty of ±0.9 V in the case of the voltage measurement AFE; ±0.08 A for the current measurement AFE and of ±0.34 ºC in the case of the PV module temperature measurement AFE. It can be seen that the higher uncertainty is related to the voltage measurement, mainly due to the stability of the ambient conditions, together with the noise present in the PV module voltage signal.

4.6 REFERENCES

[1] BIPM. Bureau International des Poids et Mesures, *Evaluation of measurement Data – Guide to the expression of uncertainty in measurement* JCGM 100:2008, corrected version 2010.

[2] A. Giordani and L. Mari, *Measurement, Models and Uncertainty. IEEE Transactions on Instrumentation and Measurement*, Vol. 6, NO. 8, August 2012.

[3] A. Ferrero and S. Salicone, *Measurement Uncertainty. Part 8 in a series of tutorials in instrumentation and measurement*. IEEE Instrumentation & Measurement Magazine, June 2006.

[4] BIPM. Bureau International des Poids et Mesures, *International Vocabulary of metrology – Basic and general concepts and associated terms (VIM)*, 3rd edition, JCGM 200:2012.

[5] W. Bich, *From Errors to Probability Density Functions. Evolution of the Concept of Measurement Uncertainty*. IEEE Transactions on Instrumentation and Measurement, Vol. 61, No.8, August 2012.

[6] A. Ferrero, M. Lazzaroni and S. Salicone, *A Calibration Procedure for a Digital Instrument for Electric Power Quality Measurement*. IEEE Transactions on Instrumentation and Measurement, 2002.

[7] M. Seapan, C. Limsakul, T. Chayavanich, K. Kirtikara, N. Chayavanich and D. Chenvidhya. *Effects of dynamic parameters on measurements of IV curve*. IEEE 33rd PVSC Photovoltaic Specialists Conference, 2008.

MODEL VALIDATION WITH EXPERIMENTAL DATA

In this chapter, the validation of the proposed mathematical model, together with the translation criteria is made on the basis of consolidated field experimental data obtained in the UMA RREE Laboratory. Both are deployed and the comparison has been made between the expected values obtained with the proposed model and the real ones. The results have allowed to quantify the maximum Relative Error that can be generated and the conditions in which it happens.

5.1 INTRODUCTION

In order to further quantify the Performance Ratio of the PV modules, it is required to understand the margin of error generated by the proposed translation model of the PV modules operational parameters from STC to Real Outdoor Conditions (ROC). By means of referred procedure, the aim is to obtain the Relative Error (RE) that the translation procedure delivers when obtained results are compared with consolidated experimental data. These data have been obtained in the UMA RREE Lab, which have been processed by calibrated instruments. This task has been developed using field data collected in the UMA RREE Lab on Yocasol PCB-195 54 cell polycrystalline 195 W PV modules shown in Figure 5.1.

Figure. 5.1. UMA RREE Lab with Yocasol PV modules

The process has an inherent error which has been quantified for each measurement. The Relative Error has been calculated, which gives an idea of the proposed model reliability.

The test assembly, together with the PV modules characterization instrumentation is shown in figure 5.2. This instrumentation assembly allows to characterize a full I-V curve with 100 measurements in less than 1 s.
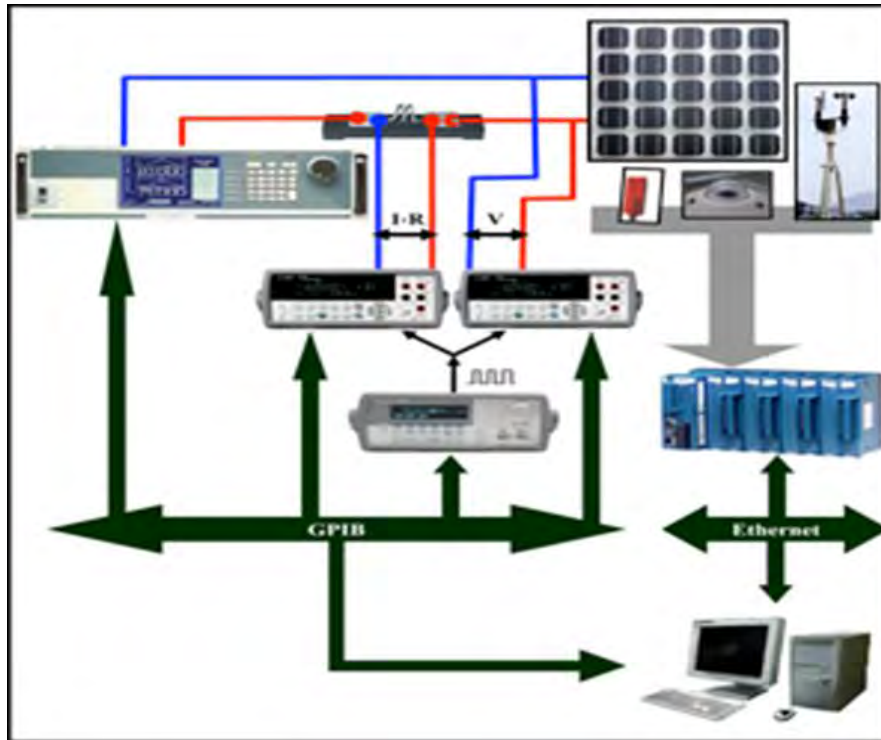
Figure. 5.2. UMA RREE Laboratory PV modules characterization test

Referred Yocasol PCB-195 modules main electrical characteristics are summarized in Table 5.1.

Table 5.1. Yocasol PCB-195 module electrical characteristics at STC

Electrical parameter	Value
Maximum output	195 W
Maximum power voltage	26 V
Maximum power current	7,50 A
Open circuit voltage	32,5 V
Short circuit current	8,26 A
Maximum output tolerance	+5%/-3%

5.2 PROPOSED MATHEMATICAL PV MODULE MODEL VALIDATION

In order to validate the proposed model, 10 measurements in different ambient outdoor conditions in a clear sky day have been considered, with irradiance values in the range between 118 to 1039 W/m^2; that is, low and high irradiance values.

The considered Operational Parameters (*OP*) are those that define the *I-V* PV module fingerprint and reported in the manufacturer´s data sheet, namely:

- *V$_{OC}$*: Open Circuit voltage
- *I$_{SC}$*: Short Circuit current
- *Pmp*: Power at Maximum Power Point (MPP)
- *Vmp*: Voltage at MPP
- *Imp*: Current at MPP

The Relative Error (*RE*) for each of the referred operational parameters has been calculated according to:

$$RE(\%) = \left| \frac{OP_i - OP_t}{OP_i} \right| \times 100 \qquad (5.1)$$

where OP_i is the generic term that refers to the real-time read parameter, while OP_t refers to the corresponding ROC translated one. Equation (5.1) has been applied to the above specified parameters.

In order to illustrate the measurements results, two cases will be described under different ROC which illustrate and justify the results further depicted in Table 5.2. The first one corresponds to a low irradiance value, and the results show very high *RE*. On the other hand, a case under a high irradiance gives *RE* much smaller for all of the analyzed *OP´s*.

Figure 5.3 represents the measured vs the model translated values of the *I-V* curve of meas. #M10, at an incident irradiance of 118 W/m^2, which makes the module to reach a temperature T_m=18,5 ºC. The solid blue line represents the STC values; the red dashed line represents the translated to ROC values, meanwhile the green dotted line depicts the read values. In this case, the resulting *RE* is of 19,2 % for I_{SC} and of 9,9 % for V_{OC} (see Table 5.2). The resulting *RE* for *Pm* is around of 24,80 %.
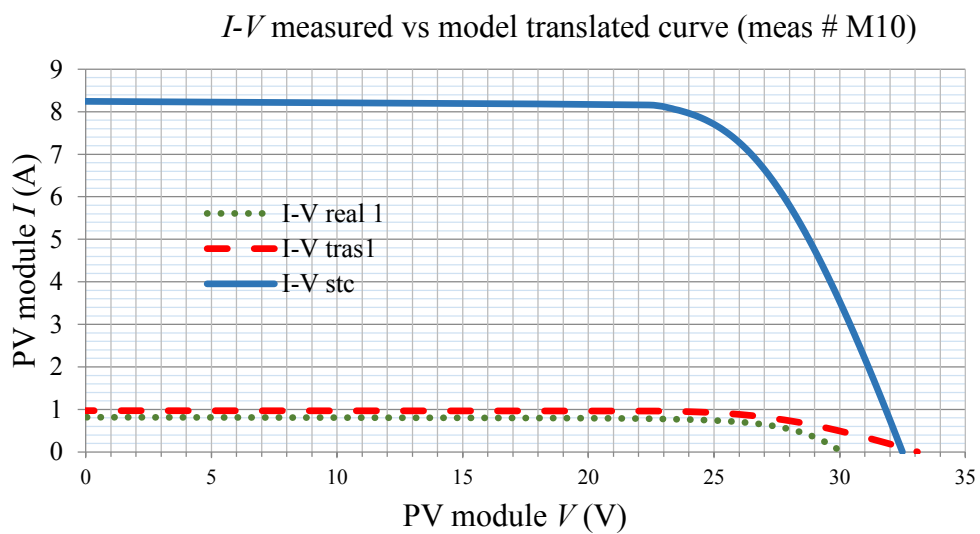
Figure. 5.3. Resulting model based translated vs measured I-V curves for #M10.

Figure 5.4 represents the measured vs the modeled translated values of the corresponding *P-V* curves. There, it can be seen that the maximum power read is sensibly smaller than the maximum expected one. Obviously, the fact that the incident irradiance is very low, the generated power is consequently also low. Additionally, probably due to an effect of the module temperature, the V_{OC} is smaller than the expected one.
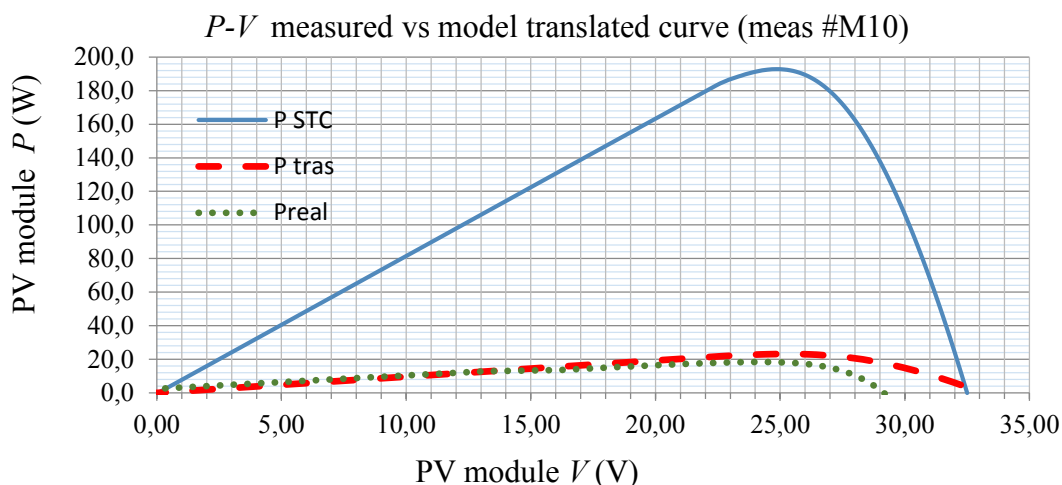
Figure.5.4. Resulting model based translated vs measured *P-V* curves for # M10.

An analysis of the results corresponding to readings under higher values of incident irradiance, gives that the *RE* resulting is significantly reduced.

Figure 5.5 corresponds to the *I-V* curve under the maximum irradiance read, of 1039 W/m^2 (meas. #M5) that makes the PV module reach a temperature T_m=33ºC, almost twice the previous value. In this case, the *RE* for I_{SC} is reported to be of 1,9 %, the V_{OC} *RE* is of 2,4 %. In this figure, the *I-V* curves at STC (solid blue line), ROC translated (dashed red line) and read (green dotted line) are depicted.
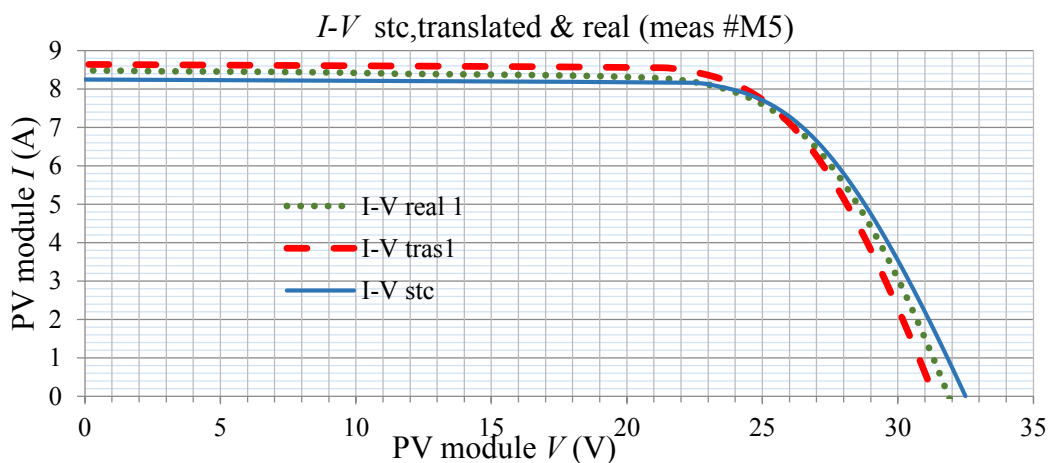
Figure. 5.5. STC, translated and measured *I-V* curves for #M5.

Which is more significant, the *RE* of the *Pm* is quantified to be of 2,3 % (Figure 5.6). This RE value is significantly smaller than the one obtained at 118 W/m^2. Consequently, the proposed model is suitable for the model based estimation of PV modules parameters to applying ambient outdoor conditions for medium to large values of the incident sun irradiance.
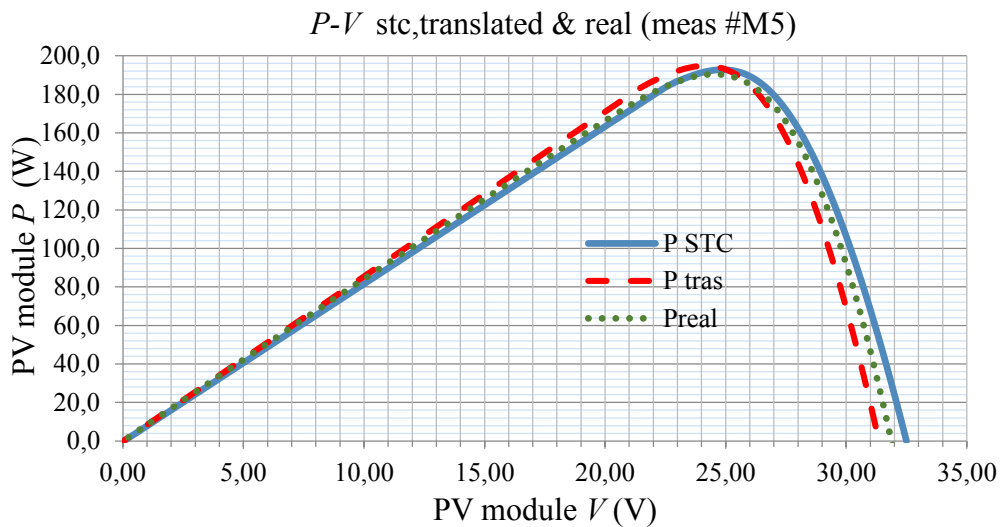
Figure. 5.6. STC, translated and measured *P-V* curves for meas. #M5

In table 5.2, a summary is made of both the model based translated values to applying outdoor conditions and the measured ones. Additionally, the Relative Error resulting in each case is also given. There, it can be seen that the *RE* increase at low irradiance values.

Table 5.2. One clear sky day long proposed model theoretical and experimentally measured PV modules operating parameters. Relative Error of most significant electrical parameters

		M1	**M2**	**M3**	**M4**	**M5**	**M6**	**M7**	**M8**	**M9**	**M10**
	Time	9:11	9:51	11:06	12:26	13:36	14:36	15:31	16:41	17:46	18:31
	T_m (°C)	14,5	19,7	24,2	31,4	33	35,4	35,3	28,8	23,9	18,5
	G (W/m²)	308	502	793	985	1039	992	878	635	344	118
I_{SC} (A)	translated	2,5	4,1	6,6	8,2	8,6	8,3	7,3	5,3	2,8	1,0
	measured	2,3	4,0	6,4	8,0	8,5	8,1	7,1	5,1	2,7	0,8
	RE (%)	**8,5**	**3,8**	**2,0**	**1,8**	**1,9**	**2,4**	**2,6**	**2,9**	**6,8**	**19,2**
V_{OC} (V)	translated	33,4	32,8	32,3	31,5	31,4	31,1	31,1	31,8	32,4	33,1
	measured	32,2	32,4	32,4	32,2	32,1	32,1	32,1	32,0	32,0	30,1
	RE (%)	**3,9**	**1,2**	**0,4**	**2,0**	**2,4**	**3,1**	**2,9**	**0,6**	**1,3**	**9,9**
P_{mp} (W)	translated	60,7	97,6	152,2	185,5	194,9	184,9	163,8	120,5	66,2	23,1
	measured	57,5	97,6	153,2	182,8	190,5	180,1	160,4	120,5	64,0	18,5
	RE (%)	**5,6**	**0,0**	**0,6**	**1,5**	**2,3**	**2,6**	**2,1**	**0,0**	**3,5**	**24,8**
V_{mp} (V)	translated	26,7	26,3	25,8	25,2	25,1	24,9	24,9	25,5	25,9	26,5
	measured	26,8	26,3	25,7	24,9	24,6	24,3	24,4	25,5	25,9	25,1
	RE (%)	**0,3**	**0,3**	**0,6**	**1,3**	**1,9**	**2,2**	**1,9**	**0,1**	**0,0**	**5,5**
I_{mp} (A)	translated	2,3	3,8	6,0	7,4	7,9	7,5	6,6	4,8	2,6	0,9
	measured	2,1	3,7	6,0	7,3	7,7	7,4	6,6	4,7	2,5	0,7
	RE (%)	**7,1**	**1,5**	**0,1**	**1,3**	**1,5**	**1,5**	**1,3**	**1,2**	**4,7**	**19,8**

From Table 5.2, it can be seen that most significant Relative Errors values appear with low values of incident irradiance for I_{SC}, V_{OC} and mainly for P_{mp} and associated V_{mp} and I_{mp}. Figure 5.7 gives an overview of the *RE* for all the operating parameters vs the evolution of the incident irradiance on the PV module. As it can be seen, the *RE* has bigger values at low irradiance levels, while in the mid ranges, the *RE* becomes much smaller.
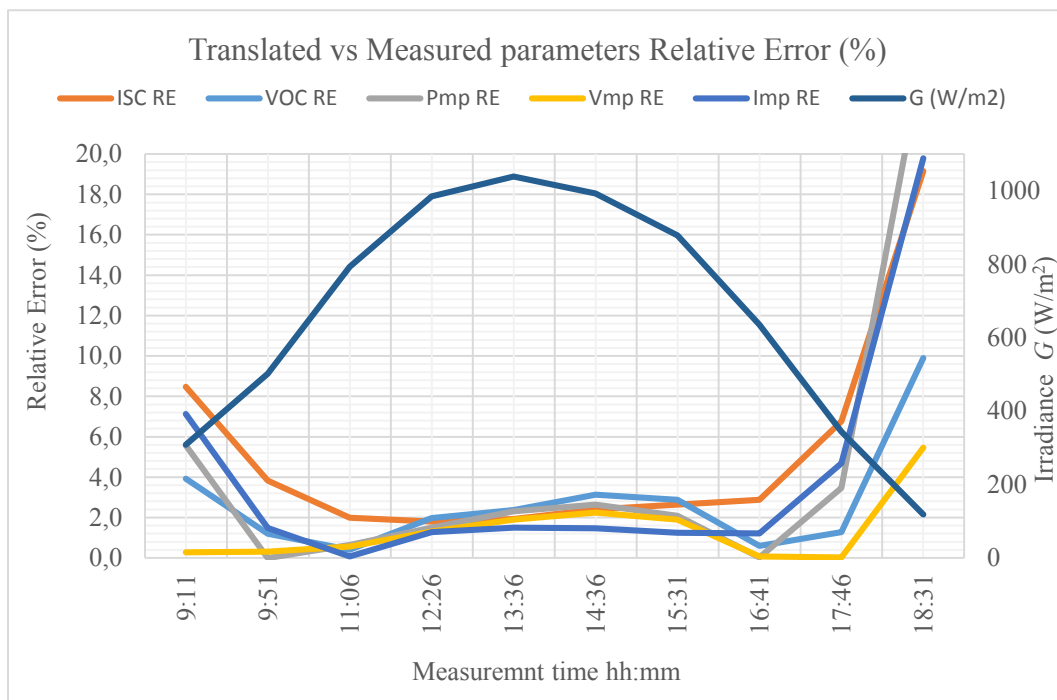
Figure. 5.7. General overview of the parameters Relative Errors, vs *G*

Regarding the maximum power point (P_{mp}) and its coordinates, the maximum power point current (I_{mp}) and the maximum power point voltage (V_{mp}), following figures depict in detail the evolution of referred parameters vs. *G* in the range of values of the outdoor measurements made. Regarding the maximum power parameter (P_{mp}), the *RE* (clear gray line) is kept < 3,5 % for irradiances > 340 W/m^2, as seen in Figure 5.8.
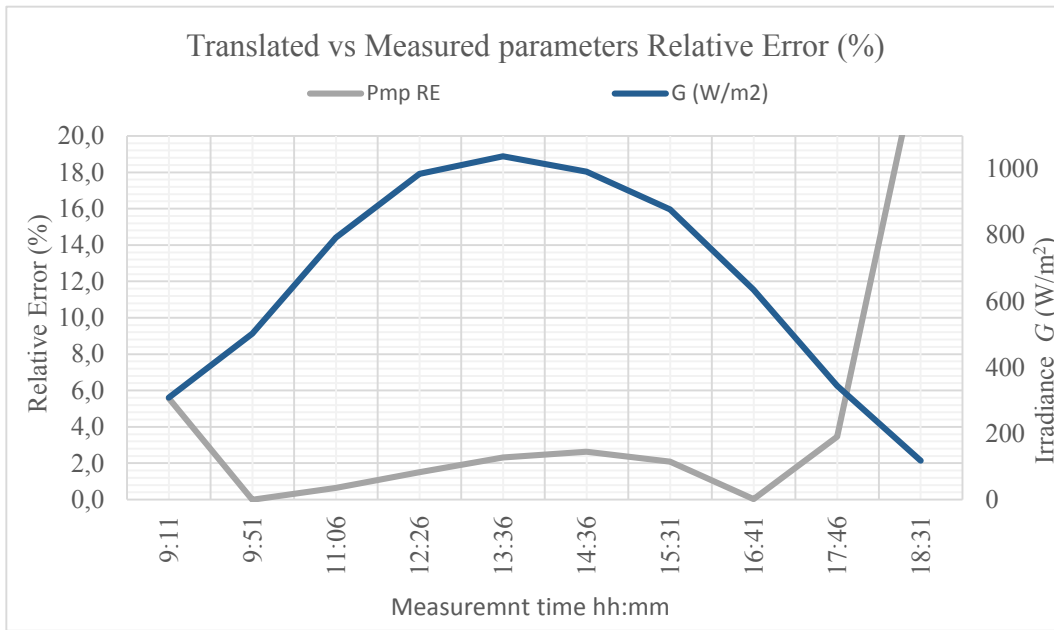
Figure 5.8. Evolution of *Pm RE* vs *G*

Figure 5.9 represents the evolution of the V_{mp} *RE* vs the irradiance. It can be seen a small increase of the *RE* in low range values, but in any case, this *RE* is kept in the boundaries of the 2 %.
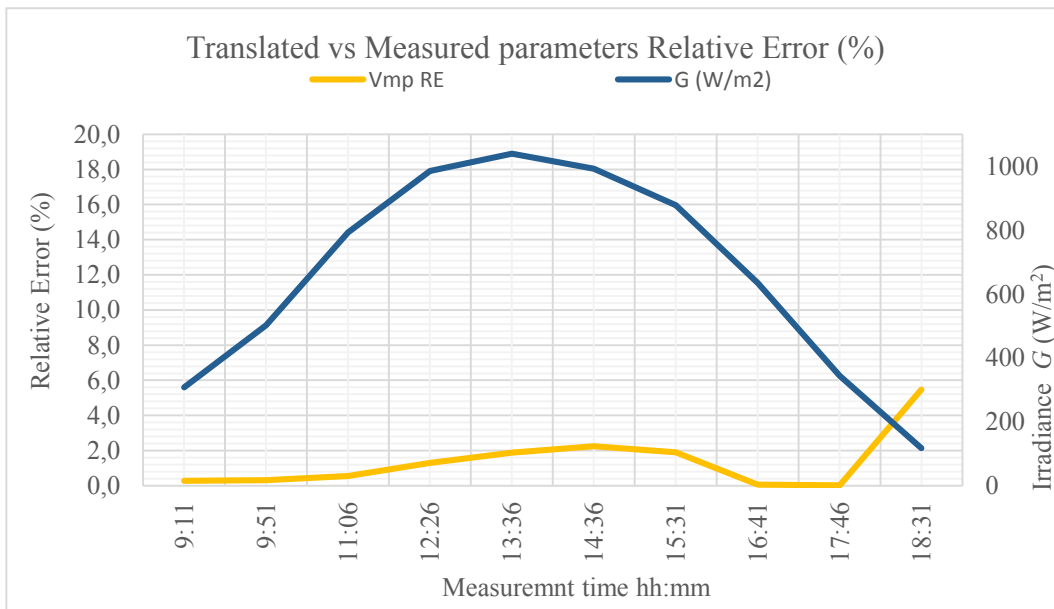
Figure 5.9. Evolution of the V_{mp} *RE* vs *G* values

5-10

Regarding I_{mp}, Figure 5.10 shows the evolution of the complementary parameter, namely the I_{mp} vs G. In the high range values, the RE is in the surrounding of the 1,5 %.
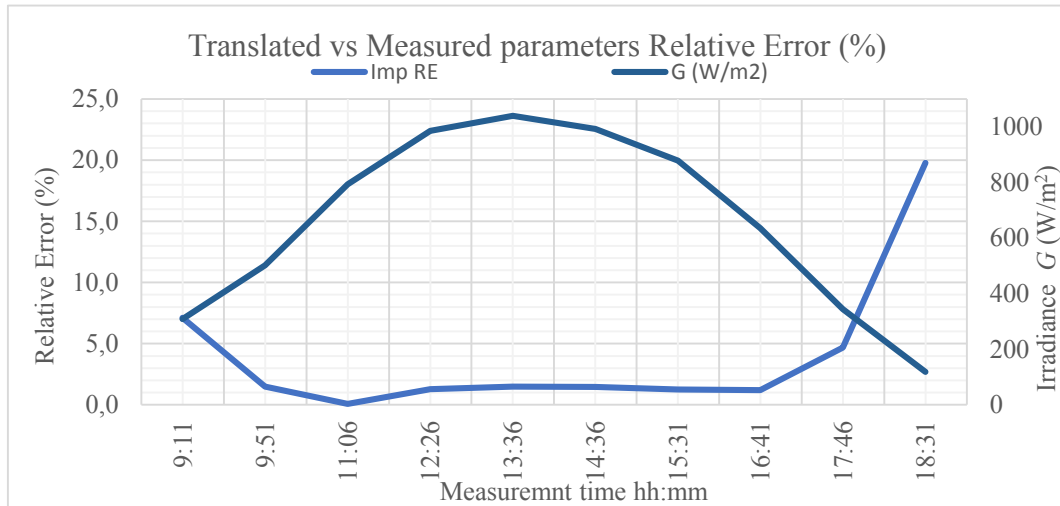
Figure 5.10. Evolution of the I_{mp} RE vs G values

In order to complete the detailed analysis, the graphs corresponding to the evolution of V_{OC} and I_{SC} operating parameters RE vs G are depicted in figures 5.11 and 5.12 respectively.
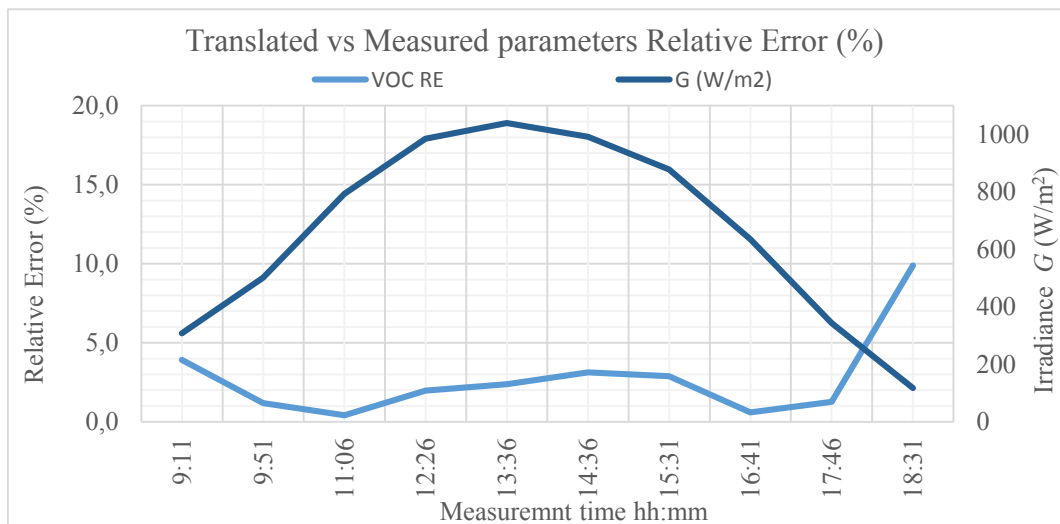
Figure 5.11. Evolution of the V_{OC} RE vs G values
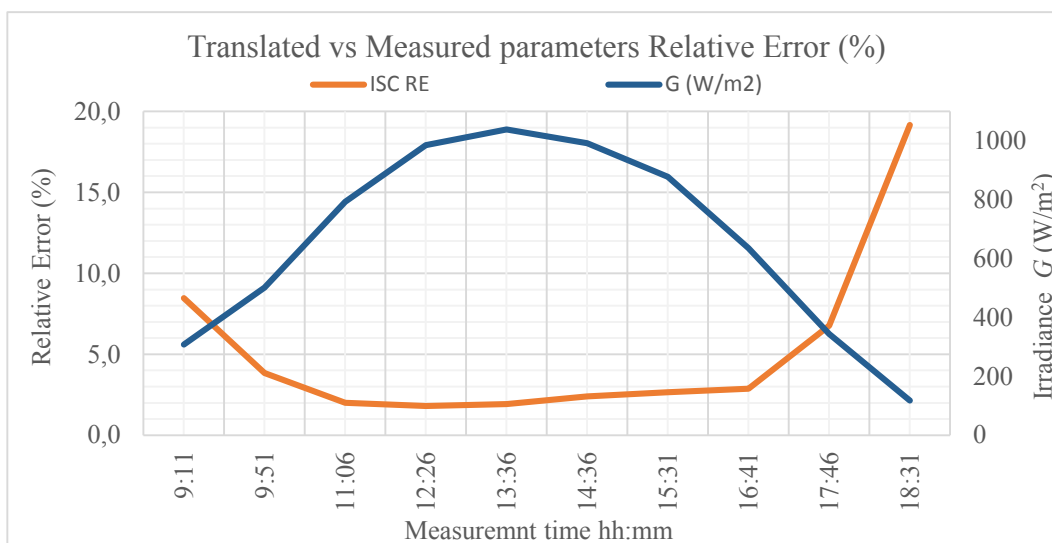
Figure 5.12. Evolution of the I_{SC} RE vs G values

Putting the focus on the incident irradiance boundaries < 200 W/m², and specifically on P_{mp} and associated V_{mp} and I_{mp} associated *RE*, in figure 5.13, it can be seen that the major contribution to the P_{mp} *RE* comes from the I_{mp} *RE*. For incident irradiances values > 200 W/m², the *RE* is kept < 2,2 % and 1,5 % respectively for V_{mp} and I_{mp}.
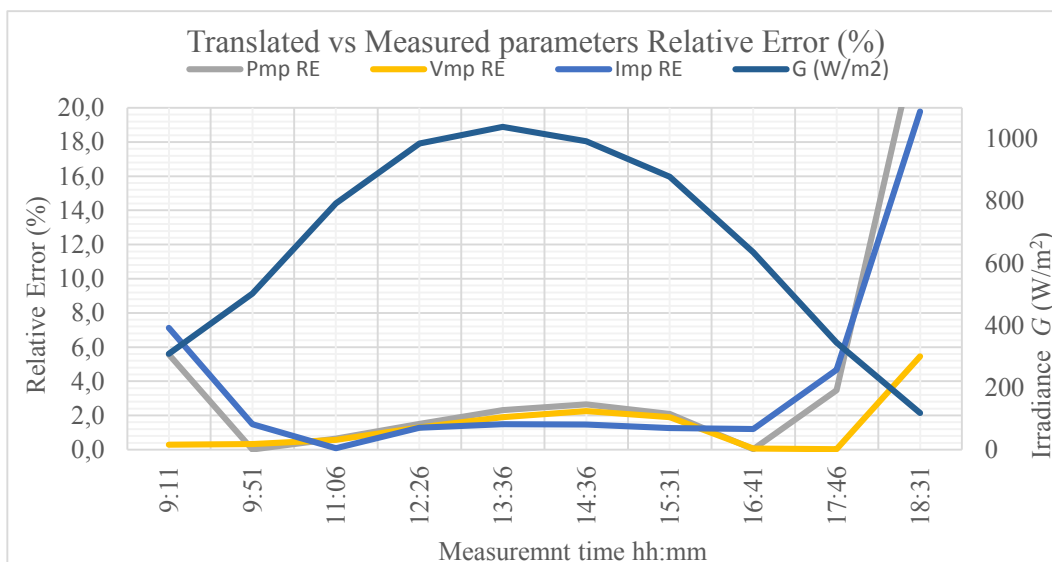
Figure 5.13. Evolution of the P_{mp}, V_{mp} and I_{mp} *RE* vs G values

5.3 CONCLUSIONS

In this chapter, the proposed translation model has been validated with consolidated experimental data obtained from the UMA RREE Lab monitored modules. These results highlight the magnitude of the proposed model generated Relative Error that acquires significant values in the low irradiation frames, roughly by < 200 W/m^2, which happens mainly at the beginning and the end of the day. Nevertheless, these errors are reduced significantly in the center day-time measurements, corresponding to higher values of irradiance (> 200 W/m^2). From a practical point of view, this is the irradiance value frame that in fact has to be considered, since the central hours of the day are the ones where the PV modules are generating the maximum power.

The results allow us to consider the model as reliable for the purpose of identifying a defective module performing under below the predicted values as per the proposed model.

Regarding the PV module maximum power generated P_{mp}, in comparison with the estimated modeled one, the maximum RE generated in the center hours is of 3,5 %. This means that all the measured values with an error above this one might be interpreted as an abnormal operation of corresponding PV module. Similar conclusions can be extracted from the other parameters considered.

Chapter 6

MODEL APPLIED TO SMCM MONITORED DATA

In this chapter, the proposed PV module model, after its validation, as described previously, is applied to the SMCM experimentally monitored PV modules parameters. The results and analysis are reported. This demonstrates the functionality of the SMCM as a PV module parameters monitoring and data transmission device. The results allow an evaluation of the real behavior of the PV modules under applying outdoor conditions and its comparison with the optimal results that should be obtained.

6.1 INTRODUCTION

The PV modules operational parameters based on mathematical model described and validated in previous chapters are now compared with the real-time data of referred PV modules and applying outdoor conditions, obtained by means of the SMCM based monitoring system. This procedure has been applied to the PV modules test assembly installed in the Málaga University Escuela Politécnica Superior Photovoltaic Laboratory (EPS PV Lab). The aim is to establish the comparison between the modelled parameters and the SMCM monitored data and according to the obtained results, evaluate the effective performance of the PV modules working under referred conditions.

This procedure has been applied to different measurements in order to validate it, which are described in this chapter. It will be demonstrated the viability of the application to quantify the PV modules operation.

6.2 EPS PHOTOVOLTAIC LABORATORY TEST ASSEMBLY DESCRIPTION

In order to validate the proposed idea of monitoring and data comparison with corresponding model, a test bench assembly has been deployed in the EPS PV Lab, comprising the PV modules, the SMCM monitoring devices, together with the additional electronic devices required for the proper operation, like the PC Central Computer System (CCS) an electronic load and laboratory measuring instruments. The test assembly layout is depicted in Figure 6.1, where it can be seen the layout of the PV modules, calibrated cell, temperature sensors, power wiring and data path. One SMCM module has been used for data monitoring and transmission of one of the PV modules and a SMCM-CCS for data reception and further routing to the PC CCS via USB.
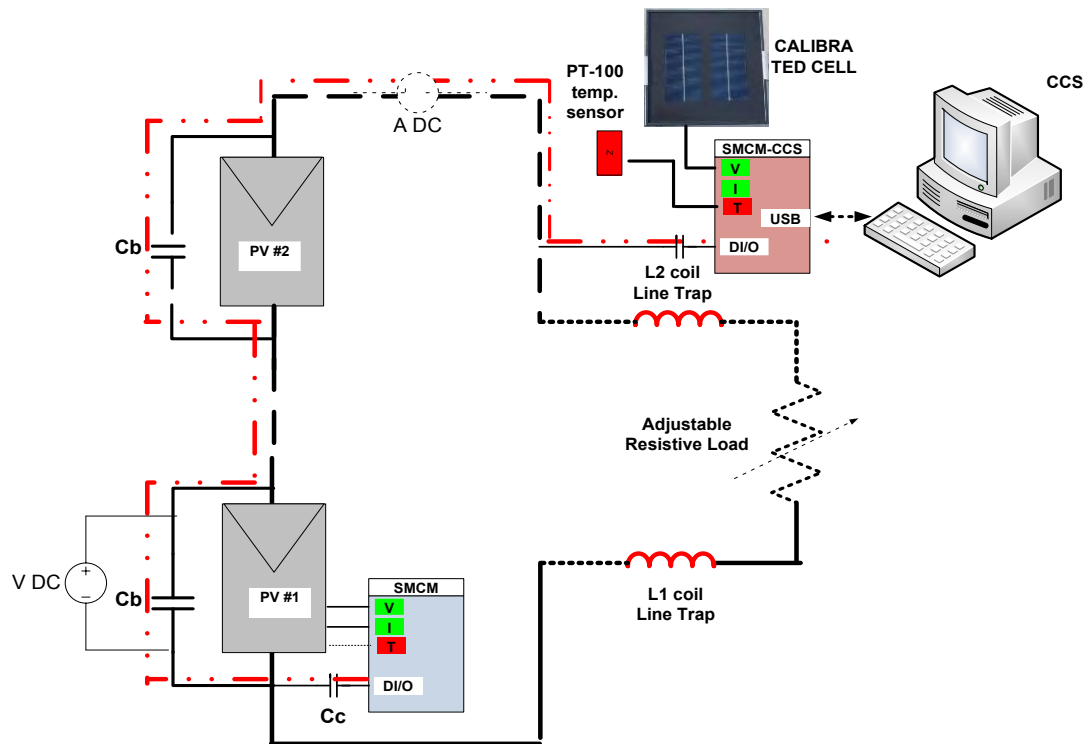
Figure 6.1. EPS PV Lab PV test bench layout

The EPS PV Lab prototype assembled is comprised of two Isofotón ISF-245 PV modules, with a PT100 RTD temperature sensor for back-plane PV module temperature monitoring (Figures 6.2 and 6.3). The effective incident irradiance is monitored by means of an Atersa calibrated photo cell and an additional Pt100 RTD is used for ambient temperature measurement. The cell has been assembled in the plane of the PV modules, so that to obtain the effective irradiance incident on their plane. This allows to have incident irradiance data compensated with tilt and orientation angles, ambient temperature and air mass index. The SMCM and SMCM-CCS are connected to the PV modules, the DC power line and the CCS computer.

The whole PV modules set has been assembled on a metallic structure, south oriented in order to comply with the optimal tilt angle, corresponding to Málaga latitude, that is of 36º as it can be seen in Figure 6.2, so as to ensure that the PV modules are able to deliver the maximum power depending on applying ambient conditions.

Figure 6.2. EPS PV Lab test bench PV module and calibrated cell assembly Test Bench structure

Figure 6.3. EPS PV Lab PV module back-plane temperature measurement with PT100 RTD

Figure 6.4. EPS PV Lab test bench incident irradiance monitoring calibrated cell detail.

Figure 6.5 shows the outdoor measurement bench, with the SMCM and SMCM-CCS modules, together with the CCS and additional laboratory instrumentation used to verify the system signals.

Figure 6.5. EPS PV Lab outdoor measurement bench.

Additionally, in order to facilitate the measurement process from indoor facility, both PV modules, the calibrated cell and temperature sensors have been electrically wired to the PV Lab. The wiring of the PV modules comprises the connections to their positive and negative terminals, as well as to the protection diodes terminals of the connecting box. All the wiring is easily accessible in the lab test bench, in order to facilitate the connection of the laboratory measurement instrumentation and the electronic loads as well as, it can be seen in Figure 6.6.
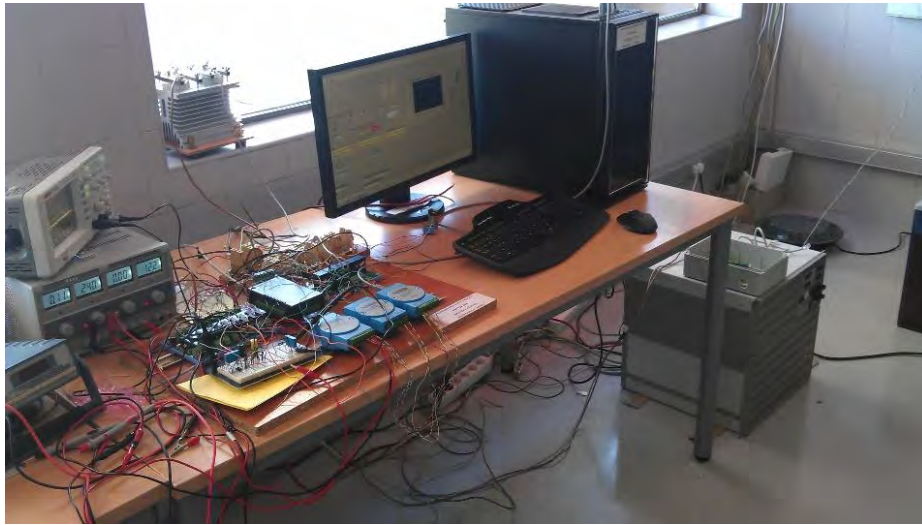
Figure 6.6. PV test assembly at the EPS PV Lab

6.2.1. Elements and instruments that compose the laboratory test bench

The different instruments and elements that constitute the laboratory test bench are:

- Digital storage 2 channels oscilloscope
- Digital multimeter
- Double power supply
- Connection rack
- PC (CCS)
- SMCM prototype
- SMCM-CCS prototype
- Adjustable electronic resistive load

- Isofoton ISF-245 PV modules (x 2)
- Atersa calibrated cell

6.2.2. Isofoton ISF-245 PV module main electrical characteristics

Main electrical parameters of the Isofoton ISF-245 PV module are included in Table 6.1. These have been extracted from the manufacturer´s data sheets. These are referred to STC conditions.

Table 6.1. Isofotón ISF-245 PV module data-sheet electrical parameters at STC

Electrical parameter	Value
Rated Power (*Pmax*)	245 W
Open-circuit Voltage (V_{OC})	37,3 V
Short-circuit Current (I_{SC})	8,70 A
Maximum power point Voltage (*Vmax*)	30,2 V
Maximum power point Current (*Imax*)	8,12 A
Efficiency	14,8 %
Power tolerance (% *Pmax*)	+/-3%

For model based translated estimation, following data have been considered: main parameters are the Nominal Operating Cell Temperature (NOCT), which is the reference for the cell temperature estimation under real outdoor conditions, and corresponding temperature coefficients, α for the PV module current, β for the voltage and γ for the PV module output power (Table 6.2).

Table 6.2. Isofotón ISF-245 PV module data-sheet operational characteristics

Electrical parameter	Value
Maximum system voltage	1000 V
Reverse current limit (series Fuse Rating)	20 A
Nominal Operating Cell Temperature (NOCT)	45+/-2 ºC
Temperature coefficient of *Pmax*	-0,464 %/K
Temperature coefficient of V_{OC}	-0,323 %/K
Temperature coefficient of I_{SC}	0,042 %/K

6.2.3. Atersa calibrated cell electrical characteristics

The effective sun irradiance in the plane of the PV modules is sensed by means of a PV calibrated cell, which gives a temperature compensated output signal in mV proportional to the incident irradiance. The main advantage of this procedure is that the calibrated cell output does also compensate the irradiance signal regarding the applying AM index, atmospheric conditions and angle of incidence. The electrical characteristics are referred in Table 6.3.

Table 6.3. Atersa calibrated cell electrical characteristic

Electrical features	Configuration 1	Configuration 2
Voltage – radiation correspondence	65 mV dc per output=1000W/m^2	100 mV dc per output=1000W/m^2
Measurement intrinsic error	+/- 0,1 %	+/- 0,2 %
Measurement error of the Reference Pattern	+/- 2,0 %	+/- 2,0 %
Impedance connected to the output	>= 10 Mohms	

The manufacturer recommends the calibration of referred cell in a qualified laboratory. In our case, this task has been performed in the UMA RREE´s lab. For the 100 mV @ 1000 W output option, the calibration constant results to be y=0,99337 x as indicated in Figure 6.7.
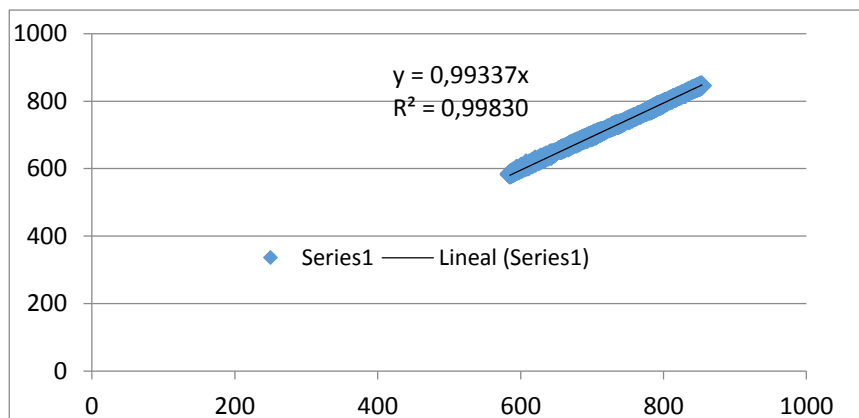
Figure 6.7. Atersa cell output signal calibration curve.

6.3 MEASUREMENT PROCEDURE

The functionality of the SMCM as a PV modules data monitoring and transmission device is demonstrated upon the results of the measurements performed in the laboratory test bench previously described. The aim is to put in value the SMCM and SMCM-CCS prototypes to validate the proposed idea. For this purpose, several experimental measures have been performed and resulting data have been used for the idea validation. The prototype assembly has been set-up for monitoring one of the PV modules operational parameters (V, I and T_m), together with the incident irradiance (G) and ambient temperature (T_a). The results together with the atmospheric conditions are depicted in following tables.

The digital counts resulting from the Analog to Digital Conversion (ADC) of the SMCM, transmitted to the SMCM-CCS through the DC power line have finally been routed to the CCS via USB.

In order to obtain corresponding voltage, current and module temperature values from the digital counts resulting from the measurement process, measuring chain equations have been applied, with their corresponding constants and coefficients, as seen previously.

The PV module Voltage (V) has been obtained applying equation (6.1):

$$V = NV_{ADC} \cdot V_q \cdot k_{VC} \qquad (6.1)$$

Where NV_{ADC} are the digital counts resulting from the AD conversion; V_q is the ADC quantization voltage (V_q=3,52 mV) and k_{VC} is the Voltage Analog Front End (VAFE) measuring chain calibrated constant (K_{VC}=11,885 V/V).

Meanwhile, the current of the PV module (I) is obtained applying the Current Analog Front End measuring chain equation:

$$I = \left[\left(NI_{ADC} \cdot V_q \cdot k_{IC} \right) - 2,5V \right] \cdot k_{ISENS} \cdot 0,5 \qquad (6.2)$$

where NI_{ADC} are the digital counts resulting from the AD conversion of the current sensor output signal; V_q is the already referred quantization voltage; k_{IC} is the

current AFE (IAFE) measuring chain calibrated constant (k_{IC}=1,1 A/A). Furthermore, k_{ISENS} is the current sensor calibrated constant (k_{ISENS} =9,6 A/V); in this case, divided by 2, since the current sensor has been connected with two loops of the PV module wire, so that to have more reliable values, as indicated in Figure 6.8.
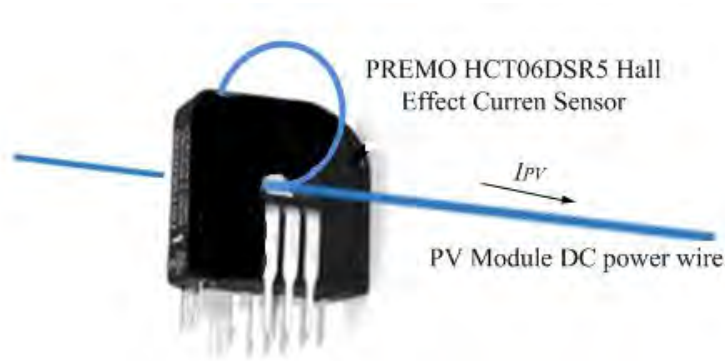
Figure 6.8. PREMO HCT06DSR5 Hall effect current set-up for non-invasive current measurement.

According to the measured module operational parameters (*V* and *I*), the resulting power output of the PV module has consequently been obtained by equation (6.3):

$$P = V \cdot I \tag{6.3}$$

Finally, the module temperature is obtained by following equation:

$$T_m = NT_{ADC} \cdot V_q \cdot k_{TC} \tag{6.4}$$

where NT_{ADC} are the digital counts resulting from the ADC of the module temperature sensor; V_q is the ADC quantization voltage (V_q=3,52 mV) and k_{TC} is the Temperature Analog Front End (TAFE) measuring chain calibrated constant (k_{TC}=24,828 V/V).

6.4 EXPERIMENTAL DATA OBTAINED WITH ISOFOTON PV MODULES

The first validation approach has been performed based on field measurements obtained in the EPS PV Lab experimental test bench, where the SMCM has been connected to one of the PV modules for V, I and T_m measurement. Additionally, a SMCM-CCS has been installed which has been in charge of the ambient incident effective irradiance monitoring, G (from the Atersa calibrated cell), the ambient temperature, T_a (by means of a Pt100 RTD) and to the CCS as a data concentrator.

In a first attempt, a total of 11 runs of 30 consecutive measurements each have been performed. This has allowed to have field data of the PV module operational parameters, under the applying outdoor conditions. For each of the runs, the 30 measurements have been tabulated and the mean and standard deviation values have been calculated. The resulting mean values and outdoor conditions are summarized in Table 6.4 and depicted in the graph of Figure 6.9 which represents the results in a similar way to the typical I-V and P-V curves, but constructed with the mean values of the 11 measurements. This justifies the lack of continuity of the curves. Despite the resulting graph, it can be seen that the procedure is capable of generating reliable data of the PV module operation.

Table 6.4. Mean values, STD deviation and outdoor conditions of readings

#	G (W/m²)	Ta (ºC)	Tm (ºC)	V (V)	I (A)	P (W)	Tm STD	V STD	I STD	P STD
1	197,3	23,4	28,0	6,8	0,92	6,32	0,06	0,42	0,02	0,40
2	201,4	23,4	31,3	12,6	0,89	11,17	0,07	0,61	0,02	0,64
3	223,2	23,8	31,7	12,8	0,92	11,78	0,07	0,64	0,01	0,58
4	199,3	23,5	33,2	20,0	0,84	16,91	0,06	0,59	0,01	0,50
5	217,4	23,6	33,1	27,8	0,85	23,56	0,06	0,47	0,02	0,68
6	274,4	24,1	33,1	31,5	0,69	21,74	0,06	0,45	0,02	0,52
7	229,0	23,1	33,2	32,1	0,55	17,77	0,07	0,42	0,01	0,45
8	203,4	24,1	33,1	32,2	0,46	14,90	0,06	0,44	0,02	0,54
9	200,4	24,0	33,0	32,4	0,39	12,54	0,08	0,44	0,02	0,63
10	204,1	24,0	33,0	32,6	0,35	11,28	0,10	0,43	0,01	0,47
11	226,6	24,1	33,0	32,7	0,32	10,40	0,07	0,44	0,01	0,42

On the basis of previously indicated equations and applying corresponding current and voltage measurement chains coefficients and constants, the resulting values of the PV module monitored voltage, current and temperature are described in Table 6.5.

This table corresponds to the 30 measurements of the run #5, which is the one that has allowed to obtain the bigger value of output power, under applying outdoor conditions, namely a sun irradiance of 217 W/m^2 and a module temperature of 33,1 ºC.

Column NI_{ADC} shows the digital counts resulting from the PV module current measurement ADC process; N_{VDC} correspond to the PV module voltage AD conversion; T refers to the module temperature; V column represents the converted resulting values of the PV module voltage; I column corresponds to the measured currents, while P_{PV} is the resulting power obtained by the product of voltage and current as specified by equation (6.3).

Table 6.5. Results of run #5
(maximum output at G=217 W/m2 and T_m=33,1ºC)

meas #	NTADC	NIADC	NVADC	T_m (ºC)	V (V)	I (A)	P (W)
1	379	691	667	33,1	27,9	0,84	23,5
2	379	691	652	33,1	27,3	0,84	23,0
3	379	691	652	33,1	27,3	0,84	23,0
4	379	691	662	33,1	27,7	0,84	23,3
5	380	692	677	33,2	28,3	0,86	24,4
6	379	692	682	33,1	28,5	0,86	24,6
7	379	692	660	33,1	27,6	0,86	23,8
8	378	691	652	33,0	27,3	0,84	23,0
9	380	692	655	33,2	27,4	0,86	23,6
10	380	692	668	33,2	27,9	0,86	24,1
11	380	693	682	33,2	28,5	0,88	25,1
12	379	692	672	33,1	28,1	0,86	24,2
13	379	691	652	33,1	27,3	0,84	23,0
14	379	691	650	33,1	27,2	0,84	22,9
15	379	691	660	33,1	27,6	0,84	23,3
16	379	692	675	33,1	28,2	0,86	24,3
17	380	692	683	33,2	28,6	0,86	24,6
18	379	692	666	33,1	27,9	0,86	24,0
19	380	691	651	33,2	27,2	0,84	22,9
20	379	692	653	33,1	27,3	0,86	23,5
21	380	692	664	33,2	27,8	0,86	23,9
22	380	691	679	33,2	28,4	0,84	23,9
23	379	691	678	33,1	28,4	0,84	23,9
24	380	692	659	33,2	27,6	0,86	23,7
25	379	691	652	33,1	27,3	0,84	23,0
26	379	691	654	33,1	27,4	0,84	23,1
27	377	688	667	32,9	27,9	0,79	22,0
28	379	691	678	33,1	28,4	0,84	23,9
29	378	690	672	33,0	28,1	0,82	23,2
30	379	690	652	33,1	27,3	0,82	22,5
		Mean values		**33,1**	**27,8**	**0,85**	**23,6**
		Standard Deviation		0,06	0,47	0,02	0,68

Additionally, several different cases are described. The *I-V* and *P-V* curves have been obtained in a single run under referred outdoor conditions. In the corresponding graphs, for comparison purposes, the STC curve, the ROC translated one and the corresponding to the instant readings are represented.

The first case analyzed corresponds to a measurement made at G=810 W/m^2 and T_m=43,9 ºC. Figure 6.9 shows the *I-V* at STC (blue solid line), translated to ROC (red dashed line) and read (green dotted line). Figure 6.10 depicts corresponding *P-V* curve. It can be seen that the read results follow the translated model.
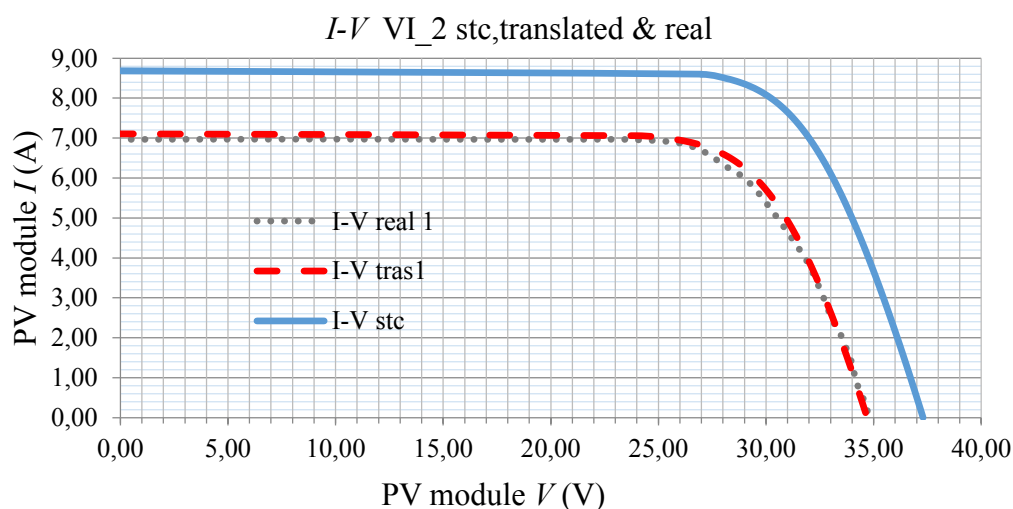
Figure 6.9. STC, translated and real measured *I-V* curves of VI_2 reading at G=810 W/m^2 and T_m = 43,9 ºC
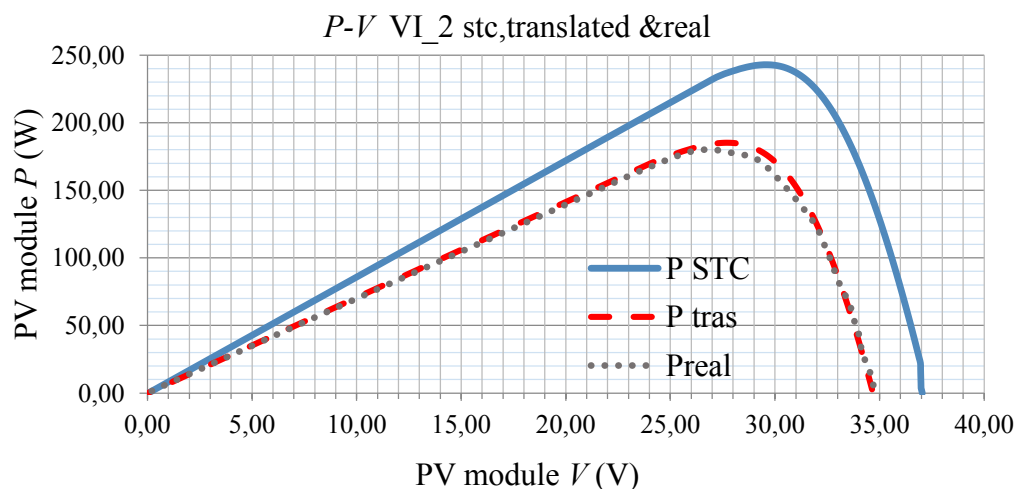
Figure 6.10. STC, translated and real measured *P-V* curves of VI_2 reading at G=810 W/m^2 and T_m = 43,9 ºC

In the second case analyzed (VI_3), which corresponds to a measurement made at G=820 W/m^2 and T_m=46,6 ºC, it will be seen the effect of partial shadowing at the boundaries of the 25 V. Figure 6.11 shows the I-V at STC (blue solid line), translated to ROC (red dashed line) and read (green dotted line). This shadowing seems to have reduced the P_{mp} and hence the module temperature at that point, which has made the open circuit voltage (V_{OC}) to result bigger than expected according to the translated curve for given outdoor conditions. In Figure 6.12 corresponding P-V STC, translated and real curves are depicted.
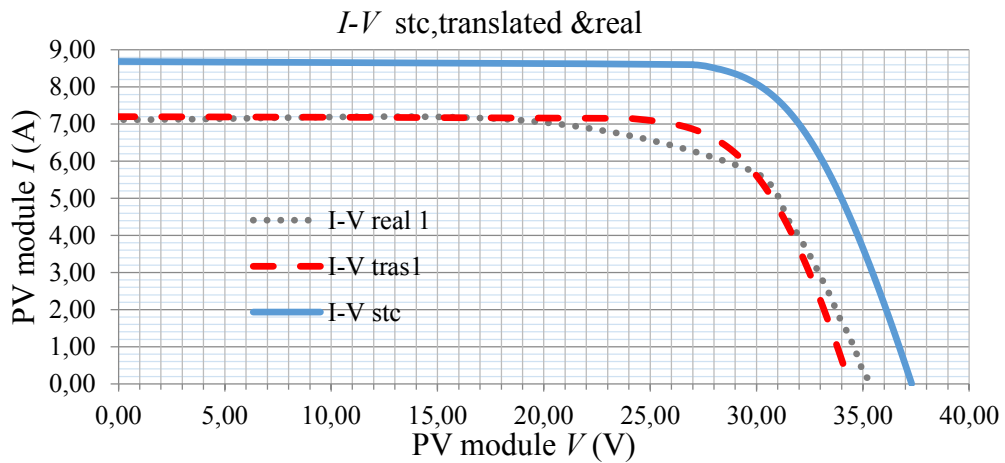
Figure 6.11. STC, translated and real I-V curves of VI_3 reading at G=820 W/m^2 and T_m= 46,6 ºC
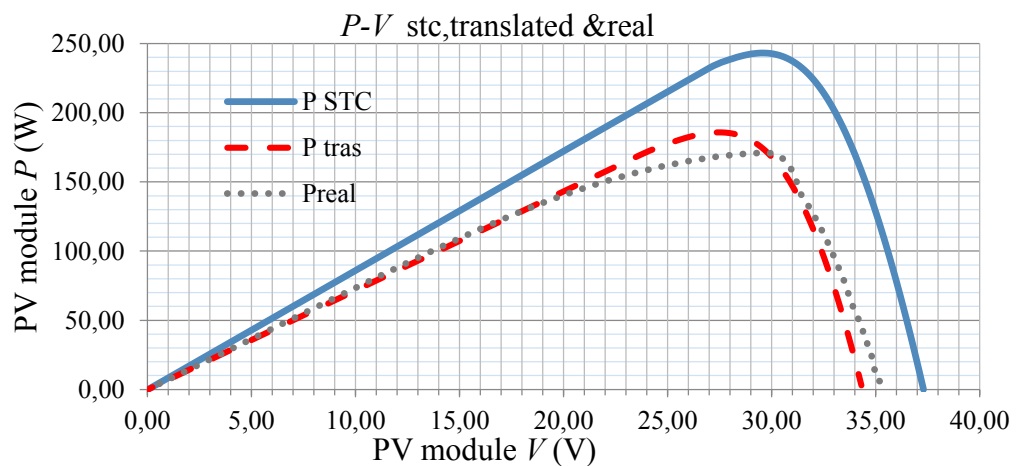
Figure 6.12. STC, translated and real P-V curves of VI_3 reading at G=820 W/m^2 and T_m = 46,6 ºC

In the third case analyzed (VI_4), the ambient conditions were G=750 W/m^2 and T_m=48,2 ºC. The curves show a behavior of the module, subject to a partial shadowing and the negative effect of the ambient temperature, which results in a significant reduction in the V_{OC} read, vs the estimated translated one. This can be seen in Figures 6.13 (*I-V* curves) and 6.14 (*P-V* curves).
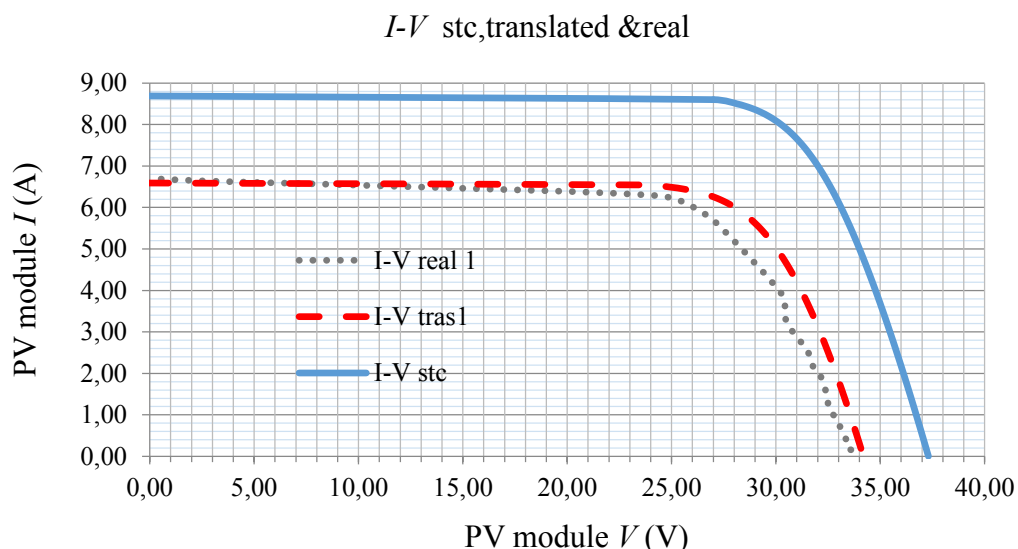
Figure 6.13. STC, translated and real time measured *I-V* curves of VI_4 reading at G=750 W/m^2 and T_m= 48,2 ºC
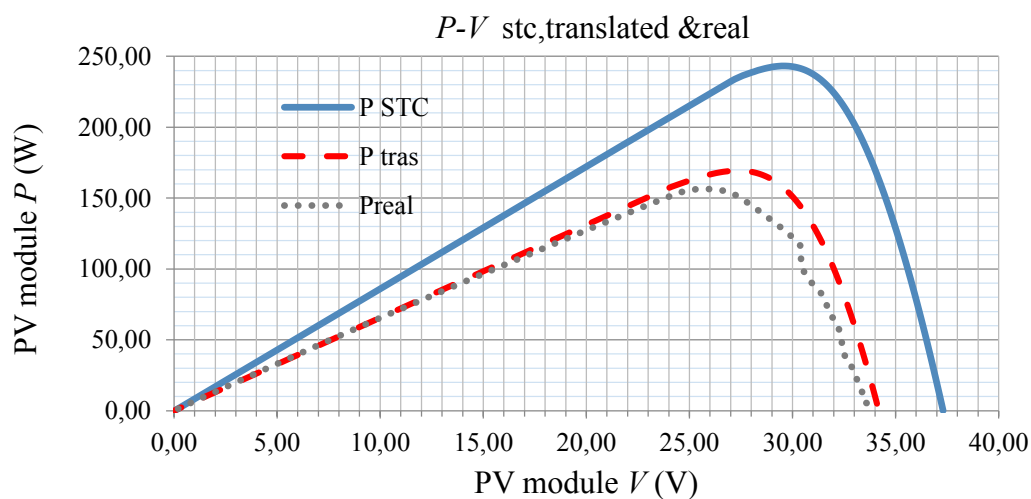
Figure 6.14. STC, translated and real time measured *P-V* curve of VI_4 reading at G=750 W/m^2 and T_m = 48,2 ºC

Finally, the fourth case analyzed corresponds to a low irradiance $G=$ 720W/m² and a module temperature of 42,3 ºC. These conditions result in a value of I_{SCt}=6.32 A) and a value of $V_{OCt=}$34.9 V and consequently, the maximum power point results to be P_{mpt}=166,6 W.

In Figure 6.15, both the STC, translated and real measured *I-V* curves are depicted. There it can be seen that the STC and translated curves are correlated. In the boundaries of V_{OC}=7 V, the graph shows the effect of a partial shadowing of the module, which significantly reduces the resulting current. Corresponding P-V curves are drawn in figure 6.16.
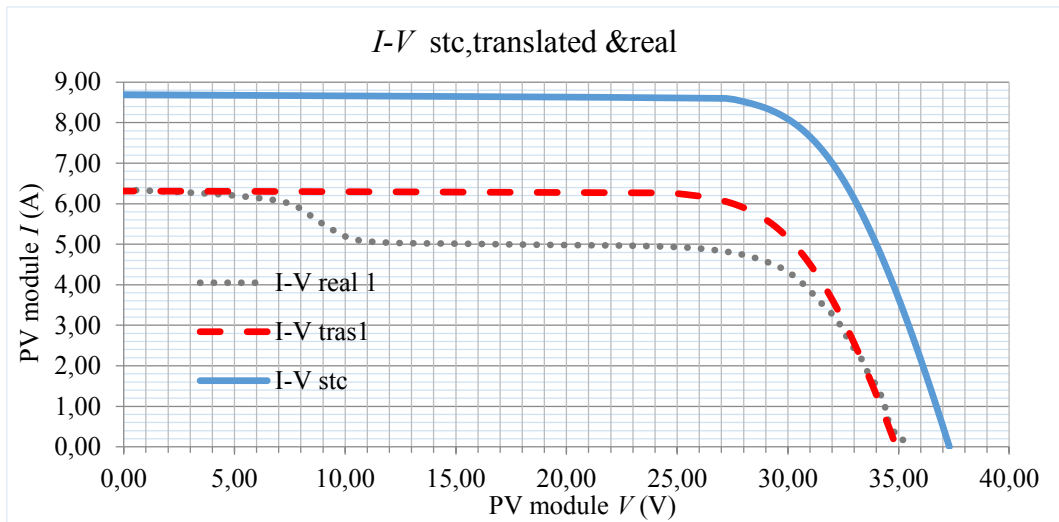
Figure 6.15. VI_1 STC, translated and measured data *I-V* curves at G=720 W/m² and a module temperature T_m=42,3 ºC.
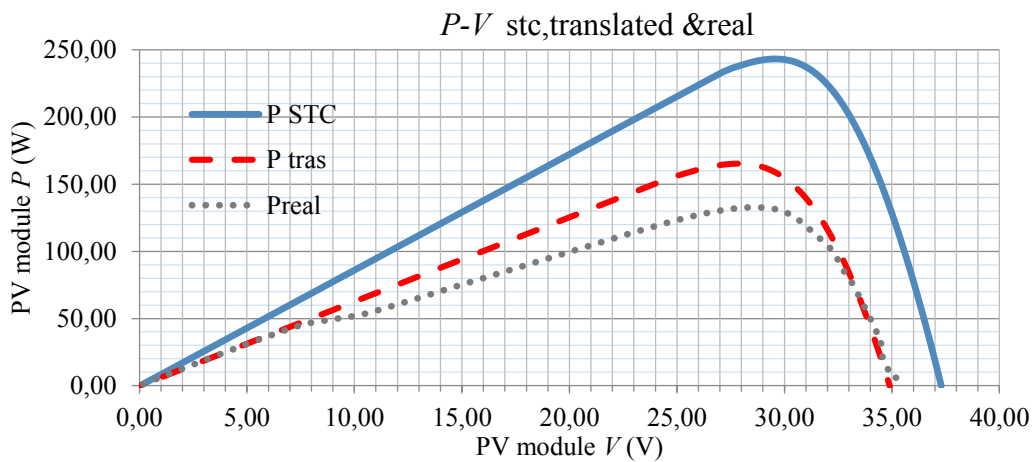
Figure 6.16. VI_1 STC, translated and measured data *P-V* curves at G=720 W/m² and a module temperature T_m=42,3 ºC.

6.5 CONCLUSIONS

The aim of described proposed SMCM and SMCM-CCS as a PV modules level monitoring system was to have the capability of real time parameters monitoring and further processing. In this chapter, the SMCM functionality has been demonstrated for data monitoring, which has made possible to get the PV module real time *I-V* and *P-V* fingerprint. This evidence has been additionally confirmed in a controlled laboratory environment with laboratory instrumentation and electronic loads and a specifically developed monitoring and data processing software.

The former challenge of proposed device is its capability to measure real time I, V and T_m values of the PV module under applying ROC, in large dimensions PV fields. The scenario in this case is significantly different. The maximum power point in which the PV module is working will depend, as previously stated on the incident irradiance and on the ambient temperature on a first step and subsequently on other factors and ambient conditions. The specific coordinates of the PV module maximum power point power will finally depend on the load faced by the PV modules assembly. Since the system is intended to be working in grid connected large PV facilities, it is considered to be working in the MPP. Hence, the initial key factors that define this point are the ambient conditions related previously. If these conditions are met, the PV module should be working properly and the maximum power expected to be obtained.

It is obvious the necessity of SMCM monitored PV modules operating parameters. Its comparison with the translated values, by means of proposed translation model helps to identify if it is working properly.

Under these premises, the SMCM system is a resourceful tool for failing PV modules real-time identification. If the measured generated power is abnormally smaller than the expected one, the corrective actions must be undertaken. This technology grants the financial operation of the whole plant, since abnormally operating modules can be immediately identified and maintenance activities can be significantly improved. This is a required way to ensure the optimal financial performance of the whole PV plant.

Chapter 7

PV MODULES PERFORMANCE RATIO ANALYSIS

Once it has been demonstrated the possibility to monitor the operational parameters at PV module level, the main advantage of proposed technology is the possibility to have real-time information of their performance, under applying operating conditions.

The Performance Ratio of a PV plant, so far, has been related to the energy it generates and the maximum energy it might supply if it were working under STC conditions. In this chapter, a specific instant Performance Ratio related to the power generated by a single PV module will be defined. This parameter gives us the power losses of the PV module, in relation with the power they might deliver under the so called standard conditions.

7.1. INTRODUCTION.

One of the parameters generally considered to know the performance of a photovoltaic system is the performance ratio (*PR*). According to the EN 61724 standard, this parameter is defined in terms of energy and is used for quantifying the overall losses of a photovoltaic system. It is usually referred as a daily *PR* value, a daily average monthly *PR* value or in many cases, as a daily average yearly *PR* value.

This parameter has been and is actually broadly used in the literature. The estimation is usually based on the system energy yield and resulting performance ratio [9]. This performance is based on manufacturer´s data sheet parameters, which are generally referred to Standard Test Conditions (STC), namely: an irradiance (G_0) of 1000 W/m^2, temperature of the cell (T_c) of 25 ºC and solar spectrum AM=1,5.

In this sense, King et al, from Sandía National Laboratories, describe in [2] a model of procedure for PV array performance estimation. This model is based on previous work presented by King et al. [3]. Furthermore, Gokmen et al. highlight the convenience of detecting faulted PV modules in [4], as well as more recently, Bastidas et al. in [5].

This topic has been treated in the literature under different scopes. Sidrach et al. in [6] analyze a 2 kWp installed in the University of Málaga, by determining the *I-V* curve of referred PV modules. Whitfield and Osterwald in [7] make the focus on the uncertainty related to the PV modules outdoor performance determination. More recently, Piliougine et al. in [8] describe the results of experimental measurements of PV modules under outdoor conditions. In most of the cases, the performance estimation is related to the amount of energy generated in a given time frame period in comparison with the maximum energy that theoretically might have been generated [10]. In the same line, B. Marion et al. in [11] consider the PV plant energy production performance, taking into account the DC/AC inverters, as Dolara et al. in [12]. Furthermore, Dolara et al. introduce a more specific instantaneous final yield in [13].

The main utility of this parameter is that it informs us about the overall losses of a PV system during a period of time, quantified in terms of energy vs. the energy it might have produced if in referred period it would have remained under the so defined as standard conditions (*PR*=1).

Consequently, the PR_{DC} is a parameter that gives us the overall losses of the module, without identifying their causes. Usually, PR_{DC}<1.0, but it might happen that PR_{DC}>1.0 if operating conditions were better than the STC ones, for which PR_{DC}=1.0 is considered.

The difference between the resulting experimental value of PR_{DC} and the corresponding value at STC (PR_{DC} =1.0) quantifies the overall Losses Factors (*LF*) under these specific operating conditions and consequently,

$$PR_{DC} = (1 - LF) \tag{7.1}$$

There are many and different adverse conditions that may negatively affect the energy performance of the PV modules.

All these losses may have a significant impact in final energy production. Although not all of them have the same influence, in general terms, this can be tabulated as per [3]. Typical values of energy losses are summarized in Table 7.1.

Table 7.1. PV plant Estimated Energy Losses Factors Values – LF_j

Item	Factor	Estimated value %	LF_j
1	Angle of Incidence	3	0.97
2	Radiation spectral conditions (depending on PV technology)	3	0.97
3	Modules mismatches	3	0.97
4	Non tracking of MPPT	1 - 3	0.99-0.97
5	Nominal power tolerance	3 to 10	0.97-0.9
6	Partial shadowing (dust, bird drops, trees leaves, etc…)	2 - 7	0.98-0.93
7	Ohmic losses	3	0.97
8	Temperature losses	3 - 10	0.97-0.9

It can be considered that:

$$LF = \Sigma(LF_j)$$
(7.2)

The losses detailed in this table refer to average energy losses and are indicative values experimentally obtained in PV installations. When the purpose is to quantify the instant power losses for PV modules prognosis purposes, its quantification cannot be based on previous losses factors.

Additionally to these losses, those due to defective modules must also be considered, which, by definition cannot be quantified initially.

In order to quantify the overall losses of the system, the energy that it has generated used to quantify the *PR* is measured at the inverter output or at the grid connection point. Nevertheless, if we want to quantify the losses produced in a specific part of the system, generator, inverter, etc... we can use the same concept of performance ratio just calculating the energy balance in this specific point of the system.

In the same way, the time frame in which the energy balance is quantified can be reduced so that to obtain an instantaneous value. In this case, the instant performance ratio relates us the losses produced in the system or in a specific part of it, at a given moment in time. Moreno-Saez et al. have already used this concept in [14].

Hence, in this work, the proposal is made to define an instantaneous performance ratio that allows us to quantify in a given moment in time the losses produced in a PV module and by extension, in a PV generator.

We define the instant performance ratio of a PV module or of a PV generator $PR^i{}_{DC}$ according to following equation:

$$PR^i{}_{DC} = \frac{\dfrac{P_i}{P_{mSTC}}}{\dfrac{G}{G_0}}$$
(7.3)

where P_i is the output power of the PV module; P_{mSTC} is the module power at STC; G is the incident global irradiance in the module surface and G_0 is the global irradiance at STC (1000 W/m²).

In our case, the instantaneous losses that a PV module can be submitted to are reflected in the resulting value of instantaneous Performance Ratio and can be divided in two major groups. On one hand, we find the losses due to the fact that the PV module is not working under the so called standard conditions. These losses are considered as non-avoidable. On the other hand, we have the losses due to a defective operation of the PV module or to abnormal conditions not related to the climatic conditions. These are mainly due to partial shadowing of the PV modules, soiling or presence of dust on its outer surface. These losses will be considered as avoidable, since by means of corresponding correcting actions, they can be suppressed.

7.2. PHOTOVOLTAIC MODULES INSTANTANEOUS PERFORMANCE RATIO ANALYSIS

In this chapter, a comparison protocol is proposed between two different concepts of PR_{DC}. Being the PV module working under Real Outdoor Conditions (ROC), an experimental value of the PR^i_{DC} is obtained, according to equation (7.3). On the other hand, a new value of PR^t_{DC} obtained by means of the ROC translated PV module operational parameters based model is proposed.

The comparative analysis of both parameters will allow to estimate the losses that each PV module is generating and their possible causes. According to the obtained results corresponding correcting actions might be programmed.

For a given sun irradiance and ambient temperature (T_a), the power generated by a PV module can be significantly constrained due to both predictable and unpredictable Losses Factors.

The correct identification of the different losses can be a simple task in case of small dimensions PV plants. Nevertheless, in huge dimensions PV plants, this can be a harsh task. As it has been seen, the so-called non-avoidable losses are related to the specific climatic conditions under which the PV module is operating. These losses can be approximately quantified, any time the operating conditions are known.

Nevertheless, the focus is put on the so-called avoidable losses, which must be correctly quantified. These losses relate us either failures of the PV generator, shadowing or presence of soiling. It is mandatory to define immediate corrective actions, so that to avoid these losses to be maintained in time. Should this happen, the cumulated financial losses could become significant if the PV module working abnormally were not immediately identified and subsequently, the causes corrected.

In our case, the focus is made on the power generated in a given moment in time and its comparison with the maximum power it could be extracted under applying outdoor conditions. Taking this into consideration, the PV modules performance estimation requires that the PV modules operating parameters, namely: voltage (V_i), current (I_i) and module temperature (T_{mi}) to be monitored [9]. This will allow us to estimate the instant electric power delivered by the PV module, under given operating outdoor conditions. Once this information is processed, by means of corresponding mathematical model, an estimation is made of the maximum power that theoretically might be generated by the PV module under outdoor existing conditions, as well as estimated Losses Factors.

The proposed analysis allows us to obtain additional information related the system losses. This procedure is not based on possible *LF* that might apply, but, nevertheless, allows to identify some of the causes of the energy yield losses.

The instant value of the module performance ratio PR^i_{DC} is calculated according to equation (7.3). This model allows to obtain the real-time performance of the PV module. Final result is basically a consequence of the different adverse conditions that might apply at a given moment in time, such as the ambient temperature, shadowing, dust, soil and possible module degradation or failure.

Taking into consideration that the power that a PV module can generate depends on ROC that apply, the ROC translated PR^t_{DC} is defined. This proposed PR^t_{DC} allows to quantify the maximum performance ratio that a PV module can generate under ROC applying conditions. It can be expressed as:

$$PR^t_{DC} = \frac{\dfrac{P_t}{P_{mSTC}}}{\dfrac{G}{G_0}} \qquad (7.4)$$

where P_t corresponds with the maximum power that the PV module might generate at ROC; P_{mSTC} is the maximum power that the PV module might generate at STC, according to the manufacturer´s data sheets; G is the incident global irradiance on the plane of the PV modules and G_0 is the reference irradiance at STC ($G_0 = 1000$ W/m^2).

This PR^t_{DC} gives a performance ratio value corrected in temperature and in effective irradiance, compensating the AOI and the incident spectral irradiance any time the global irradiance has been measured by means of a calibrated solar cell of the same technology than the PV modules. That is, this would be the maximum PR that theoretically might be obtained from the module under existing ROC, without considering other losses.

Both parameters PR^i_{DC} and PR^t_{DC} can be compared and the differences between both of them will allow to estimate the possible origin of the losses. The difference between both of them will essentially refer to losses due to shadowing (partial, total or temporary) and soil. Hence, the resulting value of PR^i_{DC} gives us the module overall real losses, while PR^t_{DC} tells us which would be the losses values at a given irradiance and temperature.

It can be expected that the value of PR^t_{DC} were bigger than the experimentally obtained value of PR^i_{DC}. If the difference between both parameters is comprised into the error margins estimated for the theoretical model, it can be deduced that the PV module is operating correctly, as it might be expected if it were under applying climatic conditions. A significant difference between both of

them would report that the module were affected of losses that cannot be explained by the specific climatic conditions under which it is working.

Consequently, once the PR^i_{DC} has been obtained, it can be deducted the overall losses that are affecting the PV module, due to applying outdoor conditions (that cannot be avoided) and other adverse circumstances that might be upgraded with corresponding corrective actions. This term is called instant losses (L^i_{DC}) and given by:

$$L^i_{DC} = 1 - PR^i_{DC} \qquad (7.5)$$

On the other hand, theoretical losses are quantified to be those that the module should have at a given irradiance and temperature, which make the module work away of the STC conditions and are considered as non-avoidable losses. This is the translated losses (L^t_{DC}) given by:

$$L^t_{DC} = 1 - PR^t_{DC} \qquad (7.6)$$

The difference between both losses factors indicates the losses that are consequence of an abnormal situation that might further be corrected, such as:

- Partial or total shadowing (permanent or temporary)
- Presence of dust and soil
- Defective PV module (defective PV cell)

This represents the effective losses (L^e_{DC}) that a PV module is submitted to and can be given by:

$$L^e_{DC} = L^t_{DC} - L^i_{DC} \qquad (7.7)$$

The procedure is summarized in the flow diagram of figure 7.1.
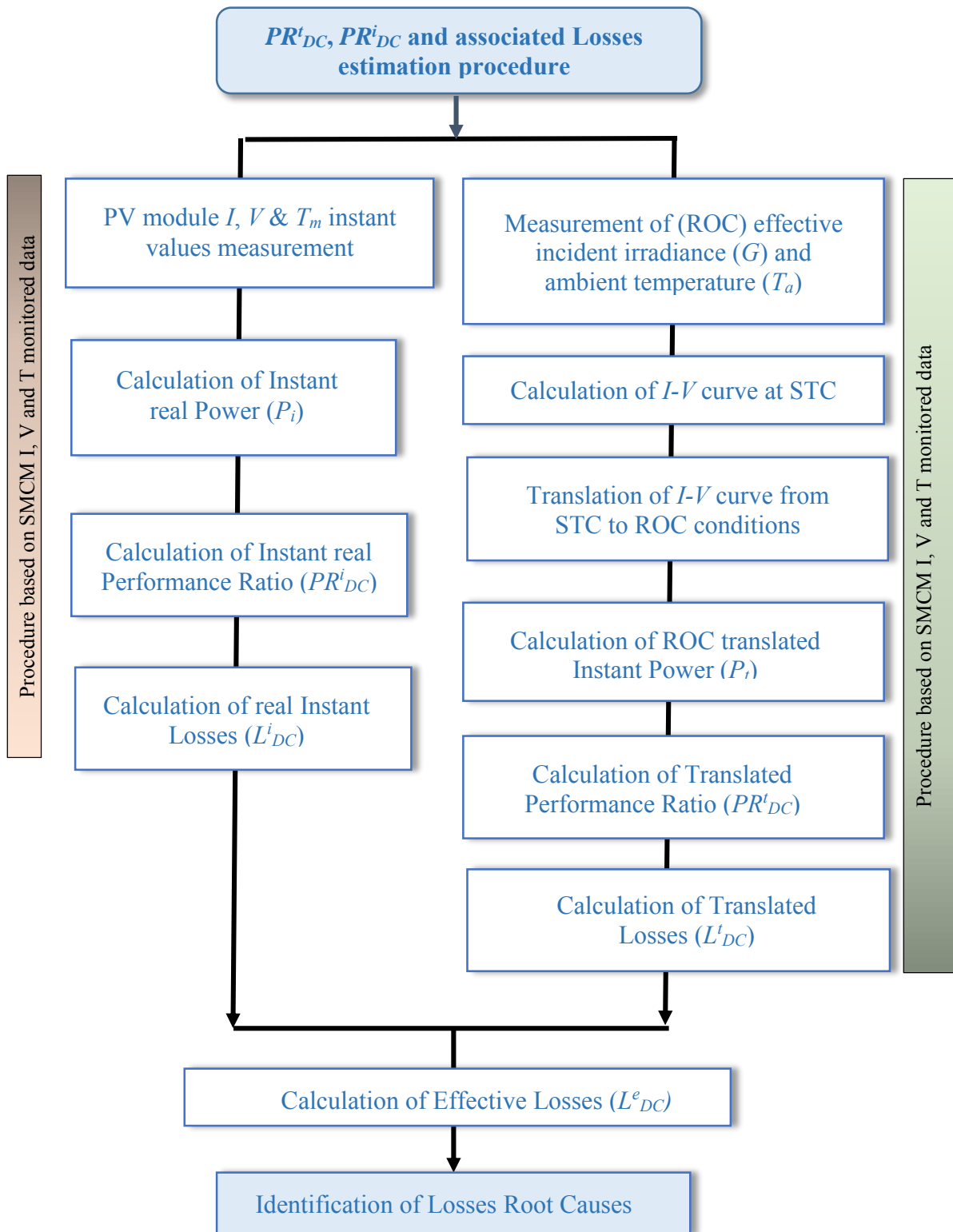
Figure 7.1. PR^t_{DC}, PR^i_{DC} and associated Losses estimation procedure

7.3. EXPERIMENTAL RESULTS

In order to demonstrate the viability of proposed procedure, several experimental data based cases have been analyzed. On one hand, proposed procedure has been applied to consolidated measurement data performed at the UMA RREE Lab. Additionally, the same procedure has been applied to experimental data obtained in the EPS PV Lab monitored data by means of the SMCM. Finally, a specific case has been analyzed, in which, in addition to the *I-V* curve measurement, the corresponding PV module has been subject to a thermography study. This has allowed to identify a PV module with a defective cell, as highlighted by the thermography.

7.3.1. Measurements on UMA RREE Lab Modules

With the aim of validating the proposed methodology, experimental *I-V* curves from the UMA RREE Lab Yocasol PV modules have been used. One clear sky day long measurements have been performed and partial shadowing have been applied in order to identify sudden significant decrease of power. Table 7.2 summarizes all the measurements performed, as well as the calculations of the different PR_{DC} like PR^i_{DC} and PR^t_{DC} and corresponding losses, namely L^i_{DC}, L^t_{DC} and the effective L^e_{DC}.

Table 7.2. Yocasol PV modules measurements performed at UMA RREE Lab

Read. Id #	Time	Ta (°C)	G (W/m2)	T_m (°C)	P_i	P_{mSTC}	P_{mt}	PR^i_{DC}	PR^t_{DC}	L^i_{DC}	L^t_{DC}	L^e_{DC}
ICV11	9:09:45	17	246	25,7	**44,11**	192,74	47,29	0,93	1,00	0,07	0,00	**-0,07**
ICV12	9:39:52	17,8	437	31,4	**79,27**	192,74	82,52	0,94	0,98	0,06	0,02	**-0,04**
ICV13	10:09:52	18,9	704	36,6	**131,97**	192,74	129,56	0,97	0,95	0,03	0,05	**0,02**
ICV14	10:39:52	20,5	719	47,4	**130,11**	192,74	131,59	0,94	0,95	0,06	0,05	**-0,01**
ICV15	11:09:52	22,1	809	55,1	**141,37**	192,74	146,25	0,91	0,94	0,09	0,06	**-0,03**
ICV16	11:39:52	24,4	884	57,1	**151,67**	192,74	157,76	0,89	0,93	0,11	0,07	**-0,04**
ICV17	12:09:52	24,8	958	55	**163,63**	192,74	169,65	0,89	0,92	0,11	0,08	**-0,03**
ICV18	12:39:52	23,2	395	41,1	**76,89**	192,74	80,86	0,92	0,97	0,08	0,03	**-0,05**
ICV19	13:09:52	23,7	457	38,6	**85,49**	192,74	84,76	0,97	0,96	0,03	0,04	**0,01**
ICV20	13:39:52	24,6	969	49,7	**167,19**	192,74	171,53	0,90	0,92	0,10	0,08	**-0,02**
ICV21	14:11:27	25,6	890	34,6	**161,50**	192,74	158,20	0,94	0,92	0,06	0,08	**0,02**
ICV27	14:35:27	25,8	854	56,2	**37,16**	192,74	152,23	0,23	0,92	0,77	0,08	**-0,70**
ICV22	15:10:52	26,7	828	60,6	**57,93**	192,74	147,57	0,36	0,92	0,64	0,08	**-0,56**
ICV23	15:34:45	26,1	731	50,6	**47,89**	192,74	131,61	0,34	0,93	0,66	0,07	**-0,59**
ICV24	16:10:45	24,9	612	38,5	**34,92**	192,74	111,66	0,30	0,95	0,70	0,05	**-0,65**
ICV25	16:34:45	26,3	478	43,3	**23,18**	192,74	87,94	0,25	0,95	0,75	0,05	**-0,70**
ICV26	17:16:45	23,5	165	24,5	**28,19**	192,74	31,46	0,89	0,99	0,11	0,01	**-0,10**

Additionally, in figure 7.2, it can be seen the evolution of PR^i_{DC} (green dotted line) and PR^t_{DC} (red dashed line) as the hours of the day are passing. In the point referred to the reading Id #ICV27, it can be seen a significant decrease of PR^i_{DC}, as a consequence of a partial shadowing that has lasted for several measurements. The minimum acceptable (given by the uncertainty of the proposed model, for a clear sky day) value of PR^t_{DC} is also represented (gray solid line).
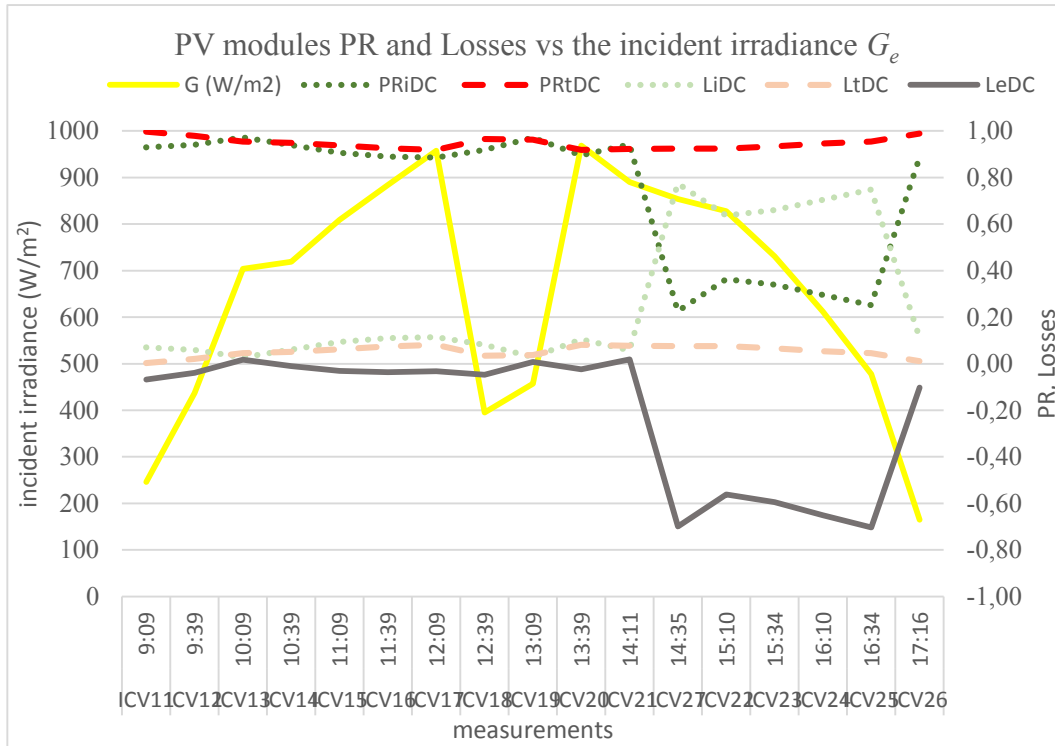
Figure 7.2. Evolution of PR^i_{DC}, PR^t_{DC}, L^i_{DC}, L^t_{DC} and L^e_{DC} vs. G

As it can be seen in Table 7.2, reading Id #ICV13 reaches the bigger resulting value of PR^i_{DC} (0,97) even bigger than the corresponding ROC translated resulting PR^t_{DC} (0,95), together with the smaller effective losses L^e_{DC} (0,02).

According to obtained data, it can be concluded that according to applying ambient conditions (T_m=36,6 ºC and G= 704 W/m^2), the proposed model says that the maximum power (P_{mt}) that might be delivered by the PV module would be 129,56 W/m^2, which signifies a PR^t_{DC} of 0,95. This result says that the losses with respect to the ideal at STC PR_{DC}=1 are 0,05.

These losses cannot be avoided. On the other hand, resulting PR^i_{DC}=0,97 indicates that the PV module is indeed delivering a better performance than the estimated one.

This can be due to the initial power tolerance given by the manufacturer (+5 %, -3 %). It can then be concluded that the PV module is performing correctly. Resulting losses are very small: L^i_{DC}=0,03; in this case, smaller than the expected ones translated to ROC, L^t_{DC}=0,05.

In the figure 7.3, corresponding *I-V* curves are depicted. On one hand, it can be seen that the *I-V* curve at STC (solid blue line), according to the data given by the manufacturer and obtained following the procedure described in chapter #2. On the other hand, the red dashed line represents the translated model from STC to ROC, as per equations (2.23) and (2.24). Finally, the green dotted line represents the curve of the measured values. It can be observed that this line follows the one corresponding to the ROC translated values. Nevertheless, starting at 24 V, it goes above it. This justifies the fact that the PR_{DCi} value were bigger than the PR_{DCt} value.
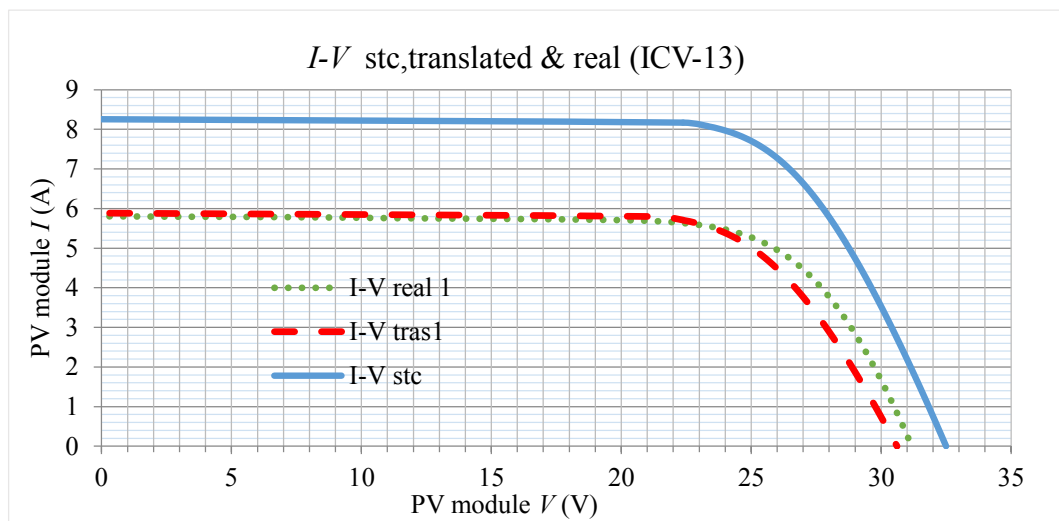
Figure 7.3. STC, translated and real *I-V* curves for Tm= 36,6 ºC and *G*=704 W/m^2

Figure 7.4 represents the *P-V* curve that illustrates previous considerations.
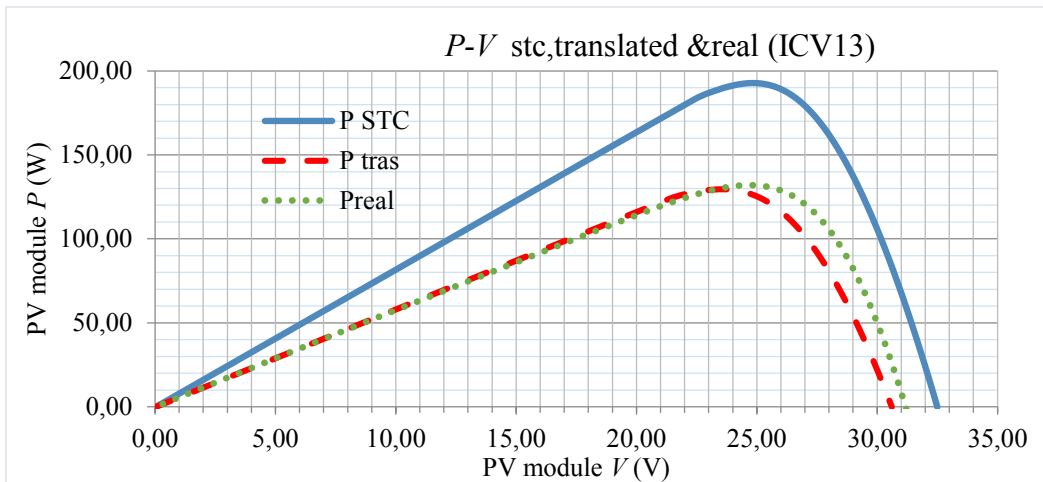
Figure 7.4. STC, translated and real *P-V* curves for T_m=36,6 ºC and G=704 W/m^2

In the opposite case, is the reading Id #ICV27 (performed at T_m=56,2 ºC and G=854 W/m^2) which represents the minor $PR\ ^i_{DC}$ (0,23), as well as the major effective losses (L^e_{DC}= -0,7). As it can be seen in figures 7.5 and 7.6, starting at 5 V, there is a significant reduction of the module current, which becomes almost null at 8,5 V. This leads to a significant reduction of the power generated.
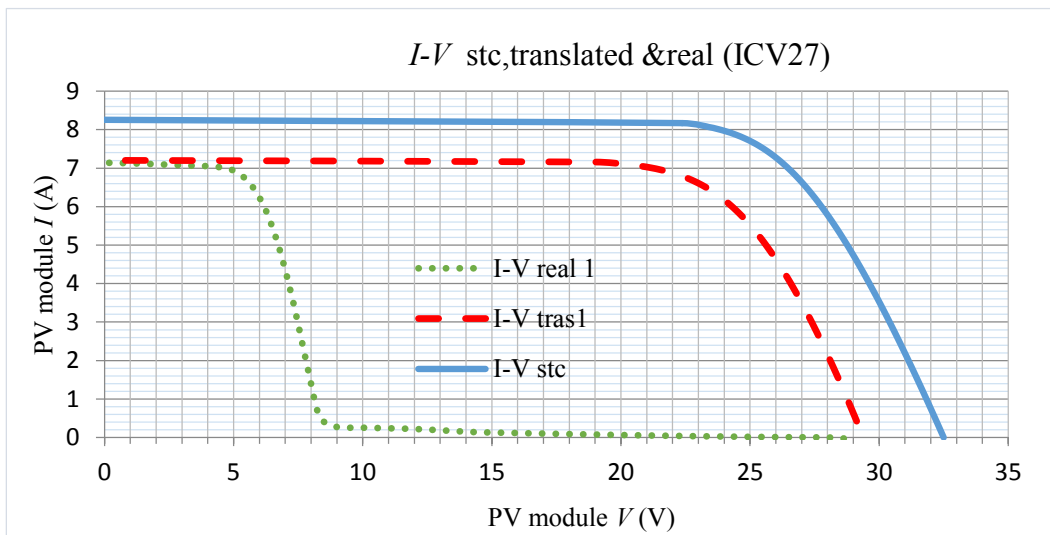
Figure 7.5. STC, translated and real *I-V* curves for T_m 56,2 ºC and G=854 W/m^2

In the same way, the graph that represents the *P-V* curves depicts previously described considerations. It can be observed that the power generated is reduced to its minimum value when the module voltage is in the surrounding of the 8,5 V.
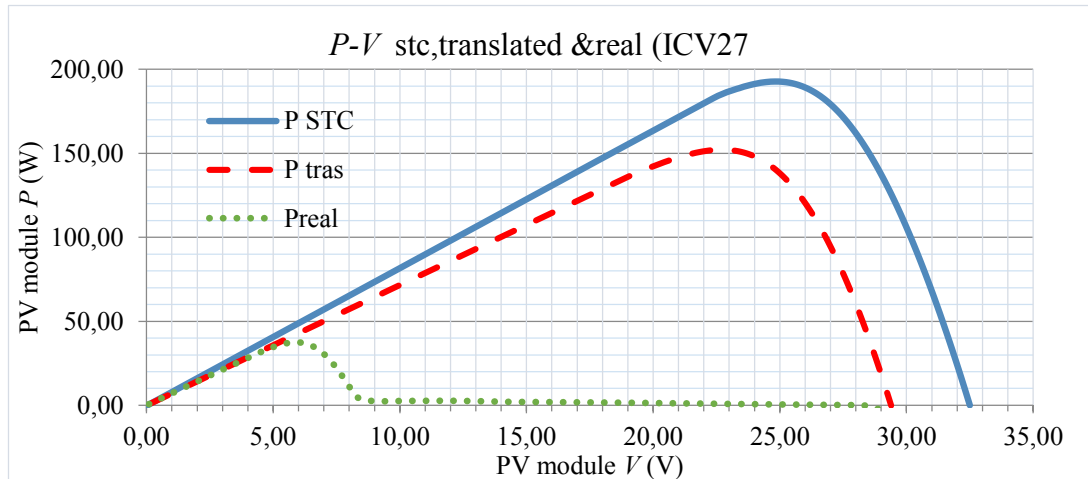
Figure 7.6. STC, translated and real *P-V* curves for T_m=56,2 ºC and G=854 W/m^2

The significant reduction of the power generated by the the module is due to a partial shadowing, which explains the low reulting value of PR^i_{DC}, as indicated by the measured power curve (green dotted line). As indicated in Table 7.2, estimated translated losses are L^t_{DC}=0,08, being PR^t_{DC}=0,92. Nevertheless, measurements based obtained PR^i_{DC} is 0,23, which represents significant losses L^i_{DC}=0,77. The model is indicating that the PV module is performing significantly below the performance it should be expected to have. In consequence, the corrective actions would indicate to identify the causes of such partial shadowing.

In between both cases, we find reading Id #ICV18. This case is very interesting, since the incident irradiance is G=395 W/m^2 and the ambient temperature is T_m=41,1 ºC; under these conditions, the power delivered by the PV module is close to 77 W, which signifies a PR^i_{DC}=0,92 and corresponding losses L^i_{DC}=0,08. Under these conditions and considering that at low power, the model presents a bigger error, the module should deliver something more than 80 W, which gives a PR^t_{DC}=0,97 with corresponding losses L^t_{DC}=0,03.

This results in effective losses L^e_{DC}=0,05 which correspond to the combined effect of different causes of losses with no excessive impact, like dust and shadowing. In fact, the results indicate that the module is working under a performance close to the one it should do under optimal conditions at ROC at that moment.

On the other hand, readings Id #ICV22, #ICV23, #ICV24 and #ICV25 report effective losses (L^e_{DC}) ranging between 0,56 and 0,70. This evidences a temporary shadowing (made ex-profeso for validation purpose) of the PV modules. This allows us to confirm the viability of the model to real-time identify a module performing much below the optimal value for given ambient conditions.

7.3.2. *Measurements on EPS PV lab modules*

In a similar way and based on measurements made on EPS PV Lab installed Isofoton ISF-245 PV modules, obtained results are herein described.

The first case analyzed (reading Id#MIV_1), corresponds to measurements made at an ambient temperature T_m=43,9 ºC and an effective irradiance G_e=810 W/m². Under these conditions, the power delivered by the PV module is P_i=177,33 W, while the maximum ROC translated value is P_t=185,09 W, which results in corresponding instant PR^i_{DC} =0,90 and translated PR^t_{DC}=0,94. According to this, the effective losses are L^e_{DC}=0,04. That is, the PV module is performing a 4 % below the maximum value it should do for applying ROC. This value is in range with the estimated error of the proposed model.

Resulting *I-V* curve appears in figure 7.7. It can be seen the evolution of the measurements (green dotted line), in comparison with the ROC translated curve (red dashed line) and the STC curve (solid blue line).
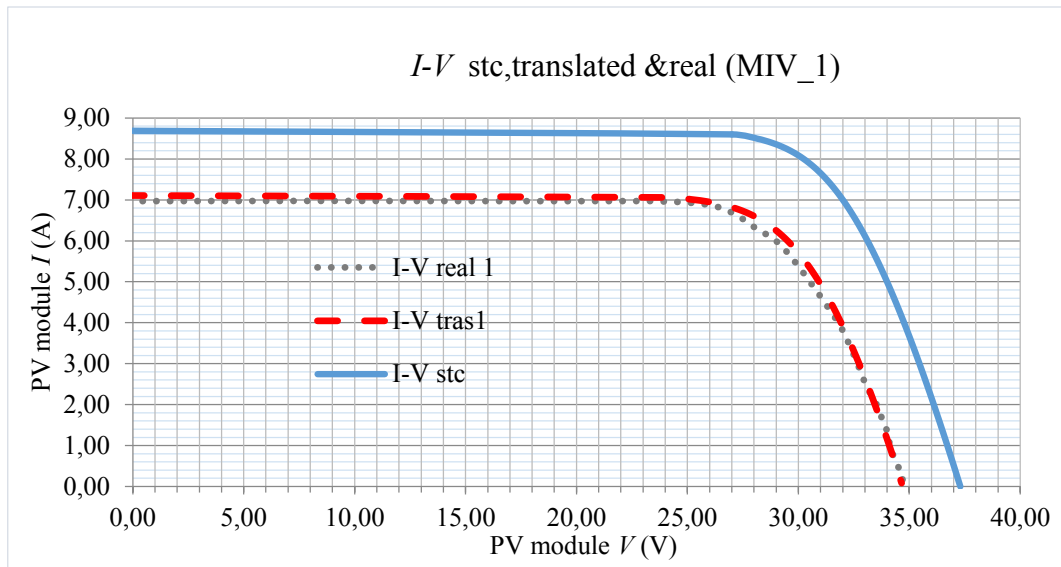
Figure 7.7. STC, translated and real *I-V* curves for T_m=43,9ºC and G= 810 W/m^2

Corresponding *P-V* curves can be seen in figure 7.8.
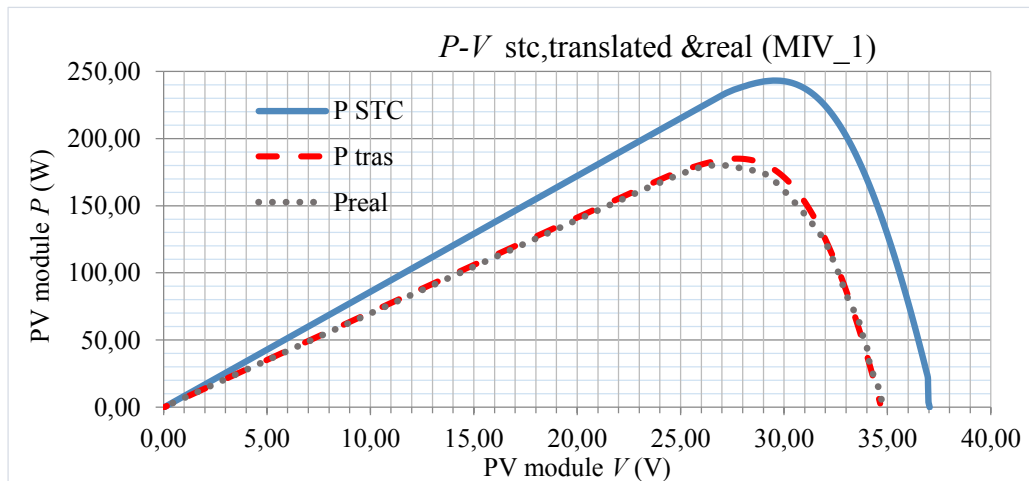
Figure 7.8. STC, translated and real *P-V* curves for T_m=43,9 ºC and G=810 W/m^2

In the second case analyzed (reading Id#MIV_3), applying conditions are an ambient temperature T_m=48,2 ºC and an incident effective irradiance G=750 W/m². Under these conditions, the ROC translated PR results to be PR_{DCt}=0,93 which represents losses L^t_{DC}=0,07. Nevertheless, real instant losses are L^i_{DC}=0,15 that correspond to a PR^i_{DC}=0,85. This results in overall losses L^e_{DC}=0,08. As it can be seen in figure 7.9, these overall losses are due to a partial shadowing that can be observed at 25 V, which reduces significantly corresponding PR.
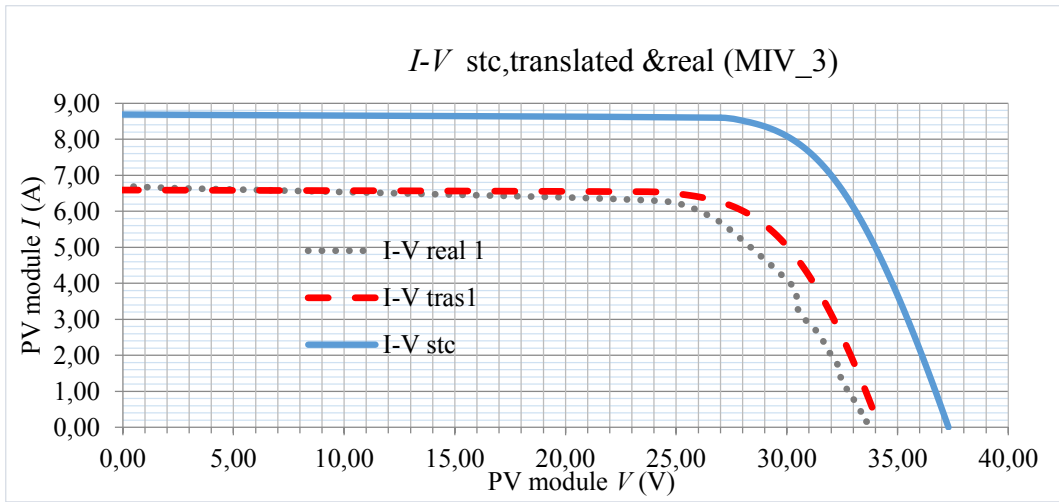
Figure 7.9. STC, translated and real I-V curves for T_m=48,2 ºC and G=750 W/m²

The PV curve of figure 7.10 illustrates what has been previously described. As it can be seen, the resulting power curve (green dotted line) goes below the curve predicted by the proposed model for applying ROC.
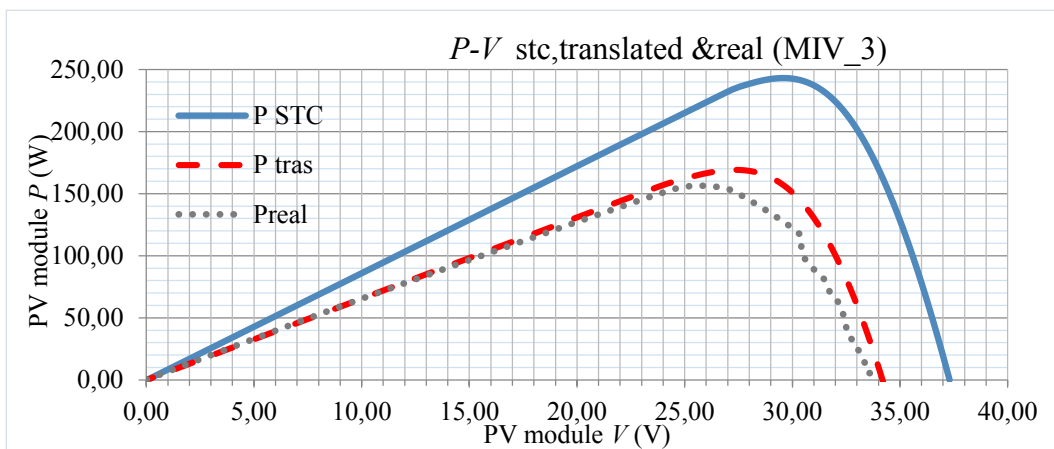
Figure 7.10. STC, translated and real P-V curves for T_m= 48,2 ºC and G=750 W/m²

In the third case analyzed, in addition to the *I-V* and T_m monitored parameters, the module temperature has also been evaluated by means of a thermophotography camera. The measurements have been made at an ambient temperature T_m=40,4 ºC and an effective irradiance *G*=650 W/m^2.

The combined effects of PV module temperature and incident irradiance on its performance have already been stated in chapter #5. The effect of the module temperature has mainly a constraint in the V_{OC} value, although as it could be seen, also on the generated power and hence on the effective performance.

Figure 7.11 shows the thermophotography of the PV modules, where it can be seen that the right-hand module has a defective cell which is operating at a higher temperature than the average of the PV module. The left-hand module is partially shadowed on the upper right-hand corner. This shadowing is affecting a higher surface of the right-hand module.
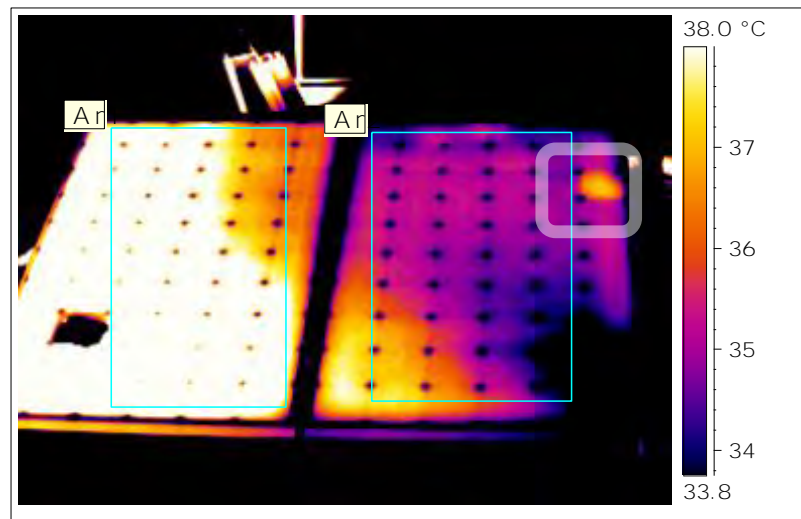
Figure 7.11. Thermophotography of Isofoton ISF-245 PV modules showing a defective cell on the upper right hand corner (courtesy of Intermal)

As it can be seen in Figures 7.12 and 7.13, which show the *I-V* and the *P-V* curves respectively, the generated power is smaller than the expected one according to the model real outdoor conditions translated curve.
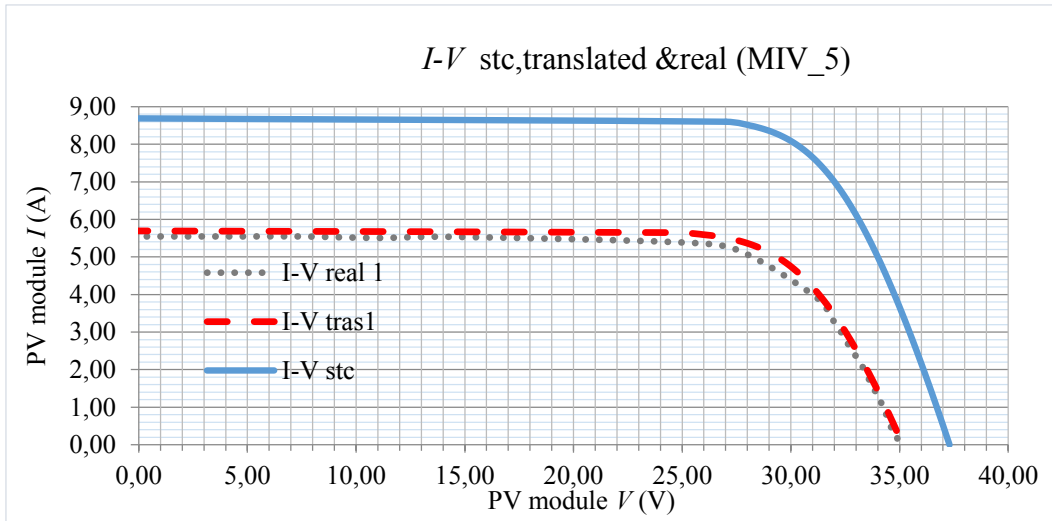
Figure 7.12. STC, translated and real *I-V* curves for T_m=40,4 ºC and G=650 W/m²
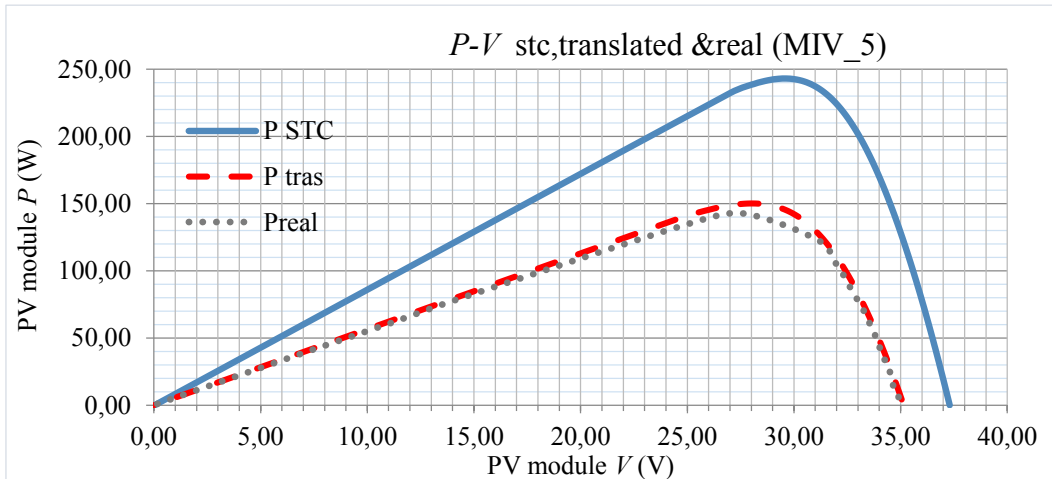
Figure 7.13. STC, translated and real *P-V* curves for T_m=40,4 ºC and G=650 W/m²

According to the translation model, the estimated PR^t_{DC}=0,97, which represents an estimated losses of L^t_{DC}=0,03. Meanwhile, the monitoring data give a reported PR^i_{DC}=0,91, that represent losses of L^i_{DC}=0,09. This means that the effective losses are L^e_{DC}= 0,06. This means that the PV module is performing around a 6 % under expected optimal value. Despite the effect of the defective cell, the low ambient temperature favorizes the PV module operation.

7.4. CONCLUSIONS

In this chapter, it has been demonstrated on one hand the viability and on the other hand the utility of having reliable data of *PR* obtained at PV module level. The PV module operating data reported by the SMCM during the monitoring process, which delivers the instant values of the PV module operational parameters *V*, *I* and T_m make possible the quantification of the Instant Performance Ratio (PR^i_{DC}). Additionally, the ROC monitored data T_a and *G* allow the estimation of the Translated Performance Ratio (PR^t_{DC}).

The model of translated PR^t_{DC}, calculated according to proposed procedure, in comparison with the PR^i_{DC} allows to reliably estimate the losses at a PV module granularity level. It is important to take into account that the PR^t_{DC} reported value is compensated in terms of effective irradiance and ambient temperature, which are field measured. The measured PR^i_{DC} is dependent upon existing ambient conditions (ROC) as well as the losses affecting the PV module.

This allows the definition of a new parameter, which has been named as effective losses (L^e_{DC}), which quantifies the power losses that are not due to the normal operation of the PV modules.

This methodology detects abnormal situations when the effective losses are bigger than the 3 %, which is the uncertainty of the proposed model.

All this makes possible a more efficient management of the PV modules maintenance operations and favourizes as well an improved yield of the PV plant, which leads to corresponding financial benefits.

From the experimental data based validated procedure it has been demonstrated the possibility to identify any PV module performing below the ratio it should be according to applying ROC.

It has also been demonstrated that the resulting effective losses can be clearly identified in case of PV modules subject to severe adverse conditions.

7.5. REFERENCES

[1] M.A. Green, K. Emery, Y. Hishikawa, W. Warta, and E.D. Dunlop, *Solar cell efficiency tables (version 43)*, Progress in Photovoltaics, Volume 22, Issue 1, pages 1–9, January 2014.

[2] D.L. King, W.E. Boyson and J.A. Kratochvill, *Photovoltaic Array Performance Model,* Sandia Report SAND2004-3535, Sandia National Laboratories, December 2004.

[3] D. King, J. Kratochvil, and W. Boyson, *Field Experience with a New Performance Characterization Procedure for Photovoltaic Arrays*, 2nd World Conference on PV Solar Energy Conversion, Vienna, 1998, pp. 1947-1952.

[4] N. Gokmen, E. Karatepe, B. Celik, and S. Silvestre, *Simple diagnostic approach for determining of faulted PV modules in string based PV arrays,* Solar Energy, Elsevier 2012.

[5] J.D. Bastidas-Rodriguez, G. Petrone, C. A. Ramos-Paja and G. Spagnuolo, *Photovoltaic modules diagnostic: an overview,* 39th Industrial Conference of the Industrial Electronics society, IECON 2013.

[6] M. Sidrach de Cardona, and Ll. Mora López, *Performance analysis of a grid-connected photovoltaic system,* Energy 24, pp 93-102, Pergamon 1999.

[7] K. Whitfield, and C.R. Osterwald, *Procedure for Determining the Uncertainty of Photovoltaic Module Outdoor Electrical Performance,* Progess in Photovoltaics Research and Applications, 9, pp 87-102, John Wiley and Sons, 2001.

[8] M. Piliougine, J. Carretero, Ll. Mora López, and M. Sidrach de Cardona, *Experimental system for current-voltage curve measurement of photovoltaic modules under outdoor conditions,* Progress in Photovoltaics: Research and Applications, 19, pp 591-602, John Wiley and Sons, 2011.

[9] L. Cristaldi, M. Faifer, A. Ferrero and A. Nechifor, *On-line monitoring of the efficiency of Photo-Voltaic panels for optimizing maintenance scheduling.* IEEE International Instrumentation and Measurement Technology Conference, May 2010.

[10] A. Luque and S. Hegedus, *Handbook of Photovoltaic Science and Engineering,* John Wiley and Sons, 2006. ISBN:978-0-471-49196-5.

[11] B. Marion, J. Adelstein, K. Boyle, H. Hayden, B. Hammond, T. Fletcher, B. Canada, D. Narang, A. Kimber, L. Mitchell, G. Rich and T. Townsend, *Perfromance Paramters for Grid-Connected PV Systems*, 31 st IEEE Photovoltaics Specialists Conference, Florida, 2005.

[12] A. Dolara, F. Grimaccia, S. Leva, M. Mussetta, R. Faranda and M. Gualdoni, *Perfromance Analysis of a Single-Axis Tracking PV System,* IEEE Journal of photovoltaics, vol.2, n. 4, 2012.

[13] A. Dolara, S. Leva, G. Manzolini and E. Ogliari, *Investigation on Performance Decay on Photovoltaic Modules: Snail Trails and Cell microcracks,* IEEE Journal of photovoltaics, vol. 4, n. 5, 2014.

[14] R. Moreno-Sáez, M. Sidrach-de-Cardona and Ll. Mora-López, *Data mining and statistical techniques for characterizing the performance of thin-film photovoltaic modules.* Expert Systems with Applications, volume 40, issue 17, Elsevier, 2013.

Chapter 8

CONCLUSIONS, FUTURE RESEARCH LINES
& SCIENTIFIC PRODUCTION

In previous seven chapters, the proposed idea to monitor at Photovoltaic Module level and the possibility to use the monitored data for the modules Performance Ratio and corresponding Losses estimation in real time has been demonstrated. In this chapter, the main overall considerations and conclusions of referred work are depicted.

8.1 GENERAL CONCLUSIONS.

The total amount of energy that a Photovoltaic (PV) Module can deliver depends not only on the PV cell technology used and the module assembly technology but more significantly on the applying outdoor ambient conditions, the so called Real Outdoor Conditions (ROC) but also on the Losses that might apply.

As it has been described in previous chapters, all the possible Losses Factors (*LF*) may significantly affect the final energy yield. Many of these adverse conditions are difficult to identify and detect. Some losses are avoidable, but some other ones must be considered as non-avoidable.

The question is: "is it possible to know how these conditions affect the energy yield of a PV power plant"? That was the question that came to me as a Master Student in may 2009 when visiting the "Olivares" PV power plant. A 9,17 MWp power plant located near Jaen. It could then be observed that the power plant was very poorly monitored. In fact a few power monitors connected to some of the strings were connected to the supervisory office, and the communications were made via radio with some "relevant" problems.

Since then, the idea to significantly increase the monitoring process granularity level began to grow up. The monitoring at PV module level became a challenge. With the support and assessment of my Thesis Directors, from the University of Málaga together with the collaboration of experienced colleagues of other Universities, it has been possible to arrive to this point, which I hope will significate the beginning of new enthusiastic projects.

Once the initial idea was put on the table, the first step was to perform a technological vigilance and state of the art prospection. This task gave us the actual status of the art. The main conclusions were that the monitoring was performed essentially at string level and in most of the cases, the information was supplied by the DC/AC inverters. No commercial devices were identified to be working at the PV module level. Nevertheless, by may 2012, a reference was found of a patent related to a similar product (US patent 200901199662, dated in july 2009). The existing monitoring systems were based on standard industrial SCADA, with data transmission based on RS-485 or via radio. In any case, these solutions are intended

to monitor at string granularity level. These expensive solutions are not adequate for monitoring at module level.

The dedicated monitoring systems, further to represent a significant cost, are usually focused for residential type installations.

The module level monitoring solutions come from the μinverter technology, where the DC/AC inversion is made at module level. In this cases, the data are transmitted via PLC but again at a significant cost and mainly for small dimension installations.

Regarding the data transmission, as it has already been said, the industrial standard RS-485, which requires additional wiring installation is the mostly used solution. The radio transmission is mainly applied for string monitoring systems, and are subject to the effect of noise and interferences. Here again, the solution is not adequate for module level monitoring. Some works published refer to the PLC based on magnetic coupling. Here the constraint is the cost of the coupling inductors.

By then, a first approach of the proposed idea had already been presented at the IEEE Powereng conference held in 2011. Its acceptance and presentation confirmed us the initial consideration that it might be a topic of interest.

The concept that has been developed since then is a complete topology that considera not only the monitoring of the PV modules operating parameters in real-time, but also the transmission of the monitored data via PLC capacitive coupling to a CCS for further processing. And all this, with the premise to comply with the requirement to be a low cost system.

Furthermore, with the available monitored data, a new Performance Ratio concept was defined so that to have a more reliable and eloquent information of the real-time performance of each one of the PV modules that configure a PV power plant.

The compliance with the initial specifications defined in terms of functionality (monitoring and data Tx/Rx) and cost as well were an important challenge. The knowledge of the state of the art of the technology allowed to presume the viability of monitoring the referred PV modules V, I and T_m parameters.

To do it at a low cost was also accessible. The challenge to transmit the data using the PLC technology would help to keep the overall system cost as tight as possible. This allowed to avoid using radio based communications systems or alternatively, the option to add a specific parallel wiring for data transmission.

Under these premises, a low cost μcontroller (TI MSP 430) based monitoring module with PLC based data Tx/Rx capabilities has been developed. Its functionality has been demonstrated and the uncertainty of its measurements have been calculated to be in the ranges of ±0,9V for the voltage measuring chain Analog Front End; ±0,084 A for the current AFE and ±0,34 ºC for the temperature measuring chain.

Further validations with consolidated data from the UMA RREE Lab have allowed to quantify the Relative Error made in the measurements of the PV module operational parameters. It has been evidenced that for irradiances < 200 W/m^2, the errors are somewhat relevant, while they are significantly reduced for higher values of irradiance. For these prototypes, a 3,5 % of RE can be considered as acceptable for irradiances values > than 200 W/m^2.

The main problem came with the field trials for data transmission. In fact, the picture of Figure 3.30 became a milestone in the project labor. It was captured after 3 months of hard field work. The redesigns, adjustments of some components that simulated the PLC based transmission path (DC power line), together with the conditioning of the signal at the end of the line in the SMCM-CCS data concentrator required a lot of work, considerations and successive trials. But all this paid the worth; finally it came the image of Figure 3.30. This figure summarizes all the undertaken tasks. The success came when we decided to bypass the PV modules with the bypass capacitors; this solved many of the problems we were facing. Finally, the values of the trap coils L1 and L2 required adjustments that could not be evidenced in the previous simulation phase.

The use of monitored data for PV module Performance Ratio estimation required also several approach trials, until the proposed model was finally concluded. The traditional Performance Ratio concept considers the generated energy (usually in AC) during a given period of time vs the maximum energy that potentially might be generated at STC, as per the EN 61724 std.

In this work, the focus has been put on the instant power generated by a single PV module, which will help to quantify the total instant power generated by the PV plant at a given moment in time. Furthermore, the availability of the power generated by the PV module at a given moment in time, knowing its temperature (T_m) and the incident irradiance on its plane, together with the theoretical power it should be generating under referred conditions, will be used for the estimation of its performance, the calculation of the losses it is submitted to. By this way, once the corrective actions have been deployed, the PV plant performance will be significantly improved. A module underperforming will be real time detected and a further estimation of the possible causes will help to organize the maintenance activities.

On one hand, it has been proposed the real-time instant performance (PR^i_{DC}) that relates the instant DC power generated by the PV module (P_{DCi}), supplied by the SMCM vs. the maximum power at STC. On the other one, the PR related to the ROC translated module power (PR^t_{DC}), considering the effective incident irradiance (G) is estimated. From these PR´s, the corresponding losses are quantified, which give real-time information of the actual performance of the PV modules.

Additionally, from previously described PR´s, resulting losses have been quantified. On one hand, we have the instant losses, given by $L^i_{DC=}1-PR^i_{DC}$, which represent the overall avoidable losses of the module; on the other hand, we have the translated losses given by $L^t_{DC=}1-PR^t_{DC}$, which quantify the non-avoidable losses that the module is submitted to. The difference of both parameters give the effective losses, as $L^e_{DC}=L^t_{DC}-L^i_{DC}$. This parameter, if reaching values bigger than the system margin of error, indicates that the corresponding PV module is underperforming.

The proposed idea was structured on three main basements: the PV module electrical mathematical model for functional parameters estimation and its translation to applying ROC; the SMCM monitored and transmitted data for further processing and finally, the translated Performance Ratio (PR^t_{DC}) estimation. The proposed idea allows in real time to detect a PV module working under expected performance and according to the results and subsequent Losses estimation, not only the defective PV module can be real-time identified, but also to conclude if the applying losses are non-avoidable ones.

It has been demonstrated that the Smart Monitoring and Communications Module (SMCM) is able to monitor the PV modules electrical parameters and its back-plane temperature and further transmit these data to the Central Computer System (CCS) via the DC power line on the basis of the Power Lines Carriers (PLC) technology.

The use of capacitors for both coupling the SMCM (instead of magnetic devices) and bypass the PV modules, have helped to define a low impedance path for data transmission and reduce the system costs.

Low cost components for the SMCM and Tx/Rx transceivers and the use of already existing DC power lines as physical communications layer have helped to keep the monitoring system deployment cost very tight. Meanwhile, the benefits in terms of avoiding production losses are significant for the project´s shareholders Return Of the Investment (ROI).

The proposed simplified mathematical models have been validated with consolidated field experimental data and further applied to the experimental test bench installed in the EPS PV Lab.

Finally, the processed information has allowed the real-time *PR* estimation and corresponding Losses which are the tool to identify PV modules performing under expected values according to ROC. This procedure improves significantly the energy yield of the PV plant, since the so called avoidable losses can be real time detected and consequently upgraded.

8.2 *FUTURE RESEARCH LINES.*

All the work developed and described in this Thesis has led to additional considerations, ideas and proposal of possible future research lines:

- Improve the design of the SMCM AFE in order to reduce the associated Uncertainty.
- Redesign the SMCM to incorporate the option of PV module isolation and obtain real-time *I-V* curve in field under existing outdoor conditions.
- Develop an Artificial Intelligence based application to identify the main losses characteristics and potential origin, failure follow-up and energy yield improvement.

- Deploy a string-based test bench to test the system with additional PV modules.

8.3 SCIENTIFIC PRODUCTION.

As a result of the activities developed in the frame of this Thesis, the stage in foreign Universities and collaborations with University of Málaga colleagues, following scientific works have been published or are under evaluation:

8.3.1   Articles in Indexed Journals

- ***PLC-Based PV Plants Smart Monitoring System: Field Measurements and Uncertainty Estimation.*** Sanchez-Pacheco, F.J. ; Sotorrio-Ruiz, P.J. ; Heredia-Larrubia, J.R.; Perez-Hidalgo, F.; Sidrach de Cardona, M. IEEE Transactions on Instrumentation and Measurement (IEEE TIM), Volume: 63 , Issue: 9 DOI: 10.1109/TIM.2014.2308972, Publication Year: 2014 , Page(s): 2215 – 2222.

- ***Real-Time Procedure to Detect Different Losses in Photovoltaic Generators by Means of Distributed Monitoring***, F.J. Sánchez Pacheco and M. Sidrach. IEEE Transactions on Industrial Informatics (Special Section: Monitoring, diagnosis, prognosis and techniques for increasing the lifetime/reliability of photovoltaic systems). (Under evaluation).

- ***Reverse Decomposition Method vs Simplified PV Module Electrical Model Comparison***, S. Merino Córdoba and F.J. Sánchez Pacheco. IEEE Transactions on Industrial Informatics; Special Section: Monitoring, diagnosis, prognosis and techniques for increasing the lifetime/reliability of photovoltaic systems. (Under evaluation).

8.3.2. Articles in International Conferences

- ***Low cost DC lines PLC based photovoltaic plants parameters smart monitoring communications and control module***. Sánchez-Pacheco, F.J.; Sotorrio-Ruiz,P.J.; Heredia-Larrubia, J.R. ;Perez-Hidalgo, F. ; Sidrach-de-Cardona,M. International Conference on Power Engineering, Energy and Electrical Drives (POWERENG), 2011 DOI: 10.1109, PowerEng.2011. 6036487. Publication Year: 2011, Pages: 1–6.

- ***Resolution of solar cells equivalent electrical model by reverse decomposition.*** Salvador Merino, F.J. Sánchez-Pacheco, Pedro Rodriguez and Carlos Sánchez. Proceedings of Applications of Computer Algebra (ACA), Málaga, 2013.

Resumen

La presente Tésis Doctoral titulada *Monitorización Distribuida en Sistemas Fotovoltaicos para la Optimización de la Eficiencia* recoge la labor realizada, las actividades llevadas a cabo, así como la descripción de los resultados experimentales que se han obtenido a lo largo de su desarrollo, y que han permitido validar la idea propuesta.

Los conceptos desarrollados en la misma tienen por finalidad la mejora significativa de la eficiencia de una planta fotovoltaica, sean cuales sean sus dimensiones, ya sea conectada a red, o bien como instalación autónoma. La cantidad de energía que una planta fotovoltaica puede generar depende en primera medida de la irradiancia incidente, así como de la temperatura ambiente, que, a la postre afectará a la temperatura de los módulos. Dicho esto, hay una serie de factores de pérdidas que pueden afectar negativamente a su rendimiento. Estos factores de pérdidas están identificados y cuantificados. Las consecuencias de los mismos van a afectar directamente a los parámetros operativos de los módulos FV. En este sentido, cobra una importancia relevante la posibilidad de disponer de información detallada de dichos parámetros operativos con un nivel de granularidad de módulo FV.

Esta Tésis ha tenido como objetivo demostrar por un lado la posibilidad de realizar la monitorización de sistemas fotovoltaicos a nivel de módulo y obtener los datos de los parámetros operativos, en tiempo real, así como poder determinar la eficiencia efectiva de los módulos, teniendo en cuenta las condiciones atmosféricas reales. Uno de los capítulos de la misma está dedicado al concepto de traslación de los parámetros basados en condiciones estándares (STC), a las condiciones atmosféricas reales de funcionamiento (ROC).

De esta manera, contando con dichos datos, se puede llegar a definir la huella *I-V* de un módulo, y, en comparación con los valores teóricos que deberían obtenerse bajo las condiciones reales de funcionamiento, determinar si el módulo FV está operando correctamente, o bien lo está haciendo por debajo de los niveles que le corresponderían por las condiciones ambientales. Las diferencias obtenidas permiten cuantificar las pérdidas asociadas.

Un módulo FV operando por debajo de su rendimiento óptimo generará unas pérdidas económicas importantes, durante el tiempo que esté trabajando en esas condiciones, y se mantendrá así mientras no se detecte. En determinadas ocasiones, las condiciones operativas en las que se encuentra un módulo FV pueden quedar enmascaradas por las condiciones en las que se encuentre la matriz en la que esté integrado. Las pérdidas por no generación se pueden acumular, lo que finalmente afectaría negativamente al rendimiento económico de la planta FV.

1. INTRODUCCIÓN

El papel que juegan las energías renovables como factor para la reducción de la huella de CO_2 es un hecho innegable. En el caso específico de la tecnología solar fotovoltaica, esta contribuye en alrededor de un 20 % a esta reducción. Adicionalmente, se puede obtener otro 23 % de reducción por la vía de la mejora de la eficiencia en la electricidad (fuente:EIA).

La cantidad de energía que un sistema FV puede suministrar depende básicamente de:

- La tecnología de la célula FV utilizada
- La tecnología de fabricación de los módulos FV (estructura, materiales aislantes, antirreflectantes, etc…)
- Condiciones atmosféricas ambientales
- Ubicación, orientación y ángulo de incidencia del sol
- Época del año y hora del día

Por otro lado, existen condiciones adversas que pueden dar lugar a una notable disminución de la energía producida. Estas pueden ser:

- Condiciones atmosféricas variables (temperatura y humedad ambientes, velocidad del viento, índice de masa espectral)

- Sombreado total o parcial, permanente o temporal, suciedad, polvo, etc…
- Degradación del módulo FV

La monitorización a nivel de panel está establecida como un requisito por la propia Agencia Internacional de la Energía (IEA), lo cual permite cuantificar con detalle el rendimiento de los módulos FV.

Los datos obtenidos permiten cuantificar el ratio de rendimiento (*Performance Ratio- PR)* a nivel de módulo FV en tiempo real. Esta información, se compara con el *PR* resultante de aplicar los procedimientos de traslación de los parámetros a las condiciones reales de operación, lo que va a permitir cuantificar las pérdidas efectivas (L^e_{DC}) a las que está sometido el módulo FV.

Uno de los objetivos ha sido el de concebir un sistema cuyo coste no supusiera una inviabilidad de la idea planteada. En este sentido, las actuaciones se han focalizado hacia:

- El coste de los componentes electrónicos del sistema
- La aplicación de la tecnología PLC para la transmisión (*Tx*) y recepción (*Rx*) de los datos
- La implementación del sistema de monitorización

La presente Tésis ha quedado estructurada de la siguiente forma: en el capítulo 2, se hace un repaso de los parámetros funcionales de los módulos FV, y su dependencia de las condiciones atmosféricas presentes; asimismo, se definen los protocolos de traslación de dichos parámetros desde las condiciones STC dadas por el fabricante en sus hojas de características, a las correspondientes por las condiciones ambientales existentes; en el capítulo 3, se describe el sistema de monitorización propuesto, la estructura del módulo de monitorización y transmisión de datos (SMCM), así como el diseño de la capa física de comunicaciones sobre la que se ha implementado la tecnología PLC; en el capítulo 4, se cuantifica la incertidumbre asociada al módulo SMCM como dispositivo de medida electrónico; en el capítulo 5, se valida el modelo propuesto anteriormente, mediante su aplicación a datos experimentales consolidados; en el capítulo 6, se aplica el mismo procedimiento a los resultados experimentales obtenidos en los módulos FV

instalados en el laboratorio de FV de la EPS; en el capítulo 7, se aplican los procedimientos anteriores para determinar y cuantificar tanto los *PR* como las pérdidas efectivas resultantes; finalmente, en el capítulo 8 se describen las conclusiones generales obtenidas.

2. *MODELOS MATEMÁTICOS Y MONITORIZACIÓN DE MÓDULOS FV*

Un módulo FV se puede asociar a un modelo eléctrico, compuesto por un generador fotovoltaico, uno o dos diodos en paralelo, y las consiguientes resistencias de pérdidas, tanto serie como paralelo. De esta manera, queda caracterizado a través de la huella que proporciona su curva característica *I-V*; la cual, a su vez, permite identificar los parámetros funcionales que el propio fabricante suministra. Esto parámetros son:

- Corriente de cortocircuito: I_{SC}
- Tensión a circuito abierto: V_{OC}
- Corriente en el punto de máxima potencia I_{mp}
- Tensión en el punto de máxima potencia V_{mp}
- Potencia máxima P_{mp}

La forma geométrica de la curva *I-V*, así como las de las envolventes I_{SC}-V_{OC}, e I_{mp}-V_{mp} definen el concepto de Factor de Forma (*Fill Factor-FF*), el cual permite atisbar el impacto de las resistencias de pérdidas y dan un orden de magnitud de la eficiencia de la tecnología utilizada en la fabricación de las células solares.

Con el objeto de simplificar la resolución del modelo matemático, se ha optado por el modelo eléctrico simplificado de un diodo, en el que la resistencia serie se omite, así como su impacto en la huella *I-V*. Esto permite pasar a una ecuación explícita, frente a la implícita que se obtendría caso de considerar dicha resistencia. Esto facilita la labor de resolución y obtención de la huella *I-V*.

Para poder evaluar el comportamiento del módulo, es necesario conocer la temperatura del mismo. El sistema aquí propuesto, concretamente, el SMCM está capacitado para poder medir la temperatura del panel posterior del mismo, tal y

como indica la normativa. Sin embargo, también se proponen dos métodos alternativos. Por un lado, se puede determinar la temperatura de los módulos a partir de la temperatura ambiente y de la velocidad del viento, o, en su ausencia, a partir del modelo basado en el parámetro denominado *Nominal Operating Cell Temperature (NOCT),* facilitado por el fabricante del módulo.

Una vez determinados dichos parámetros, se propone el método de traslación de los mismos a la condiciones ROC, las cuales nos van a permitir determinar las condiciones en las que ha de estar trabajando el módulo según la radiación incidente y la temperatura del mismo. Esto va a permitir determinar si está operando de forma satisfactoria, o bien, si al contrario, lo está haciendo de manera anómala. El procedimiento aquí descrito posibilitará evaluar las pérdidas efectivas a las que está sometido, y en tiempo real. La operatoria permite determinar los parámetros operativos a nivel de módulo, pudiéndose conseguir de esta manera, de un mapa de rendimiento de la planta completa particularizado a nivel de módulo.

En este sentido, es necesario de disponer de una infraestructura de monitorización que permita determinar en tiempo real los valores de los parámetros operativos de los módulos FV, tal y como se ha indicado anteriormente, para su posterior procesamiento y determinación de la eficiencia de los módulos. Los sistemas de monitorización existentes en el mercado no están generalmente pensados para trabajar a nivel de módulo; suelen hacerlo a nivel de *string* ó matriz. Por otro lado, los sistemas específicos, además de costosos, no suelen permitir operar con ellos, al tratarse de sistemas cerrados. Dicho esto, se consideró la posibilidad de desarrollar un sistema de bajo coste, integrable a nivel de módulo, y que utilizara las propias líneas de potencia en DC para configurar la capa física de comunicaciones, aplicando a tal efecto, la tecnología de comunicaciones por líneas de potencia.

3. *Módulo SMCM y Comunicaciones PLC*

Con el objeto de poder monitorizar los parámetros operativos a nivel de módulo fotovoltaico, se propone un sistema basado en el dispositivo denominado *Smart Monitoring and Communications Module (*SMCM*),* el cual, mediante el uso de la tecnología PLC permite, además de la captura de los parámetros, la

transmisión de los datos a un sistema computador central (CCS) para su posterior procesamiento.

El módulo SMCM es un dispositivo inteligente, basado en el μControlador MSP 430 del fabricante Texas Instruments, de coste inferior al Euro, y sin embargo, con unas grandes prestaciones. Esto ha permitido concebir un SMCM de muy bajo coste, de tal manera que no penalizara la implantación del sistema de monitorización.

Las características principales del sistema son:
- Desarrollado con componentes de bajo coste
- El sistema se puede configurar según los requisitos del cliente final
- Permite disponer en tiempo real de los parámetros operativos del módulo FV, tales como la tensión (*V*), la corriente (*I*), y la temperatura del mismo (T_m), así como de las condiciones ambientes tales como la irradiancia incidente (*G*) y la temperatura ambiente (T_a)
- Permite la representación de los datos mediante la interfaz de usuario
- Detección en tiempo real de módulos defectuosos, o bien, operando por debajo del rendimiento que se le supone
- Comunicaciones de datos mediante tecnología PLC

El SMCM está formado por los siguientes bloques:
- Bloque para la medida de la tensión del módulo (*V*)
- Bloque para la medida de la corriente generada por el módulo (*I*)
- Bloque para la medida de la temperatura del módulo, mediante una sonda PT-100
- Bloque para la transmisión (*Tx*) y recepción (*Rx*) de datos

Cada uno de ellos consta de la electrónica necesaria para el acondicionamiento de las señales que correspondan y su adecuación a la electrónica de medida para su posterior conversión a digital, mediante el μControlador.

Con el objeto de arrancar en el desarrollo, los prototipos se han implementado alrededor del kit de desarrollo *MSP430 launchpad* de TI, lo que ha permitido acortar los tiempos de montaje de los prototipos. Por otro lado, dichos

kits están dotados de una interfaz USB integrada, que ha facilitado enormemente la conectividad entre el SMCM y el CCS.

La estructura de los datos a transmitir está basada en la nomra EN 61724 (*Photovoltaic system performance monitoring. Guidelines for measurement, data Exchange and analysis*), cuya estructura es la siguiente:

Dónde cada campo corresponde a:

- Encabezado (AA$_h$): utilizado como byte de sincronización
- Número de identificación del módulo FV (XXXX$_h$)
- Temperatura del modulo FV (TT$_h$)
- Separador de campo (ASCII 44)
- Corriente del módulo FV (II$_h$)
- Separador de campo (ASCII 44)
- Tensión del módulo FV (VV$_h$)
- Fin de línea (End of Line-EOL) – (ASCII 13)

La transmisión de datos se realiza según el estándar CENELEC-B, en la banda comprendida entre los 95 y 125 kHz, que es la banda libre permitida para usuarios finales, tal y como indica la norma EN 50065-1 (*Signaling on low-voltage electrical installations in the frequency range 3 kHz to 148,5 kHz.*

Al objeto de evaluar la solución planteada por un lado, se ha llevado a cabo la simulación de la transmisión de datos en una línea que representaba una instalación de unos 1000 m de longitud, con los consiguientes componentes resistivos, inductivos y capacitivos. Se pudo observar que los datos se podían transmitir correctamente y posteriormente recuperarlos al final de la línea. Por otro lado, los armónicos generados eran prácticamente despreciables.

Sin embargo, en las pruebas reales con los prototipos y los módulos FV instalados, surgieron muchos problemas que inicialmente imposibilitaron implementar la solución prevista. Después de llevar a cabo un análisis más exhaustivo, se optó por implementar en paralelo con los módulos FV, un camino de

baja impedancia mediante condensadores de bypass acoplados a cada módulo, de tal manera que los datos transmitidos pudieran desplazarse por dicha trama, hasta tanto llegar al extremo de la línea dónde serían recogidos por el concentrador de datos y posteriormente transferidos al CCS. La adecuación de los componentes a las características de la línea por un lado y de la señal de datos transmitida por otro, permitió llegar a resultados positivos, pudiendo recuperar íntegramente los datos al final de la línea PLC.

4. *ESTIMACIÓN DE LA INCERTIDUMBRE DEL SMCM*

El SMCM es en definitiva un módulo de medida de parámetros eléctricos para su posterior conversión a formato digital y transmisión. Como tal dispositivo de medida, los resultados que proporciona no están exentos de incertidumbre. La cuantificación de dicha incertidumbre se ha llevado a cabo aplicando la norma IEC-98, procedente del procedimiento "*Guide for the Uncertainty Measurement*" propuesto por la Oficina Internacional de Pesos y Medidas de Paris. Dicho procedimiento contempla dos tipos de incertidumbres en función del método seguido para su cuantificación; por un lado, las denominadas incertidumbres de tipo A se obtienen mediante medidas repetitivas del parámetro a evaluar; por otro lado, las de tipo B se obtienen a partir de las especificaciones de los fabricantes de los componentes utilizados en la lectura de los parámetros operativos del módulo FV. En este sentido, se han identificado tres posibles contribuciones a la incertidumbre generada por el SMCM:

a) Contribución de las constantes de calibración de las cadenas de medida de los parámetros operativos (*V, I* y T_m) u(C)

b) Incertidumbre estándar debida a la inestabilidad de las condiciones ambientes que aplican al módulo FV, u(R)

c) Contribución a la Incertidumbre estándar debido a las derivas de los componentes electrónicos que conforman el SMCM.

Esta estimación se ha llevado a cabo para cada una de las cadenas de medidas, obteniéndose los siguientes resultados:

– Medida de la tensión: uC(k_{VM})= ±0.062 V

- Medida de la corriente: uC(k_{IM})=±0.13 A
- Medida de la temperatura: uC(k_{TM})=±0.015 ºC

Adicionalmente, la incertidumbre debida a la inestabilidad de las condiciones ambientales ha dado los siguientes resultados:

- Medida de la tensión: uR(V)=±0.442 V
- Medida de la corriente: uR(I)=±0.013 A
- Medida de la temperatura uR(Tm)=±0.095 ºC

Finalmente, en cuanto a la deriva de los componentes, las incertidumbres obtenidas son las siguientes:

- Medida de la tensión: uD(V)=±0.107 V
- Medida de la corriente: uD(I)=±0.065 A
- Medida de la temperatura: uD(Tm)=±0.24 ºC

Los valores resultantes quedan recogidos en la siguiente tabla siguiente:

Tabla 1. Uncertainty estimation of voltage, current and temperature measuring chains

Source	Type	Value	Divis.	Sens Coeff	Standard Uncertainty
$uR(V_{PV})$	A	0,442	1	1	0,442
$uC(V_{PV})$	A	0,062	1	1	0,062
$uD(V_{PV})$	B	0,107	1,73	1	0,062
				combined uncertainty	**0,451**
				coverage factor	**2,000**
			Voltage AFE expanded uncertainty (±V)		**0,901**
$uR(I_{PV})$	A	0,013	1	1	0,013
$uC(I_{PV})$	A	0,013	1	1	0,013
$uD(I_{PV})$	B	0,065	1,73	1	0,038
				combined uncertainty	**0,042**
				coverage factor	**2,000**
			Current AFE expanded uncertainty (±A)		**0,084**
$uR(TV_{PVBp})$	A	0,095	1	1	0,095
$uC(T_{PVBp})$	A	0,015	1	1	0,015
$uD(TV_{PVBp})$	B	0,242	1,73	1	0,140
				combined uncertainty	**0,170**
				coverage factor	**2,000**
			PV BP Temp. expanded uncertainty (±ºC)		**0,340**

5. *VALIDACIÓN DEL MODELO EN BASE A DATOS EXPERIMENTALES*

Los modelos matemáticos del módulo FV, de los parámetros operativos, así como su traslación a las condiciones ROC para su posterior comparación se ha llevado a cabo partiendo de datos procedentes de módulos FV instalados en el Laboratorio de EERR de la UMA, los cuales han sido caracterizados mediante instrumentación de laboratorio calibrada. La disponibilidad de dichos datos ha permitido contrastar los valores estimados con los reales y asi determinar el error que se genera al aplicar dicho procedimiento.

Este proceso previo es fundamental para posteriormente poder cuantificar el Ratio de Rendimiento (*Performance Ratio*) de los módulos trabajando en determinadas condiciones ambientales conocidas.

Los módulos en cuestión son del fabricante Yocasol; y tienen las siguientes características:

Tabla 2. Yocasol PCB-195 module electrical characteristics at STC

Electrical parameter	Value
Maximum output	195 W
Maximum power voltage	26 V
Maximum power current	7,50 A
Open circuit voltage	32,5 V
Short circuit current	8,26 A
Maximum output tolerance	+5%/-3%

El procedimiento ha consistido en generar los valores de la curva *I-V* a partir del modelo propuesto, según las condiciones ambientales reportadas, y posteriormente contrastar los resultados obtenidos para así poder cuantificar el error relativo (RE) resultante de la aplicación del proceso.

A tal efecto, se han tabulado 10 medidas, hechas en distintas condiciones; se han obtenido los correspondientes curvas *I-V* a condiciones STC, las cuales han sido posteriormente trasladadas a ROC y se ha cuantificado el error relativo en los parámetros más importantes; esto es, la corriente de cortocircuito (I_{SC}), la tensión a circuito abierto (V_{OC}), así como la potencia en el punto de máxima potencia (MPP) (P_{mp}) y sus correspondientes coordenadas de tensión (V_{mp}) y corriente (I_{mp}). Los resultados obtenidos están resumidos en la tabla siguiente:

Tabla 3. One clear sky day long proposed model theoretical and experimentally measured PV modules operating parameters. Relative Error of most significant electrical parameters

		M1	M2	M3	M4	M5	M6	M7	M8	M9	M10
	Time	9:11	9:51	11:06	12:26	13:36	14:36	15:31	16:41	17:46	18:31
	T_m (ºC)	14,5	19,7	24,2	31,4	33	35,4	35,3	28,8	23,9	18,5
	G (W/m^2)	308	502	793	985	1039	992	878	635	344	118
I_{SC} (A)	translated	2,5	4,1	6,6	8,2	8,6	8,3	7,3	5,3	2,8	1,0
	measured	2,3	4,0	6,4	8,0	8,5	8,1	7,1	5,1	2,7	0,8
	RE (%)	**8,5**	**3,8**	**2,0**	**1,8**	**1,9**	**2,4**	**2,6**	**2,9**	**6,8**	**19,2**
V_{OC} (V)	translated	33,4	32,8	32,3	31,5	31,4	31,1	31,1	31,8	32,4	33,1
	measured	32,2	32,4	32,4	32,2	32,1	32,1	32,1	32,0	32,0	30,1
	RE (%)	**3,9**	**1,2**	**0,4**	**2,0**	**2,4**	**3,1**	**2,9**	**0,6**	**1,3**	**9,9**
P_{mp} (W)	translated	60,7	97,6	152,2	185,5	194,9	184,9	163,8	120,5	66,2	23,1
	measured	57,5	97,6	153,2	182,8	190,5	180,1	160,4	120,5	64,0	18,5
	RE (%)	**5,6**	**0,0**	**0,6**	**1,5**	**2,3**	**2,6**	**2,1**	**0,0**	**3,5**	**24,8**
V_{mp} (V)	translated	26,7	26,3	25,8	25,2	25,1	24,9	24,9	25,5	25,9	26,5
	measured	26,8	26,3	25,7	24,9	24,6	24,3	24,4	25,5	25,9	25,1
	RE (%)	**0,3**	**0,3**	**0,6**	**1,3**	**1,9**	**2,2**	**1,9**	**0,1**	**0,0**	**5,5**
I_{mp} (A)	translated	2,3	3,8	6,0	7,4	7,9	7,5	6,6	4,8	2,6	0,9
	measured	2,1	3,7	6,0	7,3	7,7	7,4	6,6	4,7	2,5	0,7
	RE (%)	**7,1**	**1,5**	**0,1**	**1,3**	**1,5**	**1,5**	**1,3**	**1,2**	**4,7**	**19,8**

Como consecuencia del análisis de los resultados obtenidos, se ha podido cuantificar el RE en los distintos tramos de irradiancia para cada uno de los parámetros considerados. Se ha podido comprobar que dicho error es mayor en los rangos de irradiancia inferiores a los 200 W/m^2. En dichas condiciones, el comportamiento de los módulos FV no llega a ser crítico, ya que entre otras cosas, la temperatura que alcanzan no es excesiva, quedando esencialmente influenciados por la ambiente.

En definitiva, el método propuesto ofrece unos resultados razonables en el sentido de que no aporta grandes niveles de incertidumbre. En los tramos centrales, el RE correspondiente a la máxima potencia no supera el 2.6 %. Esto es, cualquier módulo que proporcione una potencia inferior al 2.6 % del valor teórico que le correspondiera a las condiciones climáticas que apliquen se puede catalogar como un dispositivo trabajando por debajo del rendimiento óptimo, o bien defectuoso.

6. *APLICACIÓN DEL MODELO A DATOS OBTENIDOS MEDIANTE LOS SMCM*

Una vez que los modelos matemáticos de los parámetros del módulo FV, así como su traslación a las condiciones reales de operación han sido validados y el error relativo cuantificado, procede aplicar dichos procedimientos a los datos obtenidos en el proceso de monitorización en tiempo real utilizando los SMCM´s.

En este caso, se han utilizado los módulos FV de Isofotón instalados en el laboratorio de FV de la EPS. El sistema está formado por dos módulos FV, un SMCM adosado a uno de ellos, el cual se encarga de monitorizar los parámetros operativos del mismo, tales como la tensión (V), la corriente (I), y su temperatura (T_m) y transmitirlos al CCS, utilizando el propio cableado de potencia mediante tecnología PLC . Adicionalmente, otro módulo SMCM-CCS hace la función de concentrador de datos y asimismo, captura los datos procedentes de la célula calibrada, la cual proporciona el valor de la irradiancia incidente en el plano de los módulos FV, y por otro lado, del sensor de temperatura (Pt-100) el cual permite medir la temperatura ambiente.

Por otro lado, el conjunto está dotado de la siguiente instrumentación y equipamiento de laboratorio:

- Osciloscopio Digital de 2 canales
- Multímetro Digital
- Fuente de alimentación dual
- Rack de conexionado
- PC (CCS)
- Prototipo de SMCM
- Prototipo de SMCM-CCS
- Cargas electrónicas ajustables

La configuración del sistema queda recogido en la figura siguiente:
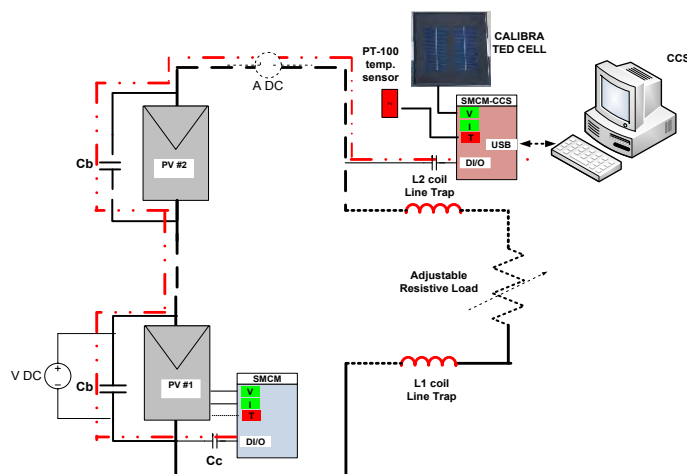
Los parámetros eléctricos más importantes facilitados por el fabricante y referidos a condiciones STC están recogidos en la tabla 4.

Tabla 4. Isofotón ISF-245 PV module data-sheet electrical parameters at STC

Electrical parameter	Value
Rated Power (*Pmax*)	245 W
Open-circuit Voltage (V_{OC})	37,3 V
Short-circuit Current (I_{SC})	8,70 A
Maximum power point Voltage (*Vmax*)	30,2 V
Maximum power point Current (*Imax*)	8,12 A
Efficiency	14,8 %
Power tolerance (% *Pmax*)	+/-3%

El procedimiento de medida ha consistido en conectar el SMCM a uno de los módulos FV, medir los valores instantáneos de la tensión (*V*), corriente (*I*) y temperatura (*Tm*) del mismo, así como los valores de la irradiancia incidente y de la temperatura ambiente, mediante el SMCM-CCS, para que, posteriormente a la correspondiente conversión Analógica/Digital (ADC), se puedan tener los datos digitalizados. Una vez obtenidos los datos, en el CCS, mediante las

correspondientes ecuaciones de conversión a los equivalentes parámetros de ingeniería, se pueden restituir los valores obtenidos.

Se han realizado un total de 11 tandas de medidas cada una de las cuales ha constado de 30 lecturas consecutivas del mismo parámetro, tratando de independizar el procedimiento a posibles variaciones de las condiciones ambientales existentes en un momento determinado. De cada una de las tandas de medidas de los diferentes parámetros, se ha cuantificado asimismo la desviación estándar resultante. El resumen de los resultados obtenidos queda recogido en la tabla 5.

Tabla 5. Mean values, STD deviation and outdoor conditions of readings

#	*G* (W/m^2)	*Ta* (ºC)	*Tm* (ºC)	*V* (V)	*I* (A)	*P* (W)	*Tm* STD	*V* STD	*I* STD	*P* STD
1	197,3	23,4	28,0	6,8	0,92	6,32	0,06	0,42	0,02	0,40
2	201,4	23,4	31,3	12,6	0,89	11,17	0,07	0,61	0,02	0,64
3	223,2	23,8	31,7	12,8	0,92	11,78	0,07	0,64	0,01	0,58
4	199,3	23,5	33,2	20,0	0,84	16,91	0,06	0,59	0,01	0,50
5	217,4	23,6	33,1	27,8	0,85	23,56	0,06	0,47	0,02	0,68
6	274,4	24,1	33,1	31,5	0,69	21,74	0,06	0,45	0,02	0,52
7	229,0	23,1	33,2	32,1	0,55	17,77	0,07	0,42	0,01	0,45
8	203,4	24,1	33,1	32,2	0,46	14,90	0,06	0,44	0,02	0,54
9	200,4	24,0	33,0	32,4	0,39	12,54	0,08	0,44	0,02	0,63
10	204,1	24,0	33,0	32,6	0,35	11,28	0,10	0,43	0,01	0,47
11	226,6	24,1	33,0	32,7	0,32	10,40	0,07	0,44	0,01	0,42

En la tabla 6 se recogen las 30 lecturas correspondientes a la medida #5, realizadas estando el módulo FV a una temperatura de 33,1 ºC y sometido a una irradiancia de 217 W/m^2. En la citada tabla, aparecen los valores digitales de las lecturas, los cuales, aplicados a las correspondientes ecuaciones de conversión permiten obtener los valores de tensión, corriente y temperatura del módulo.

Tabla 6. Results of run #5
(maximum output at G=217 W/m2 and T_m=33,1ºC)

meas #	NTADC	NIADC	NVADC	T_m (ºC)	V (V)	I (A)	P (W)
1	379	691	667	33,1	27,9	0,84	23,5
2	379	691	652	33,1	27,3	0,84	23,0
3	379	691	652	33,1	27,3	0,84	23,0
4	379	691	662	33,1	27,7	0,84	23,3
5	380	692	677	33,2	28,3	0,86	24,4
6	379	692	682	33,1	28,5	0,86	24,6
7	379	692	660	33,1	27,6	0,86	23,8
8	378	691	652	33,0	27,3	0,84	23,0
9	380	692	655	33,2	27,4	0,86	23,6
10	380	692	668	33,2	27,9	0,86	24,1
11	380	693	682	33,2	28,5	0,88	25,1
12	379	692	672	33,1	28,1	0,86	24,2
13	379	691	652	33,1	27,3	0,84	23,0
14	379	691	650	33,1	27,2	0,84	22,9
15	379	691	660	33,1	27,6	0,84	23,3
16	379	692	675	33,1	28,2	0,86	24,3
17	380	692	683	33,2	28,6	0,86	24,6
18	379	692	666	33,1	27,9	0,86	24,0
19	380	691	651	33,2	27,2	0,84	22,9
20	379	692	653	33,1	27,3	0,86	23,5
21	380	692	664	33,2	27,8	0,86	23,9
22	380	691	679	33,2	28,4	0,84	23,9
23	379	691	678	33,1	28,4	0,84	23,9
24	380	692	659	33,2	27,6	0,86	23,7
25	379	691	652	33,1	27,3	0,84	23,0
26	379	691	654	33,1	27,4	0,84	23,1
27	377	688	667	32,9	27,9	0,79	22,0
28	379	691	678	33,1	28,4	0,84	23,9
29	378	690	672	33,0	28,1	0,82	23,2
30	379	690	652	33,1	27,3	0,82	22,5
		Mean values		**33,1**	**27,8**	**0,85**	**23,6**
		Standard Deviation		0,06	0,47	0,02	0,68

Con el objeto de ilustrar los resultados obtenidos, se presentan algunas de las gráficas resultantes. La siguiente que se muestra corresponde a una medida realizada a una irradiancia de 810 W/m^2, estando el módulo FV a una temperatura de 43,9 ºC. La línea continua de color azul representa la curva correspondiente a condiciones STC; la línea roja de trazos representa la correspondiente trasladada a condiciones reales de operación (ROC), mientras que la línea verde de puntos representa los valores leidos en tiempo real.

I-V VI_2 stc,translated & real

P-V VI_2 stc,translated &real
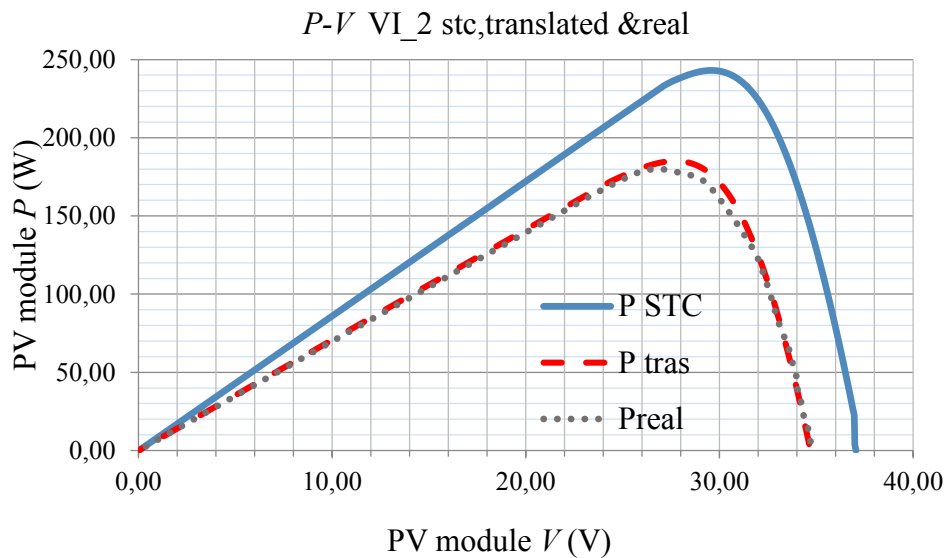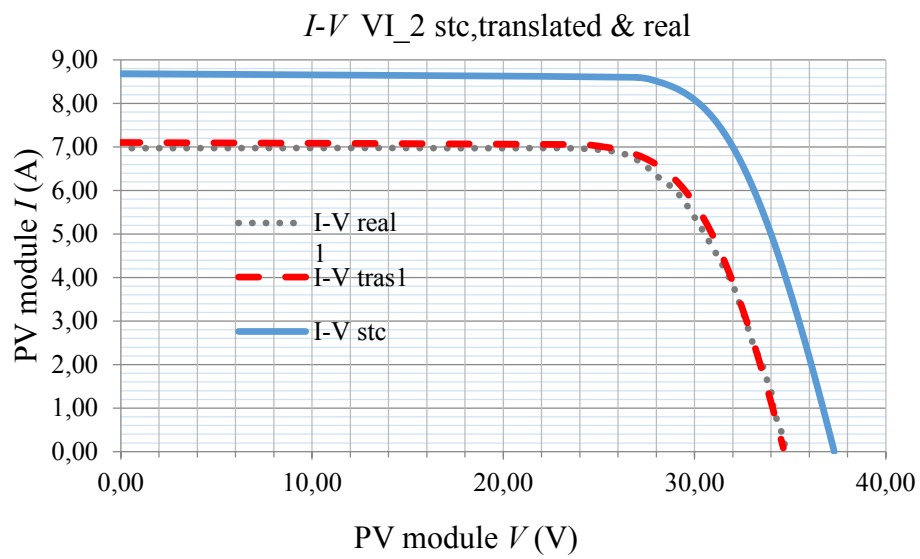
Mediante este procedimiento, se ha podido demostrar la viabilidad de utilizar los SMCM como dispositivos de monitorización en tiempo real de los parámetros operativos de los módulos FV y obtener a partir de los mismos las correspondientes huellas *I-V* y *P-V*. El alcance del punto de máxima potencia va a depender inicialmente de la irradiancia incidente, y de la temperatura ambiente en primera instancia, y, posteriormente de los posibles factores de pérdidas que puedan aplicar. En el caso de un planta conectada a red, se supone que los módulos FV van a estar trabajando en el MPP, por lo que se supone que han de estar suministrando la máxima potencia de que son capaces en las condiciones a las que están sometidos, siempre que estén operando correctamente. Esto se puede comprobar comparando los valores leidos de los parámetros, con los obtenidos por el procedimiento de traslación a condiciones ROC. Queda por lo tanto evidenciada la conveniencia de monitorizar en tiempo real con los SMCM para poder así identificar módulos FV operando por debajo del rendimiento que teóricamente le correspondería. De ser así cabría emprender las acciones correctoras pertinentes.

7. *ANÁLISIS DEL PERFORMANCE RATIO DE LOS MÓDULOS FV*

Las pérdidas a las que puede estar sometido un módulo FV se pueden reflejar en el correspondiente *Performance Ratio (PR)*, y se pueden dividir en dos grandes grupos. Por un lado, tenemos las pérdidas debidas al hecho de que el módulo FV no está trabajando bajo las consideradas condiciones estándares STC. Estas se consideran como inevitables. Por otro lado, están las pérdidas debidas a una mala operación del módulo FV, o bien a condiciones anormales momentáneas no atribuibles a las condiciones climáticas. Estas pueden ser debidas a un sombreado total o parcial, momentáneo o duradero, polvo, suciedad en los módulos, etc… Estas pérdidas son consideradas como evitables, y mediante las correspondientes acciones correctoras, pueden ser suprimidas.

En este sentido, en este capítulo, se propone un protocolo de comparación entre dos conceptos diferentes de *PR*. Estando el módulo FV trabajando en unas determinadas y conocidas condiciones reales (ROC), se obtiene un *PR* experimental denominado PR^i_{DC}. Por otro lado, está el nuevo concepto de *PR* obtenido a partir de los datos trasladados a ROC, y denominado PR^t_{DC}.

El análisis comparativo de ambos *PR* va a permitir cuantificar las pérdidas a las que está sometido el módulo FV, así como sus posibles causas.

La cantidad de energía eléctrica que una planta FV puede generar, ya sea conectada a red, o de forma autónoma depende inicialmente de la eficiencia de la célula FV para unas determinadas condiciones ambientales. Bajo estas condiciones, la energía generada puede verse notablemente constreñida debido tanto a factores de pérdidas (*LF*) predecibles como impredecibles.

En este caso, el foco se ha puesto en las denominadas pérdidas evitables, las cuales han de poder ser cuantificadas correctamente. Estas pérdidas son debidas o bien a fallos del módulo FV, sombreados o presencia de suciedad presente en la superficie de los módulos. Una vez identificado el módulo operando por debajo del rendimiento óptimo en las condiciones que apliquen, es necesario emprender las acciones correctoras oportunas, para, de esta manera, intentar conseguir que el módulo vuelva a proporcionar la máxima energía que fuera capaz, evitando las pérdidas económicas que se pudieran ocasionar si el módulo siguiera trabajando por debajo del rendimiento óptimo.

El procedimiento aplicado queda resumido en la figura siguiente:

PR^t_{DC}, PR^i_{DC} and associated Losses estimation procedure

Procedure based on SMCM I, V and T monitored data

Procedure based on SMCM I, V and T monitored data

PV module I, V & T_m instant values measurement

Measurement of (ROC) effective incident irradiance (G) and ambient temperature (T_a)

Calculation of Instant real Power (P_i)

Calculation of I-V curve at STC

Calculation of Instant real Performance Ratio (PR^i_{DC})

Translation of I-V curve from STC to ROC conditions

Calculation of real Instant Losses (L^i_{DC})

Calculation of ROC translated Instant Power (P_t)

Calculation of Translated Performance Ratio (PR^t_{DC})

Calculation of Translated Losses (L^t_{DC})

Calculation of Effective Losses (L^e_{DC})

Identification of Losses Root Causes

Aplicando dicho procedimiento a las medidas experimentales realizadas, se han obtenido los siguientes resultados, recogidos en la tabla 7.2:

Table 7.2. Yocasol PV modules measurements performed at UMA RREE Lab

Read. Id #	Time	Ta (ºC)	G (W/m2)	T_m (ºC)	P_i	P_{mSTC}	P_{mt}	PR^i_{DC}	PR^t_{DC}	L^i_{DC}	L^t_{DC}	L^e_{DC}
ICV11	9:09:45	17	246	25,7	**44,11**	192,74	47,29	0,93	1,00	0,07	0,00	**-0,07**
ICV12	9:39:52	17,8	437	31,4	**79,27**	192,74	82,52	0,94	0,98	0,06	0,02	**-0,04**
ICV13	10:09:52	18,9	704	36,6	**131,97**	192,74	129,56	0,97	0,95	0,03	0,05	**0,02**
ICV14	10:39:52	20,5	719	47,4	**130,11**	192,74	131,59	0,94	0,95	0,06	0,05	**-0,01**
ICV15	11:09:52	22,1	809	55,1	**141,37**	192,74	146,25	0,91	0,94	0,09	0,06	**-0,03**
ICV16	11:39:52	24,4	884	57,1	**151,67**	192,74	157,76	0,89	0,93	0,11	0,07	**-0,04**
ICV17	12:09:52	24,8	958	55	**163,63**	192,74	169,65	0,89	0,92	0,11	0,08	**-0,03**
ICV18	12:39:52	23,2	395	41,1	**76,89**	192,74	80,86	0,92	0,97	0,08	0,03	**-0,05**
ICV19	13:09:52	23,7	457	38,6	**85,49**	192,74	84,76	0,97	0,96	0,03	0,04	**0,01**
ICV20	13:39:52	24,6	969	49,7	**167,19**	192,74	171,53	0,90	0,92	0,10	0,08	**-0,02**
ICV21	14:11:27	25,6	890	34,6	**161,50**	192,74	158,20	0,94	0,92	0,06	0,08	**0,02**
ICV27	14:35:27	25,8	854	56,2	**37,16**	192,74	152,23	0,23	0,92	0,77	0,08	**-0,70**
ICV22	15:10:52	26,7	828	60,6	**57,93**	192,74	147,57	0,36	0,92	0,64	0,08	**-0,56**
ICV23	15:34:45	26,1	731	50,6	**47,89**	192,74	131,61	0,34	0,93	0,66	0,07	**-0,59**
ICV24	16:10:45	24,9	612	38,5	**34,92**	192,74	111,66	0,30	0,95	0,70	0,05	**-0,65**
ICV25	16:34:45	26,3	478	43,3	**23,18**	192,74	87,94	0,25	0,95	0,75	0,05	**-0,70**
ICV26	17:16:45	23,5	165	24,5	**28,19**	192,74	31,46	0,89	0,99	0,11	0,01	**-0,10**

De forma gráfica, los resultados obtenidos se han agrupado en la siguiente figura, en la que se puede ver la evolución de los *PR*, así como de las pérdidas efectivas ($L\ ^e_{DC}$).
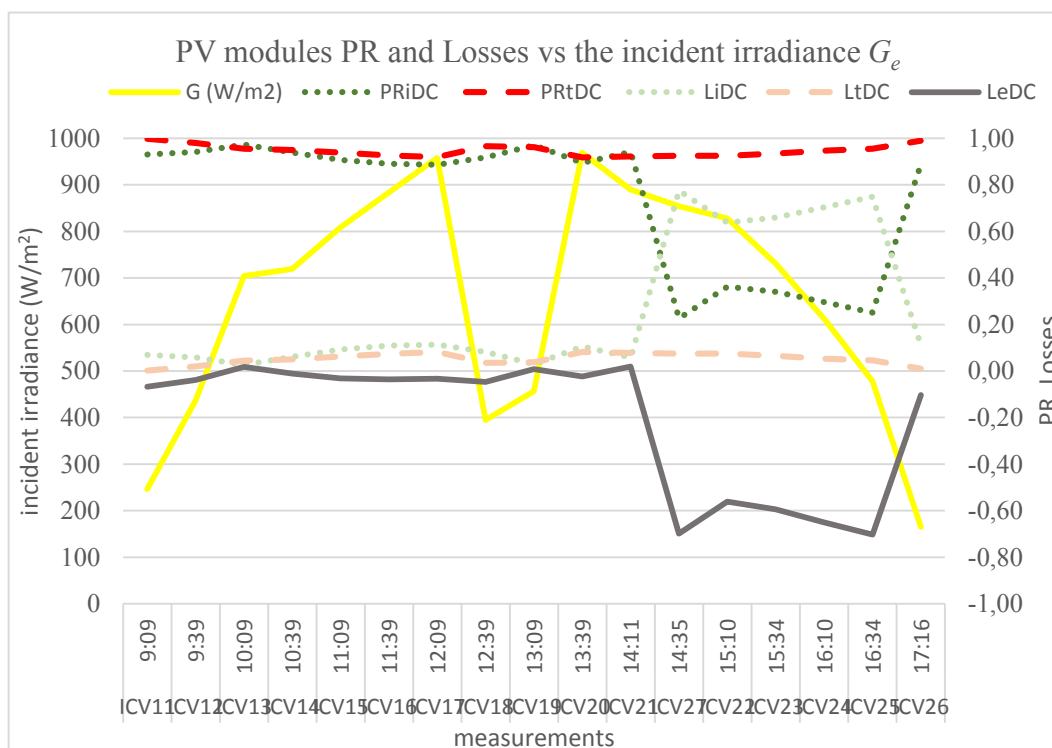
En dicha gráfica, se puede ver la evolución del denominado PR_t, (línea de trazos roja) el cual nos indica el rendimiento óptimo del módulo FV teniendo en cuenta las condiciones ROC que aplican. A partir de las 14:11 h, se produce un sombreado del módulo monitorizado, lo cual da lugar a una bajada drástica de la potencia suministrada, y por extensión del PR^i_{DC} correspondiente. Así se mantiene durante un tiempo. Esto nos indica claramente que el dispositivo está operando por debajo del rendimiento óptimo dado para las condiciones reales aplicables. Se puede observar asimismo que el $PR\ ^t_{DC}$ se mantiene estable, incluso en intérvalos de baja radiación, tal y como ocurre entre las 12:09 h y las 13:39 h. En la misma medida que evoluciona el PR^i_{DC}, lo hace el factor de pérdidas efectivas L^e_{DC}, tal y como indica la línea de trazos y doble punto de color verde oscuro.

Mediante este procedimiento, el módulo FV que presenta unas pérdidas superiores al 3 % se supone que está operando por debajo del rendimiento óptimo. Las pérdidas asociadas se deben a circunstancias de las denominadas "evitables", por lo que las acciones correctoras han de estar enfocadas a subsanar las circunstancias anómalas, para así tratar de conseguir que el módulo FV vuelva a generar la máxima potencia que pudiera, en función de las condiciones ROC aplicables.

Este procedimiento permite optimizar en consecuencia la eficiencia de una planta FV, identificando y advirtiendo en tiempo real de un módulo no operando correctamente.

8. *Conclusiones Generales y Líneas de Investigación Futuras*

Como colofón del trabajo presentado en esta Tésis Doctoral, se ha podido constatar la posibilidad de monitorizar a nivel de módulo FV los parámetros operativos, comparar los resultados obtenidos con los trasladados a condiciones ROC, mediante los procedimientos descritos, y, finalmente determinar los *PR* correspondientes y consecuentes pérdidas efectivas L_e. Mediante una electrónica de bajo coste, utilizando la propia línea de potencia como capa física para la tansmisión de los datos, se ha podido implementar un sistema de monitorización que permite la identificación en tiempo real de un módulo FV operando por debajo del rendimiento que le correspondiera de forma óptima en las condiciones en las que estuviera trabajando. De esta manera, se puede optimizar el rendimiento de una planta FV, asegurando el ROI lo antes posible, mediante la identificación de las causas de las pérdidas.

En cuanto a las posibles líneas futuras, se han identificado las siguientes:

- Mejora del diseño de la electrónica de acondicionamiento de las señales del SMCM para reducir la incertidumbre asociada
- Rediseñar el SMCM para permitir el aislamiento del módulo FV, así como la obtención en tiempo real de la huella I-V.
- Desarrollar una aplicación basada en la Inteligencia Artificial para la identificación de las causas de pérdidas a partir de los datos obtenidos.

Adicionalmente, como resultado de este trabajo, se ha obtenido la siguiente producción científica:

Articulos en publicaciones indexadas

- ***PLC-Based PV Plants Smart Monitoring System: Field Measurements and Uncertainty Estimation.*** Sanchez-Pacheco, F.J. ; Sotorrio-Ruiz, P.J. ; Heredia-Larrubia, J.R.; Perez-Hidalgo, F.; Sidrach de Cardona, M. IEEE Transactions on Instrumentation and Measurement (IEEE TIM), Volume: 63 , Issue: 9 DOI: 10.1109/TIM.2014.2308972, Publication Year: 2014 , Page(s): 2215 – 2222.

- ***Real-Time Procedure to Detect Different Losses in Photovoltaic Generators by Means of Distributed Monitoring***, F.J. Sánchez Pacheco and M. Sidrach. IEEE Transactions on Industrial Informatics (Special Section: Monitoring, diagnosis, prognosis and techniques for increasing the lifetime/reliability of photovoltaic systems). En revisión.

- ***Reverse Decomposition Method vs Simplified PV Module Electrical Model Comparison***, S. Merino Córdoba and F.J. Sánchez Pacheco. IEEE Transactions on Industrial Informatics; Special Section: Monitoring, diagnosis, prognosis and techniques for increasing the lifetime/reliability of photovoltaic systems. En revision.

Artículos en Conferencias internacionales

- ***Low cost DC lines PLC based photovoltaic plants parameters smart monitoring communications and control module***. Sánchez-Pacheco, F.J.; Sotorrio-Ruiz,P.J.; Heredia-Larrubia, J.R. ;Perez-Hidalgo, F. ; Sidrach-de-Cardona,M. International Conference on Power Engineering, Energy and Electrical Drives (POWERENG), 2011 DOI: 10.1109, PowerEng.2011. 6036487. Publication Year: 2011, Pages: 1–6.

- ***Resolution of solar cells equivalent electrical model by reverse decomposition.*** Salvador Merino, F.J. Sánchez-Pacheco, Pedro Rodriguez and Carlos Sánchez. Proceedings of Applications of Computer Algebra (ACA), Málaga, 2013.